_____

TECHNISCHE UNIVERSITÄT WIEN
Vienna University of Technology

D I P L O M A R B E I T

MID-IR transmission spectroscopy of proteins in aqueous solution with an External Cavity Quantum Cascade Laser

ausgeführt am Institut für

Angewandte Physik

der Technischen Universität Wien

unter der Anleitung von Ao.Univ.-Prof. Dr. Martin Gröschl und

Ao.Univ.-Prof. Dipl.-Ing. Dr. techn. Bernhard Lendl

durch

Christian Kristament, Bsc

Leibnizgasse 20-28/2/10, 1100 Wien

_____ _____

Datum Christian Kristament, BSc

Content

Abstract

A room temperature operated pulsed external-cavity quantum cascade laser (EC-QCL) was used for transmissions measurements of proteins in aqueous solution in the mid-infrared region between 1565 cm^{-1} and 1730 cm^{-1}. The high emission power of the laser (up to 800 mW in pulsed mode operation) has enabled transmission measurements through path lengths of 40 µm and more at the 1645 cm^{-1} absorption band of water (ν_2-band, bending vibration). The large absorption of water in this spectral region limits the usable layer thicknesses in a FTIR measurement to about 8-12 µm, which causes lower LODs (limit of detection). This and the opportunity for building a portable and robust device are the two main advantages of the laser technology. The wide tuning range of the laser made it possible to measure spectrally broad absorption bands which are typical for liquids. As a part of this thesis the protein content from milk samples was measured at spectral region of the amide I band. The amide I band of proteins is beneficial as it allows the determination of their secondary structure. Due to the partial overlap of the ν_2 - band of water, the measurement of proteins in aqueous solution is a major challenge. Furthermore, the water absorption band raises additional problems such as the large temperature dependence of the band shape and intensity. For this reason, it was also a part of this thesis to examine the temperature dependence of aqueous solutions in the mid-IR region relevant for the measurement of proteins. To ensure reproducibility, a fully automated measurement system was set up for that purpose.

Zusammenfassung

Ein bei Raumtemperatur betriebener gepulster External-Cavity Quanten Kaskaden Laser wurde für Transmissionsmessungen von Proteinen in wässriger Lösung im mittleren Infrarot eingesetzt. Die hohe Emissionsleistung (im gepulsten Modus - bis zu 800mW) des Laser ermöglichte es im Bereich der Biegeschwingung von Wasser (bei 1645 cm^{-1}) durch Flusszellen von 40µm und mehr Transmissionsmessungen durchzuführen. Die große Absorption von Wasser begrenzt die einsetzbaren Schichtdicken in einem FTIR auf ca. 8-12µm, was die Nachweisgrenzen der Analyten sehr stark beschränkt. Dies und die Tatsache, dass aus einem Lasersystem ein portables und robustes Messgerät entwickelt bzw. aufgebaut werden kann, sind zwei der wichtigsten Vorteile der Lasertechnologie. Der weite Tuning Bereich des Lasers, welcher sich von 1565 bis 1730cm^{-1} erstreckt, machte es möglich, breite Flüssigkeitsabsorptionsbanden aufzunehmen. In weiterer Folge sollte der Proteingehalt von Milchproben im Bereich der Amid I Bande vermessen werden. Die Amid I Bande von Proteinen gibt Aufschluss über die Sekundärstruktur von Proteinen. Durch die partielle Überlappung der ν_2-bande von Wasser, ist die Messung von Proteinen in wässriger Lösung eine große Herausforderung. Weiters wirft die Wasserabsorptionsbande weitere Probleme auf, wie zum Beispiel die große Temperaturabhängigkeit der Absorptionsspektren. Aus diesem Grund war es ebenfalls Teil dieser Arbeit die Temperaturabhängigkeit von wässrigen Lösungen im Bereich der Amid I Bande zu untersuchen. Um die Reproduzierbarkeit zu garantieren, wurde ein vollautomatisiertes Messsystem aufgebaut.

1 Introduction

In dairy industry the milk quality is tightly controlled. Among the various parameters that are monitored the amount of protein in milk is of interest. Furthermore, one specific protein, the casein, is of particular interest therein. One popular way to determine the protein content is the analysis by means of FTIR-spectroscopy in the mid-IR region. The major disadvantage of mid-IR measurements of aqueous solution, as e.g. milk, is the strong water absorption in this spectral region. Because of the strong absorption band at about 1645 cm^{-1}, it is impossible to measure the amide I band, which overlaps with the strong water band, in aqueous solution at higher path lengths (higher than 12 µm) with conventional FTIR-spectrometers due to the low intensity emitting thermal light sources (globar) used therein. These extremely thin layer thicknesses tend to clog easily the flow cell. For this reason the measurements must usually be performed in a spectral region apart from the water band at 1645 cm^{-1} such as the region of the amid II band to determine the amount of proteins in milk while keeping the path length of the measurement cell short. Keeping the path length of the absorbing sample short causes low detection limits. Another possibility would be using a Quantum Cascade Laser (QCL) which offer much higher spectral power density than conventional thermal emitters used in FTIR spectrometers. Hence, they allow transmission measurements of aqueous solutions at reasonable optical path lengths in the mid-IR region. In order to cope with the broad absorption bands typical for dissolved analytes QCLs with a broad spectral coverage are required. This requirement is fulfilled by broadly tuneable External Cavity (EC-)QCLs. Also the possibility of building a compact and robust setup due to the laser technology without moving mirror of an interferometer is an important advantage. Details on this new type of mid-IR source are presented in section 1.1.

The most significant benefit when measuring the amid I band is the opportunity to determine the secondary structure of proteins, such as α-helix, β-sheet and random coil structure. Furthermore, the amid I band is stronger than the amid II band which increase also the limit of detection. The major disadvantage of measuring the amid I band is the overlapping bending vibration band of liquid water as mentioned previously.

A frequently applied counter measure to enable the investigation of the amid I band using mid-IR spectroscopy is to extract the proteins or to establish a solution in D_2O, which does not possess an absorption band overlapping the amid I band.

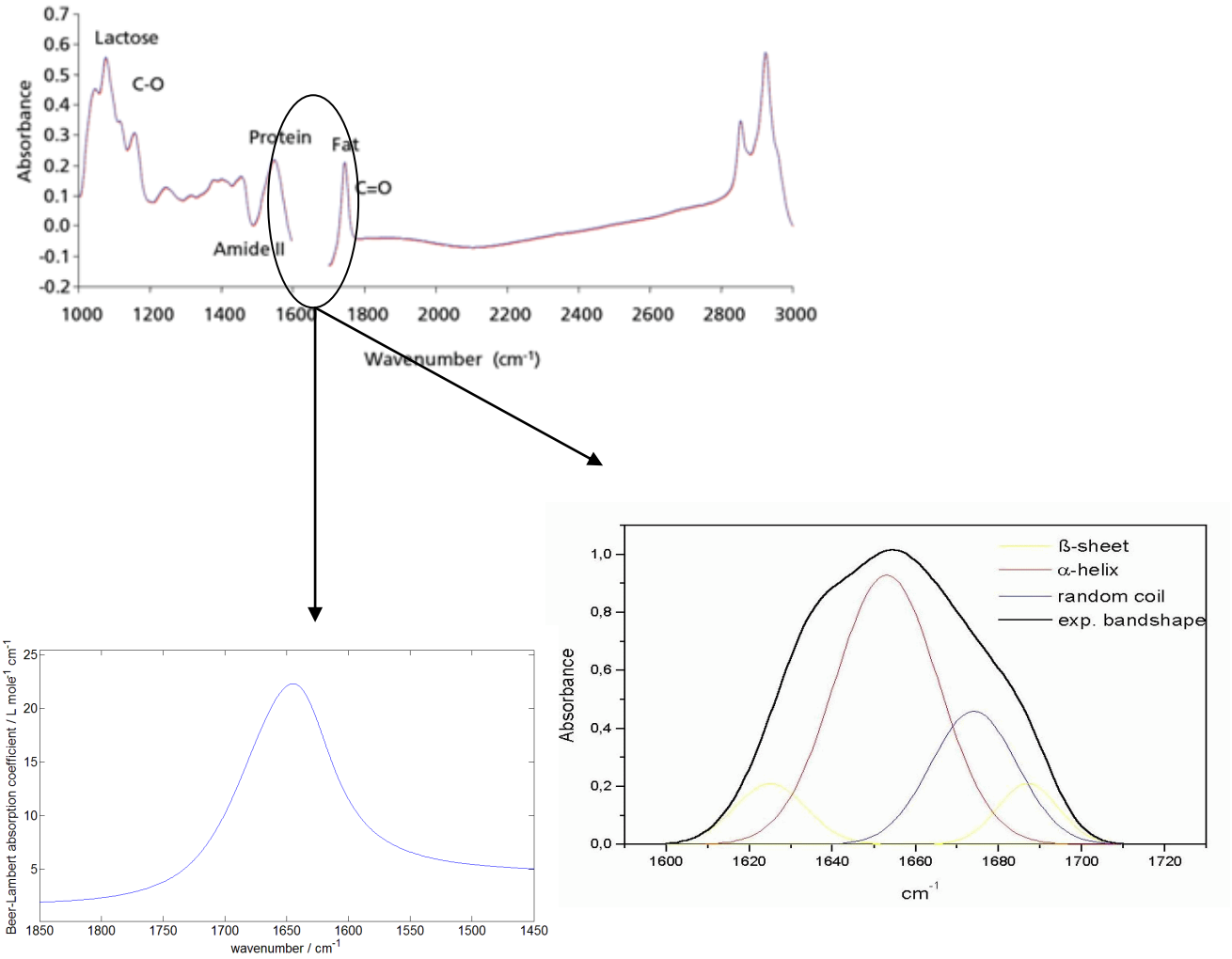

Figure 1 – MilkoScan spectrum of milk (top, reproduced from [33]) compared with the water absorption band at 1645cm^{-1} (left, data obtained from [14]) and a spectrum of the overlapping amid I band (right, reproduced from [6])

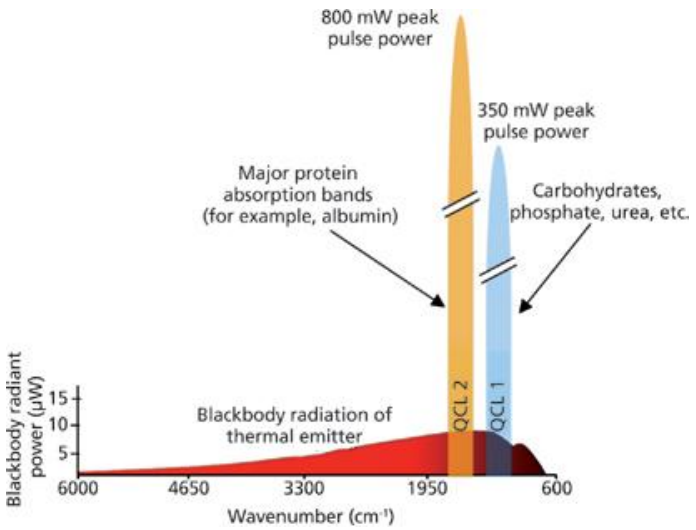

Figure 2 – Comparison of the light emission between a globar and a QCL [18]

A popular commercial product which relies on mid-IR optical analysis of milk is the MilkoScan of the FOSS GmbH. It is used to determine the quality of milk by an FTIR-spectroscopic measurement. For this reason the device is not able to measure the amid I band of milk samples (aqueous solution), which is shown in Figure 1 and mentioned above.

Another issue when measuring in aqueous solutions is the dependence on the temperature of the water absorption spectra which may cause a great error. Hence, an emphasis on the temperature stabilization of the flow cell is a prerequisite.

1.1 Quantum Cascade Laser

Quantum cascade lasers are semiconductor lasers that emit in the mid- and far-infrared spectral region. The theoretical function of the QCL is based on a theory which was developed in the year 1971 by Kazarinov and Suri's [15]. The first successful experimental demonstration took place in the year 1994 by Jerome Faist [16]. QCLs emit light due to intersubband transition of electrons within a conduction band. Modern QCLs can be operated at room temperature. The spectral region that can be achieved spreads from about 2 – to 200 µm [17].

1.1.1 Construction and working principle of a QCL

The structures of QCLs are made of thin semiconductor layers with a thickness of a few nanometers. Figure 3 shows the typical structure of a QCL. A layered structure of different materials and thicknesses determines the size of the band gap. The photon energy and the wavelength are determined by the band gap of the gain material such as for example GaAs and AlGaAs. This layered structure form a cascade of quantum wells when a voltage across the layers is applied. The function of the laser depends on the correct thickness of the single layers and the right doping of the semiconductor. The wavelength of a QCL is dependent on the thickness of the semiconductor layer and not the material in the first place. As a result many wavenumbers can be covered by the same laser material by adjusting the thickness of the semiconductor layers [18]. This is the major difference to conventional interband laser (=diode lasers) whose emission wavelength is solely determined by the employed material.

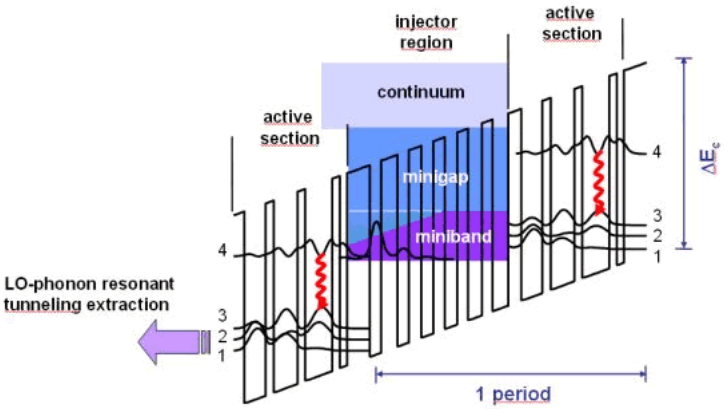

Figure 3 – Typical structure of a quantum cascade laser [17]

In Figure 3 the operation principle of a QCL is shown schematically. Upon application of a voltage across the layers, photons are emitted in the active areas by electronic transitions. Then the electrons which were used for the transitions are collected in the injector areas and are reused for another transition in the next active zone. In a QCL active regions and injector regions repeat periodically.

"From the injector miniband the electrons are injected into the upper laser energy level (4) of the active section. Here the laser transition by emitting photons takes place*. After that, the lower laser energy level (3) is emptied by LO-phonon emissions and the electrons enter the next stage by tunnelling (see figure 3)." [17]*

A quantum cascade laser usually contains 20-30 such active layers which are called cascades. The consecutive active regions are located on sloping energy levels.

1.2 Mid-IR transmission spectroscopy with quantum cascade lasers

The mid-IR region is defined as the part of the electromagnetic spectrum between 2.5µm and 50µm. Absorption of IR-light is due to vibrational excitation of covalently bonded atoms or groups and rotational excitation of molecules [10]. The transferred energy contains information on functional groups, intra- und intermolecular interactions.

1.2.1 Molecular vibrations

The interaction of a molecule with electromagnetic radiation is directly proportional to the dipole moment of the molecule. Absorption or emission of radiation is therefore only observed when it is accompanied by a change of the dipole moment of the molecule. Therefore, the structure of a molecule is crucial for the observation of radiation. So, for example, diatomic molecules consisting of the same atoms (eg N2, O2) show no change in the dipole moment and therefore they do not absorb radiation. Thus IR-active vibrations require changeable (induced) dipole moments to get an absorption response in the IR-region; otherwise molecules without changeable dipole moment are called IR-inactive [22]: *"Each atom has three degrees of freedom, corresponding to motions along any of the three Cartesian coordinate axes (x, y, z). A polyatomic molecule of n atoms has 3n total degrees of freedom. However, 3 degrees of freedom are required to describe translation, the motion of the entire molecule through space. Additionally, 3 degrees of freedom correspond to rotation of the entire molecule. Therefore, the remaining 3n– 6 degrees of freedom are true, fundamental vibrations for nonlinear molecules. Linear molecules possess 3n– 5 fundamental vibrational modes because only 2 degrees of freedom are sufficient to describe rotation. Among the 3n– 6 or 3n– 5 fundamental vibrations (also known as normal modes of vibration), those that produce a net change in the dipole moment may result in an IR activity and those that give polarizability changes may give rise to Raman activity. Naturally, some vibrations can be both IR- and Raman-active" [1].*

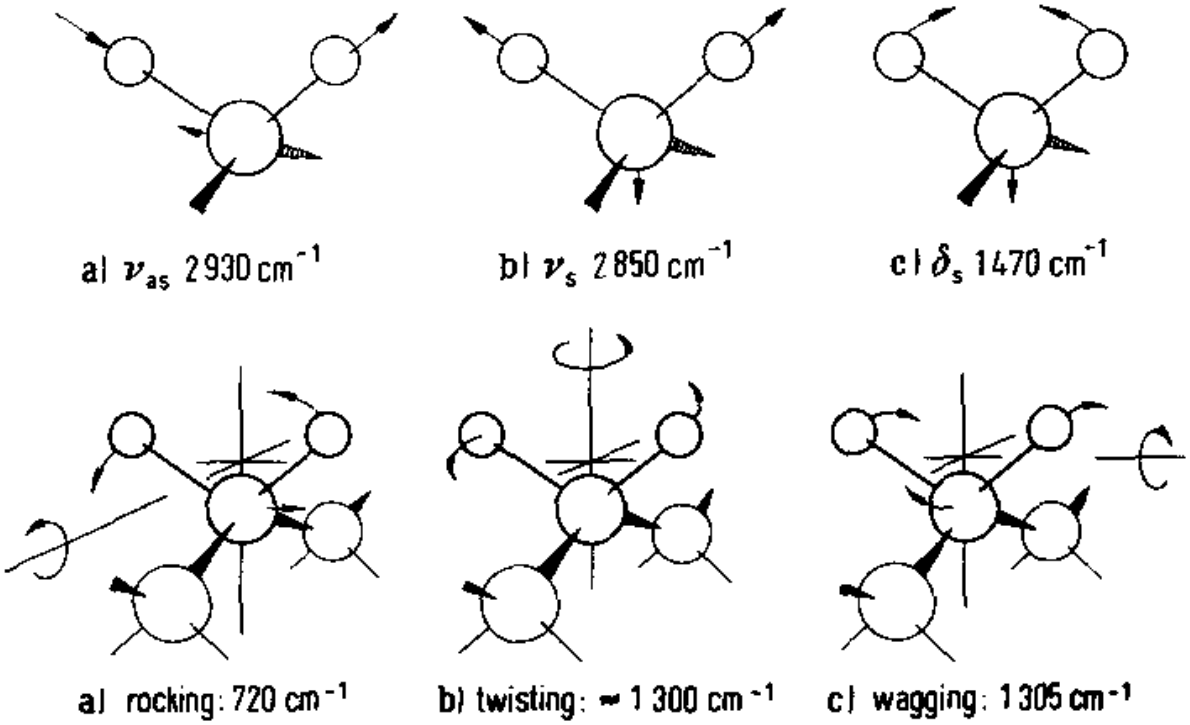

Figure 4 – Vibration modes of the CH_2-group of methylen [1]

The fundamental molecular vibrations have descriptive names. Among them are the following types [1]:

1) Stretching (asymmetric and symmetric stretching)
2) Bending
3) Scissoring
4) Rocking
5) Twisting
6) Wagging

In addition to these basic types of vibration combinations thereof are found, too. Figure 4 exemplary shows the CH_2-group modes of methylen and the characteristic reciprocal centimeters of each mode. Not all theoretically possible vibration may be observed in practice: "*The total number of observed absorption bands is generally different from the total number of fundamental vibrations. It is reduced because some modes are not IR active and a single frequency can cause more than one mode of motion to occur. Conversely, additional bands are generated by the appearance of overtones (integral multiples of the fundamental absorption frequencies), combinations of fundamental frequencies, differences*

of fundamental frequencies, coupling interactions of two fundamental absorption frequencies, and coupling interactions between fundamental vibrations and overtones or combination bands (Fermi resonance)" [1].

1.2.2 Absorption in the mid-IR-spectral region

During the absorption of IR-light by a molecule, the molecule goes to a higher excited state of vibration. The intensity of an absorption band is proportional to the square of the change in the dipole moment relative to the equilibrium state. In case of stretching vibrations, for instance, the change in the dipole moment is caused by a change in bonding lengths and at bending vibrations by changes in bonding angles [21][22].

The different energy levels are given by the energy states of the quantum harmonic oscillator which is shown in equation (1.1). The harmonic approximation is valid for low quantum state numbers.

$$E_n = h\,\nu\left(n + \tfrac{1}{2}\right) \tag{1.1}$$

E … energy
ν … oscillation frequency
h … Planck constant
n … quantum number

The frequency, at which a specific vibrational mode absorbs electromagnetic radiation, depends on the reduced mass of the involved atoms, the force constant of the chemical bond, the strength of interactions with adjacent atoms and the coupling with other molecular vibrations. For a diatomic molecule (different atoms) it is calculated by [21][22]:

$$\nu = \frac{1}{2\pi}\sqrt{\frac{k}{\mu}} \tag{1.2}$$

k … force constant
μ … reduced mass

The concentration of a dissolved sample is determined by first measuring the intensity (I_0) of the transmitted light through the solvent without the sample (matrix) followed by a measurement of the intensity transmitted through the sample containing solution. If d is the path length of the transmission cell, ϵ the absorption coefficient and c the molar concentration of the sample, the transmitted light intensity can be calculated with formula (2) [10].

$$T = \frac{I}{I_0} = 10^{-\epsilon dc} \tag{2}$$

From equation 2 follows the Beer-Lambert law for the absorption of IR-light:

$$A = log_{10}\left(\frac{I_0}{I}\right) = \epsilon dc \tag{3}$$

An important aspect of the Lambert-Beer law is that the concentration is linearly correlated with the absorption signal. Thus, a linear calibration curve can easily be calculated.

1.3 Properties of liquid water in the mid-IR spectral region

In this thesis water was used as solvent (=background) for the measurements, so it was important to pay attention to the properties of water with regard to its interactions with mid-IR radiation. Figure 5 shows the possible molecular vibrations of the water molecule. Due to the low weight of the H atom the amplitude of the vibrations are large [13].

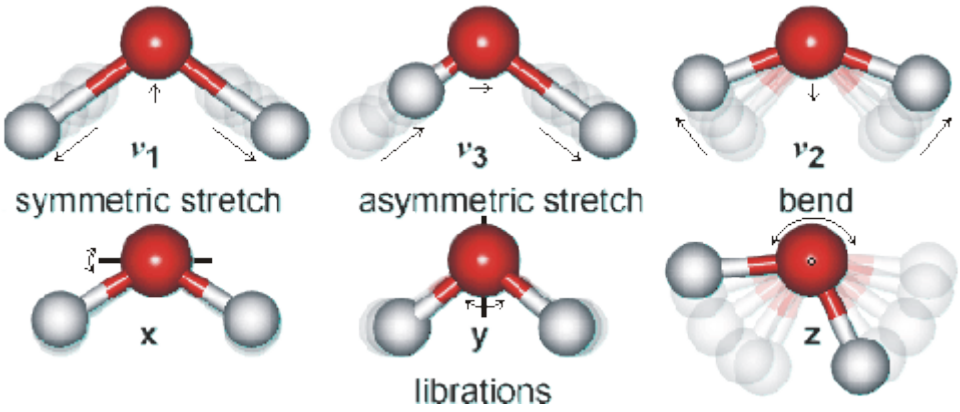

Figure 5 – Molecule vibrations of liquid water: the arrows show the movements of the dipole moments, which change in the direction of the oxygen atoms [13]

Main vibrations of liquid ordinary and heavy water				
Vibration(s)	**liquid H2O (25°C)**		**liquid D2O (25°C)**	
	***v*, cm-1**	**E0, M-1 cm-1**	***v*, cm-1**	**E0, M-1 cm-1**
V_2	1643.5	21.65	1209.4	17.10
combination of v_2 + libration	2127.5	3.46	1555.0	1.88
v_1, v_3 , and overtone of v_2	3404.0	100.61	2504.0	69.68

Table 1 - maximum of the several absorption bands of liquid water (reproduced from [13])

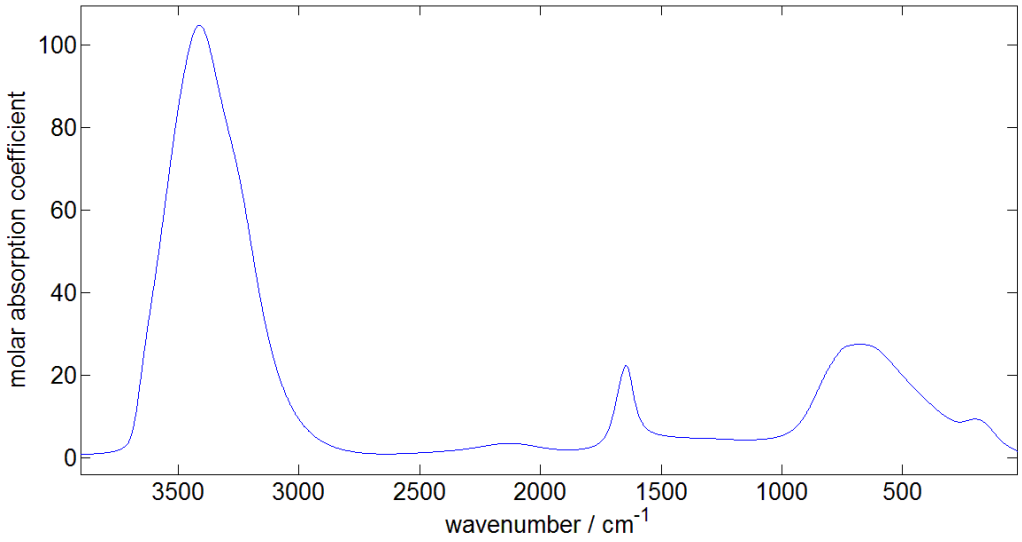

Figure 6 – Molar absorption coefficient of water (H_2O) at 25°C (data obtained from [14])

In Figure 6 the molar absorption coefficient of water at 25°C in the range between 1-4000 cm^{-1} [14] is shown. The band positions are summarized in Table 1 [13]. The frequencies of the stretching and bending vibrations depend on the strength of the intra- and intermolecular hydrogen-bonds. In liquid water the stretching vibration shifts towards higher frequencies if the temperature is increased. This effect can be explained by weakening of the intermolecular hydrogen-bonds and strengthening the covalent O-H bonds, respectively. On the other hand the bending vibration band shifts towards lower frequencies because of a weakening of the intermolecular hydrogen-bonds. Furthermore, it becomes stronger and narrower. Increasing temperature lowers the intensity of the stretching bands.

Also the pressure on water changes the position of its vibration band: "*Increasing the pressure on water decreases the O⋯O distances so increasing the covalent O-H distances and lowering their stretch frequency. Raised pressure also causes a reduction in long, weak or broken bonds and an increase in bent and short, strong hydrogen bonds." [13]*

Figure 7 shows the temperature effects on the fundamental vibration band, which are mentioned in table 1.

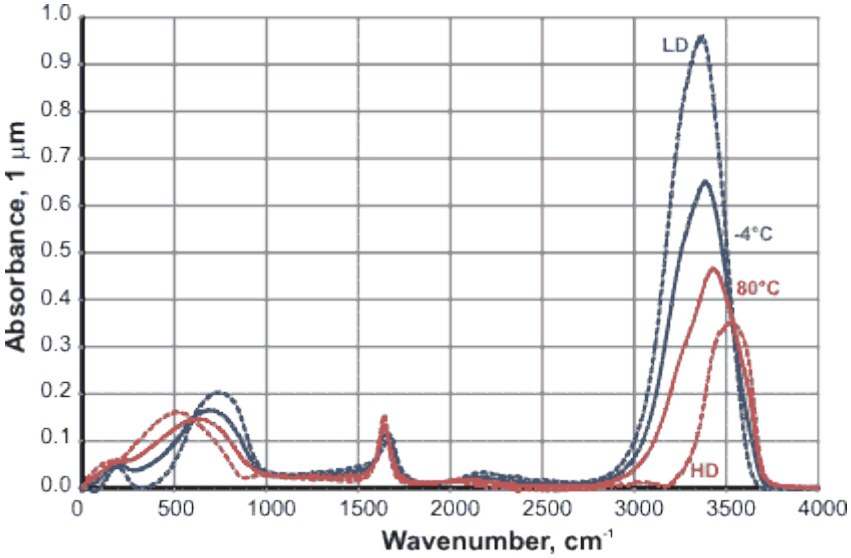

Figure 7 – Temperature effects on water vibration bands [13]

1.4 Influence of the thermal expansion of the measurement cell on the measured absorption.

The calculation of the thermal expansion of the spacer in the flow cell is calculated based on the linear approximation with a linear expansion coefficient. [19]

$$L \approx L_0(1 + \alpha \cdot \Delta T) \tag{4}$$

$$\alpha = \frac{1}{L}\frac{dL}{dT}$$

L_0 … length before expansion

L … length after expansion

α … linear expansion coefficient

Subsequently, the change of absorption induced by this thermal expansion can be calculated by equation 1, using the value of ΔL, which was calculated by equation 4 [10]:

$$\varepsilon \cdot c \cdot \Delta L = \Delta A \quad (5)$$

ΔA … change of the absorption

ΔL … expansion of the spacer (path length)

c … concentration

ε … molar absorption coefficient

Considering a temperature change of T = 10 K with a layer thickness of L = 50 µm and a linear expansion coefficient α = 21 × 10-5 K^{-1} of PTFE, the error by using (3) and (4) (where c = 55.56 mol^{-1}, ε = 22.3086 l mol^{-1} cm^{-1} based on the data of John Bertie of water at 1645 cm^{-1}) results in:

$$\Delta A \approx 13\ mAU$$

This error is added to the errors caused by changing the strength of the hydrogen bonds so an accurate temperature stabilization of the flow cell is necessary.

1.5 Analysis of protein in mid-IR-region

1.5.1 Introduction in proteins

Proteins are linear biological polymers which are composed of about only twenty different amino acids. These amino acids are the monomers which form the polymer. Building an amide bond is due to linking one amino acid with the carboxylic acid group which is shown in Figure 8a. This amide bond is called peptide bond by protein chemists. When two amino acids linked together by an amide bond it is called dipeptide. Furthermore, a polypeptide is built when many amino acids are linked together by amide bonds (see figure 8b). A polypeptide consists of a backbone and sidechains [2].

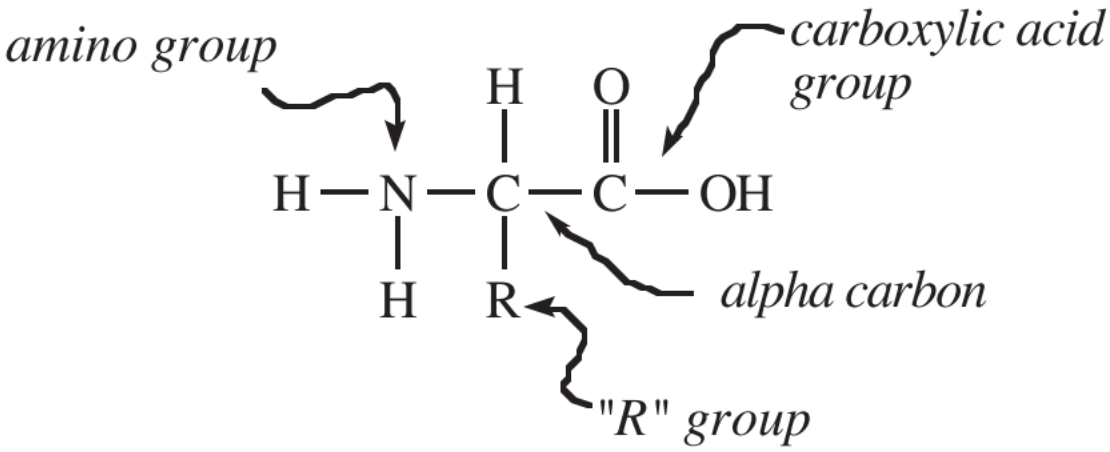

Figure 8a – Basic structure of an amino acid [2]

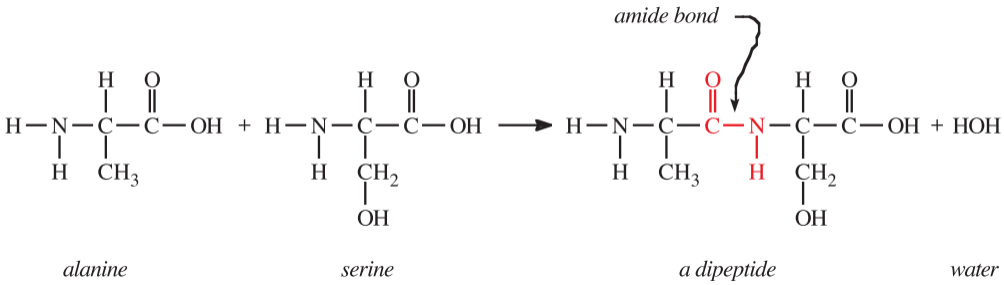

Figure 8b – Schematic illustration building a polypeptide [2]

The backbone of each polypeptide consists of the amide nitrogen, the alpha carbon and the carbonyl carbon. Due to the number of different (hundreds of amino acid unit) the number of the possible sequences explodes [2]. Proteins basically appear in three structures: primary, secondary and tertiary structure. The structure determines the function of proteins or requires the structure for their function respectively.

The primary structure of proteins indicates the amino acid sequence of the peptide chain. The secondary structure refers to a local sub-structure which is built by hydrogen bonds between main-chain peptides. The main and most important types of secondary structures are the α-helices and β-sheets which are periodic structures. They should not be confused with random coil und unfolded polypeptide chains (see Figure 9a).

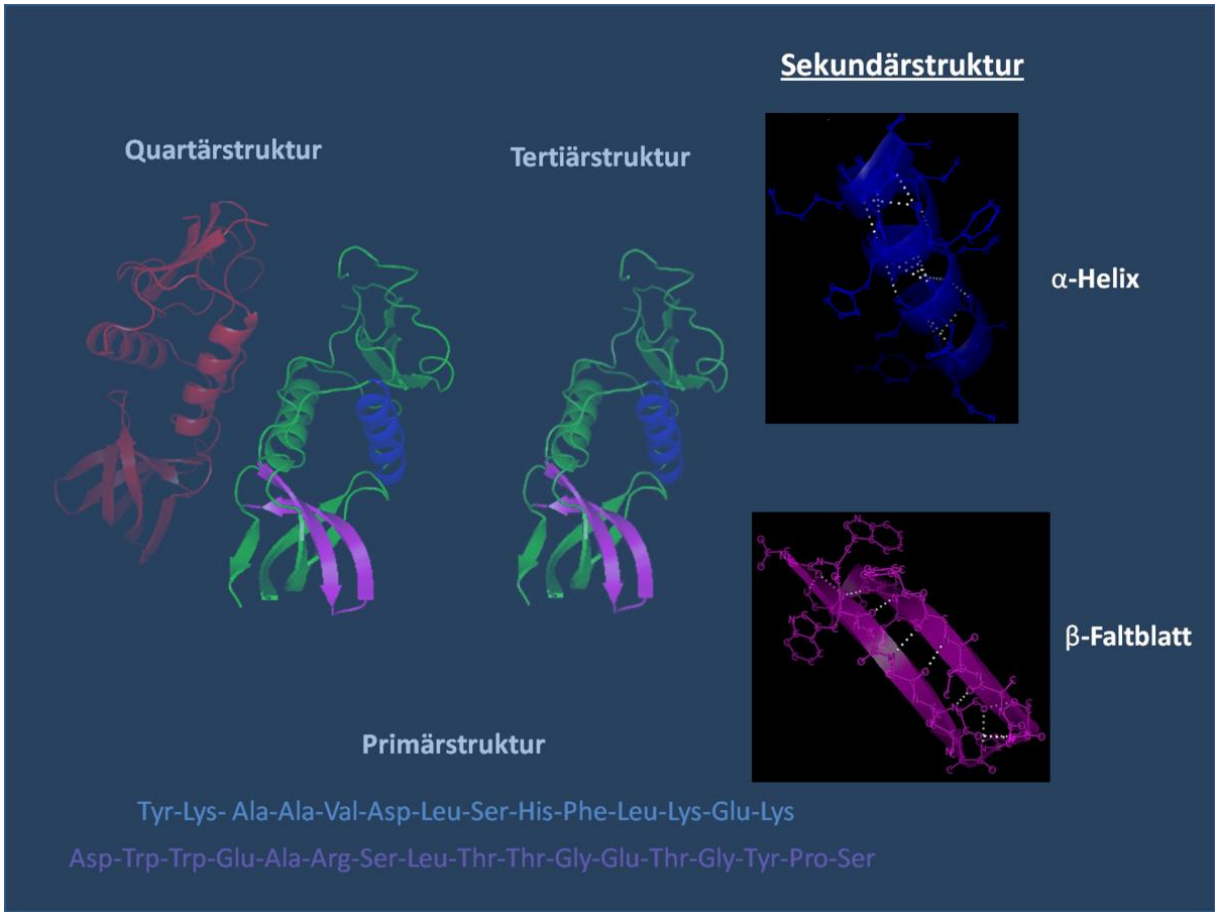

Figure 9a – Schematic illustration of the different structures. [23]

Tertiary structure means when various elements of secondary structure packed tightly together to form a well-defined 3-dimensional structure. The folding is due to hydrophobic interaction. However, these interactions are weak, so the protein can be easily denatured [2] [20].

The primary mechanism responsible for the secondary structure is that the amides form hydrogen bonds to each other which influence the absorption spectrum. Hence absorption spectra of the different structures are characteristic and can be measured in the mid-IR-region. However, amides like to be exposed to water, because they can form hydrogen bonds with water, which can influence the mid-IR absorption spectrum of proteins in aqueous solutions [2].

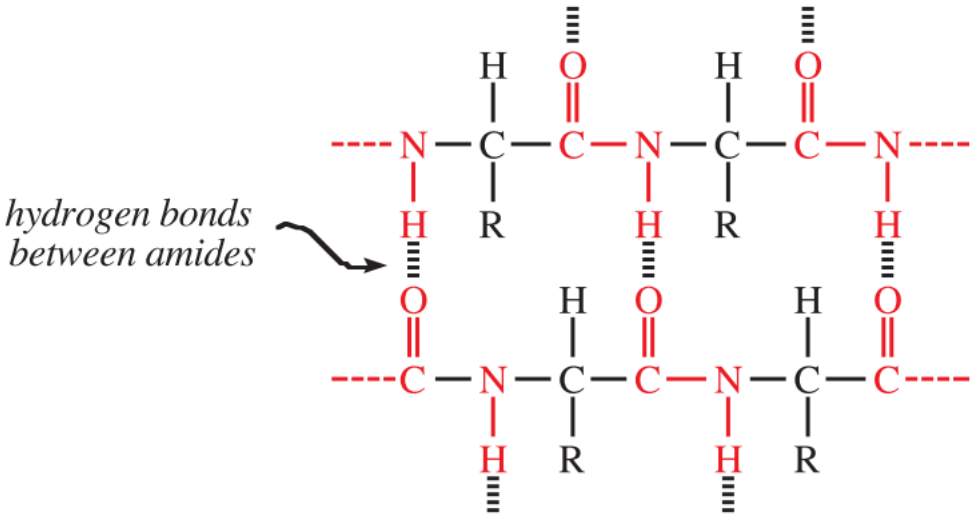

Figure 9b – Hydrogen bonds that form between amides causing protein folding [2]

1.5.2 Mid-IR-spectroscopy for the analysis of secondary structures of proteins

For the understanding of biological reactions, infrared spectroscopy is becoming increasingly important, especially since it provides information (i.e. secondary structures) that cannot be obtained by methods of structural analysis such as NMR, electron microscopy and X-ray structure analysis. A protein results in mid-IR absorption over a broad spectral range because of the peptide backbone (amide bands) and the amino acid side chains. Hence, it is difficult to determine the individual input of each amino acid. [4][6].

Proteins can give rise to nine absorption bands in the mid-IR spectral region, which are named amid A, B and I-VII band [3]. The characteristic wavelengths are shown in Table 2 [4] and Figure 10 [6].

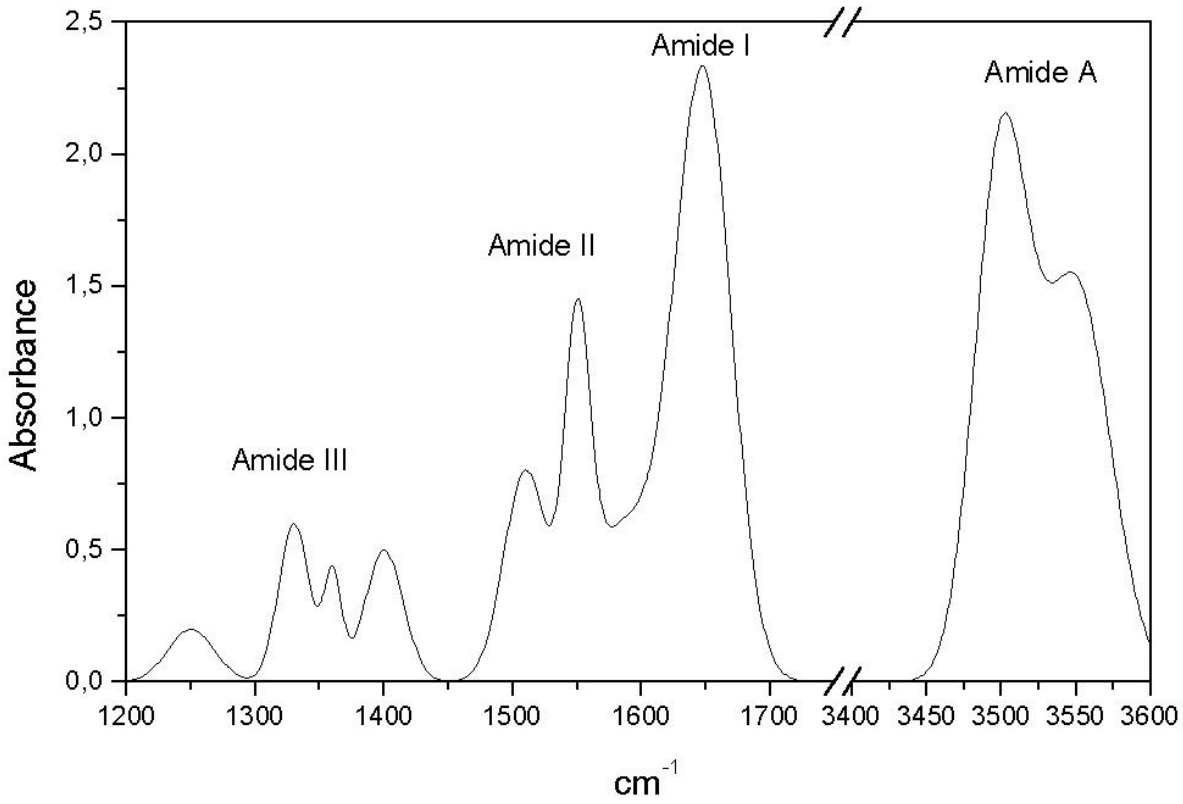

Figure 10 - IR-absorption bands of the peptide groups [6]

Some particular important bands among these nine are the amide I and II since they provide information of the secondary structure of proteins. Because of the high complexity depending on the details of the force fields, side chains and hydrogen bonding, the remaining bands have little importance in protein conformational studies. Thus, this work concentrates on the amide I band. The N-H bending (40-60%) and C-N stretching (18-40%) vibration is responsible for the amid II band and is not as suitable to predict the secondary structure of protein as the amide I band. The amide I band is almost exclusive the consequence of the C=O stretching (70-85%) vibration of the peptide group [4]. Because of this reason the amide I band was chosen for analysis of the protein's secondary structure with an EC-QCL in the mid-IR-region.

Designation	Approximate frequency (cm^{-1})	Description
Amide A	3300	NH stretching
Amide B	3100	NH stretching
Amide I	1600–1690	C=O stretching
Amide II	1480–1575	CN stretching, NH bending
Amide III	1229–1301	CN stretching, NH bending
Amide IV	625–767	OCN bending
Amide V	640–800	Out-of-plane NH bending
Amide VI	537–606	Out-of-plane C=O bending
Amide VII	200	Skeletal torsion

Table 2 - Characteristic vibrations of the polypeptide group (reproduced from [3])

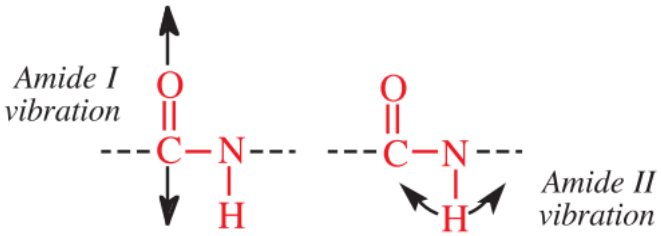

Figure 11 - Vibrations responsible for the amid I and II band in the infrared spectra of proteins and polypeptides [2]

One difficulty in analyzing the amide I band is that all responses of the different conformations (α-helix, β-sheet, …) of proteins show significant overlap. In order to differ the several absorption band components, a Fourier self-deconvolution (see Figure 12) method for separating the absorption bands can be used. [2]

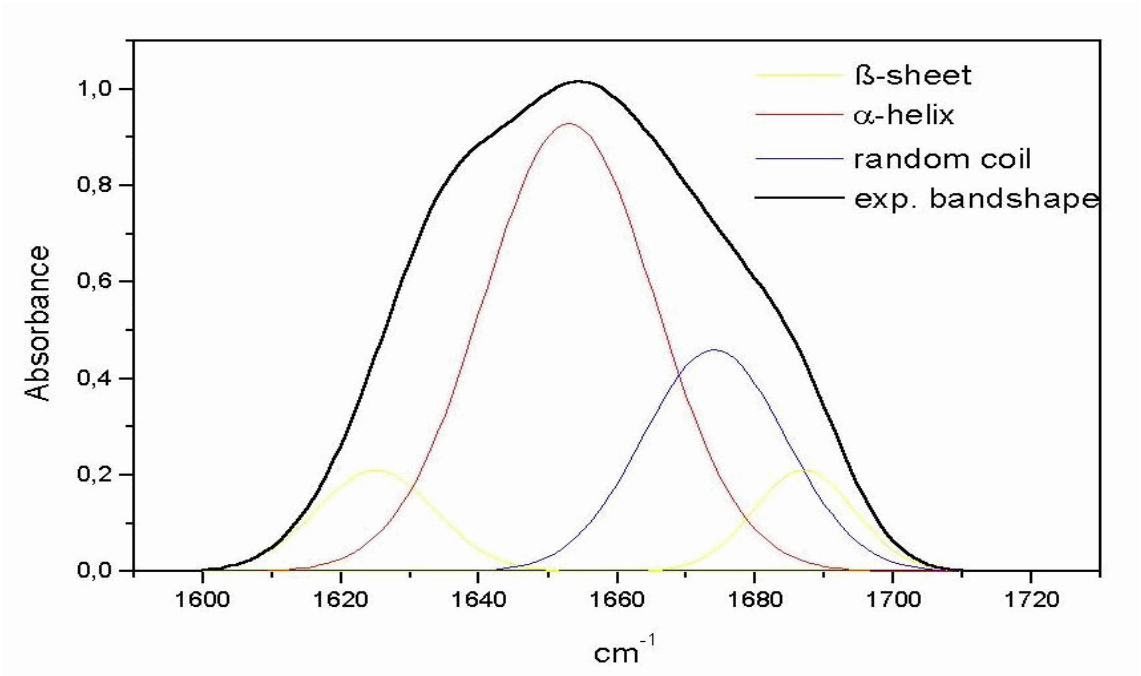

Figure 12 - Example of a deconvolution of an amide I band [6]

Secondary structure	Band position in $^1H_2O/cm^{-1}$		Band position in $^2H_2O/cm^{-1}$	
	Average	Extremes	Average	Extremes
α-helix	1654	1648–1657	1652	1642–1660
β-sheet	1633, 1684	1623–1641, 1674–1695	1630, 1679	1615–1638, 1672–1694
Turns	1672	1662–1686	1671	1653–1691
Disordered	1654	1642–1657	1645	1639–1654

Table 3 - Assignment of amid I band positions to secondary structure [4]

1.5.3 Casein

One of this thesis' goals was to determine the quality of cow milk by measuring the protein amount with laser spectroscopy like mentioned in chapter 1. According to that the most important of cow milk protein is casein, because it is vital for the production of cheese and yoghurt. So a short introduction of casein spectra is necessary.
The protein content of milk is typically 2.9-5.0 % [8] of which casein is about 79-83%. [8]

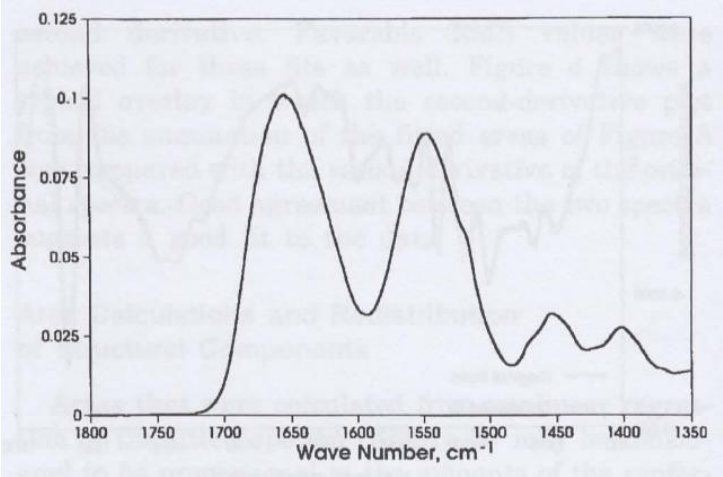

Figure 13 – Typical spectrum of casein (reproduced from [24])

Figure 13 shows a typical IR-spectrum of casein. The envelope of the absorption band changes with different conformations [24]. The conformation of proteins changes with the temperature, pH-level, and the presence of other substances present in milk. For this reason it is important to pay attention on the temperature and the pH-value of the sample solution.

1.6 Properties of cow milk

Cow milk is composed of approximately 87% water and 13% dry substances. The relative composition of dry substances is as follows [8]:

- Water 84.5-89.5%
- Fat 2.5-6.0%
- Proteins 2.9-5.0%
- Lactose 3.6-5.5%
- Minerals 0.6-0.9%

These constituents of milk differentiate between different breed of cows and between individual cows, so the composition is not well defined. At first the quality of milk is defined by the casein content, furthermore it is defined by the fat content, pH-level, calcium ion activity, sugar and phosphate content. These single contents can influence the IR-spectrum [24]. Figure 14 shows a spectrum of milk measured with the MilkoScan. This figure clearly shows that this Instrument only measures the protein amount by the amid II band. This restriction is imposed by the strong water absorption band. With the QCL technology used in this thesis it should be demonstrated that the amide I band in aqueous solution can be measured, thereby delivering valuable additional information about the sample.

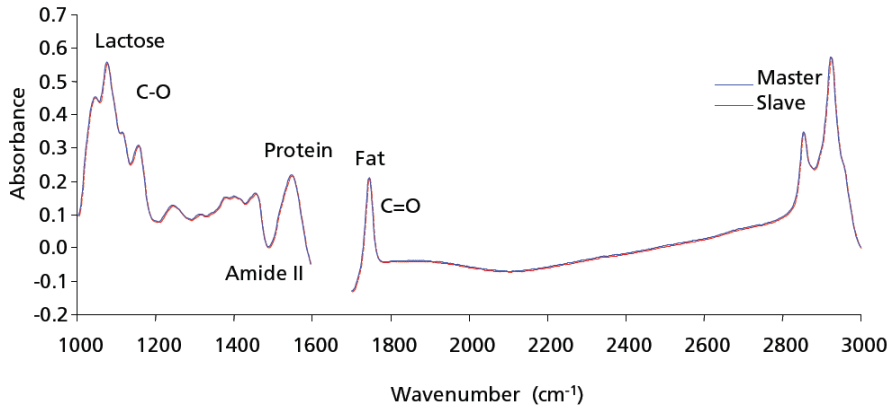

Figure 14 – Spectrum of milk measured by a MilkoScan [33]

2. Materials and Methods

2.1 Equipment/Setup

Figure 15a and 15b show the basic setup, used in all measurements. All experiments took place in an air-conditioned laboratory and the setup was mounted on an air-cushioned table, which attenuated mechanical vibrations. Reproducible results were achieved by setting up a software-controlled automated sampling system (ATLAS software system [30] [28]). As can be seen in Figure 15a, the setup consists of 4 main components:

- External Cavity Quantum Cascade Laser + driver (Daylight Solutions, USA)
- Sample handling components (temperature stabilized flow cell + selection valve + syringe pump)
- Data acquisition components
- PC for controlling and data acquisition

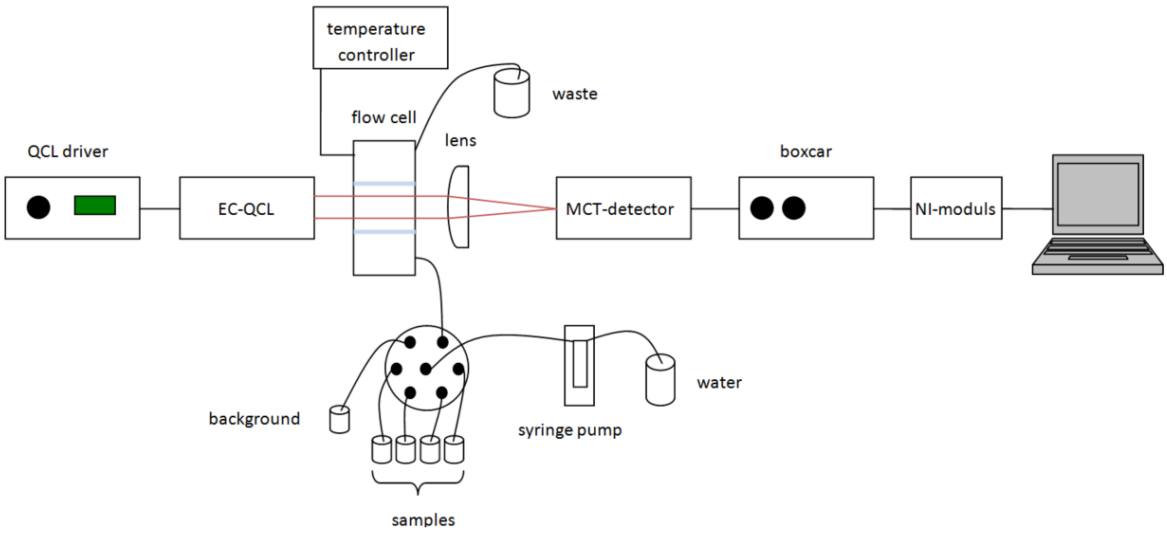

Figure 15a – Schematic illustration of the measurement system (the boxcar integrator and the NI-modules (DAC and ADC) are described in section 2.1.5)

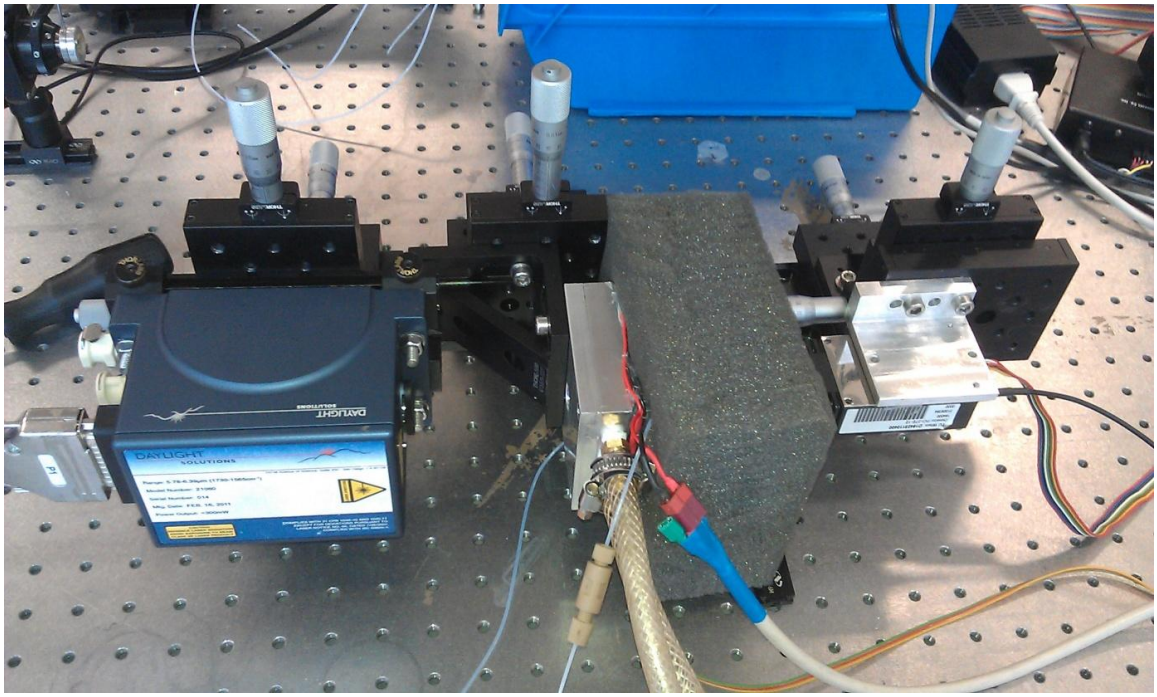

Figure 15b - Setup for protein measurements

To suppress the noise in the infrared spectrum, generated by water vapor bands (see chapter 1.3), the whole setup was positioned under a hood purged with dry air (see Figure 16).

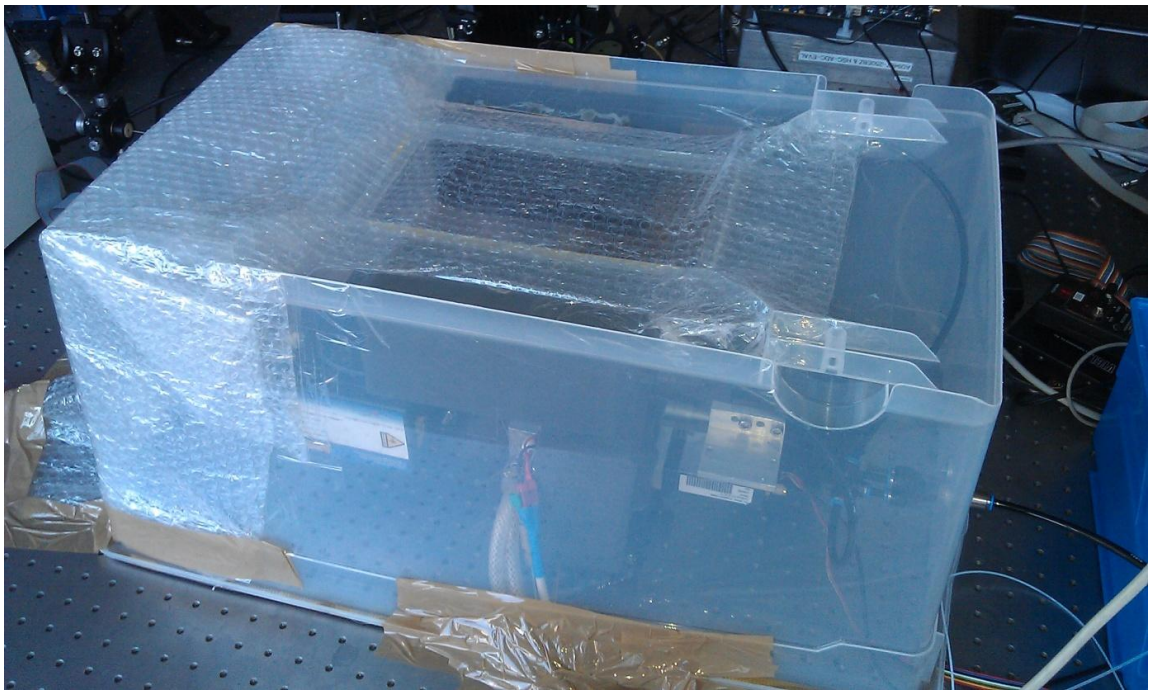

Figure 16 - Setup with a dry air purged hood

2.1.1 Data acquisition equipment

The data acquisition system consisted of the following components:

- Vigo System MCT-detector MIPAC-xx, MIPDC-xx Series (thermoelectric cooled)
- WT Boxcar mit Anzeige REV_C (built in house)
- National Instruments CompactRIO System
- Textronik TSD 210

A schematic of the data acquisition system is shown in Figure 15a.

a) Vigo MCT-detector

The Vigo System MCT-Detector of the MIPAC-xx, MIPDC-xx Series is a thermoelectric cooled detector, which can be operated at room temperature. Because of this reason it is perfect equipment for the measurements in this thesis. The basic structure is shown in Figure 28.

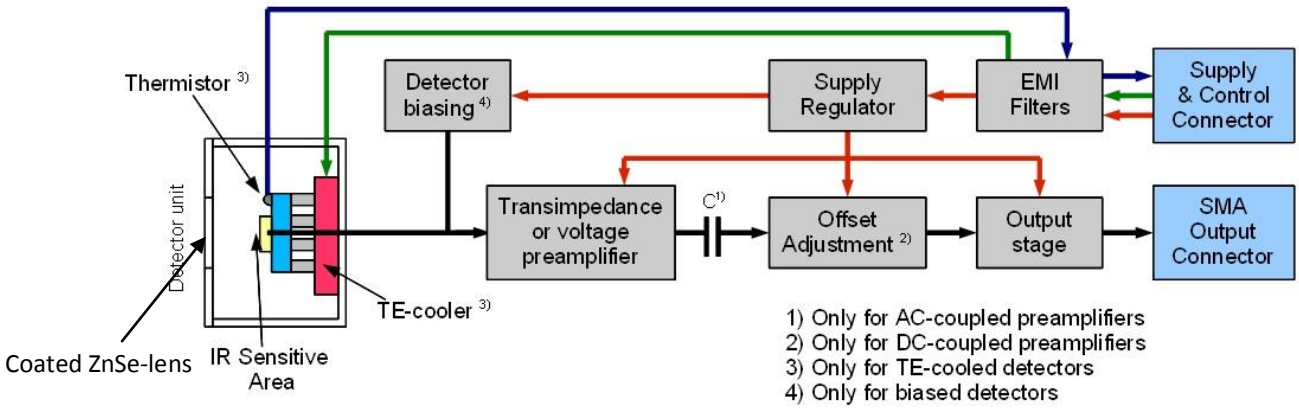

Figure 28 – basic structure of the Vigo MCT-detector of the MIPAC-xx, MIPDC-xx Series [31]

b) Boxcar integrator

The boxcar integrator was used for extraction and noise suppression of instantaneous voltage values from alternating voltages. The basic structure of the device is shown in Figure 30.

Figure 29 – WT Boxcar mit Anzeige REV_C [25]

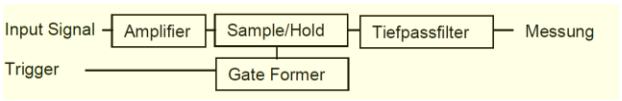

Figure 30 - Basic structure of the WT Boxcar mit Anzeige REV_C [25]

The boxcar integrator was used for the detection of noisy pulsed signals emitting by the EC-QCL. The laser was exclusively operated in pulsed mode, hence the boxcar system was necessary to generate a DC-signal, which could be measured by an analog-digital converter (ADC) (NI DAQ 9239, National Instruments) and processed by a PC.

c) NI (National Instruments) CompactRIO system and modules

For data acquisition a CompactRIO System of National Instruments was used, which was equipped with 4 I/O modules (see figure 31). For the Data acquisition of the DC signal from the boxcar a 24-bit ADC (NI DAQ 9239, NI) was used. The same module was used to read the temperature sensors of the flow cell. Furthermore, a 16-bit DAC (NI 9263, NI) was used to adjust the temperature of the flow cell. For triggering the laser scans (laser scan = tuning the Laser over all adjusted wavenumbers) a digital I/O module from NI was used (NI 9401, NI).

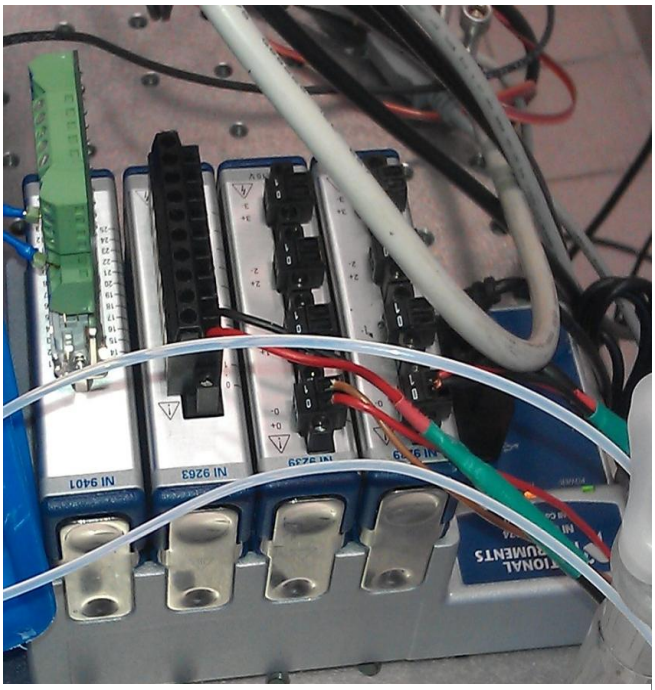

Figure 31 – NI CompactRIO System with 4 I/O modules

2.1.2 External Cavity Quantum Cascade Laser

Figure 17 – EC-QCL from Daylight Solutions (1565.06-1729.30cm^{-1})

For the measurements an external cavity quantum cascade laser (further EC-QCL) with suitable driver electronics for driving and cooling the laser element from Daylight Solutions was used (see Figure 17, described in [35]). The spectral tuning range located between 1565.06 and 1729.30cm^{-1}. In order to avoid unwanted heating of the sample by the laser beam, the laser was operated in pulsed mode with a low duty cycle (5% max, 500ns pulse duration), because heating of the proteins may cause changes in their molecular properties. The wide spectral tuning range of the laser allows the measurement of the amid I band of proteins. The maximum emission power density of the laser was 800mW in pulsed mode at the highest driving current. In Figure 18 the CW (continuous wave) emission power vs. laser current is shown. The emission power of the laser vs. the adjusted wavenumbers is shown in Figure 19 (pulsed mode operation), measured with a power meter (Solo 2 Power Meter, Gentec Electro Optic Inc.). In pulsed mode, which was used during all measurements the average power amounts to 30mW. Figure 18 shows a lower laser output power because the shown measurement was captured in pulsed mode of the EC-QCL and in Figure 19 in CW mode was measured. Because of averaging of the pulsed signal by the power meter Figure 18 shows a lower power curve.

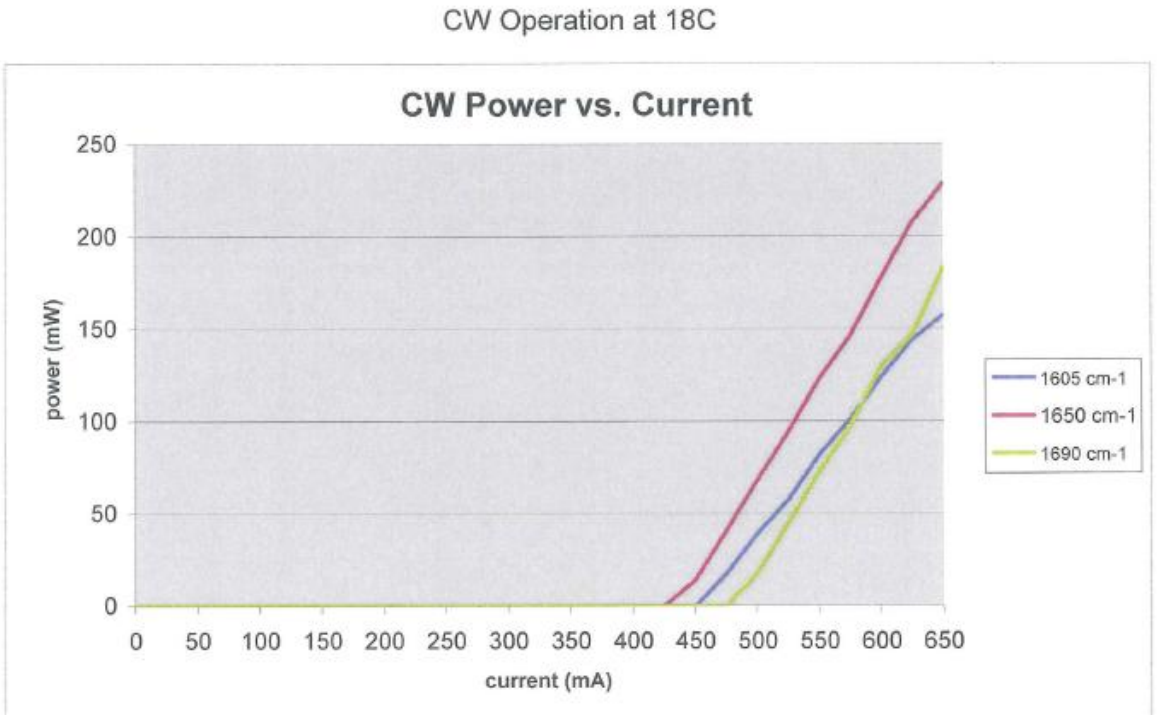

Figure 18 - Emission power vs laser current from the EC-QCL

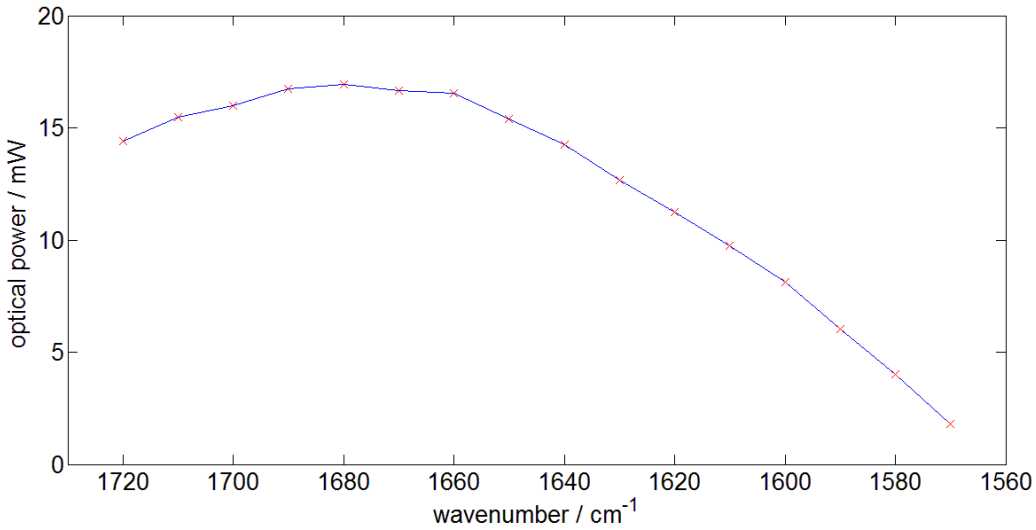

Figure 19 - Optical power measured by a power meter (measured at 1000mA, 250ns, 100kHz)

2.1.3 Peltierelement-controller (TEC-Controller)

As a part of this thesis a TEC-controller for temperature stabilization of the flow cell was designed and assembled. The controller had to guarantee a relative temperature accuracy of +/- 0.005K (for the explanation of this limit see 3.1.2) and should also be able to heat and cool (bipolar). Figure 20 shows an image of the fully assembled device. Two TEC-elements with 42 W electrical power was used to provide sufficient thermal energy. An addition of the experimental work a user manual was written for correct use of the device. The schematic diagram can be found in the Appendix A.

To adjust the temperature via a PC, a control software (Labview, National Instruments) was written, so it was possible to use the established ATLAS system (described in [30]) for remote operation. This software was also used for recording temperature logs during the measurements.

Figure 10 – Bipolar TEC-controller

2.1.4 Measurement cells

All flow cells were designed for the use with the same Ca_2F windows (38x19x3 mm, LxBxH). The cells consisted of a rear window, a spacer, which determined the optical path length, and a front window, having two holes for sample inlet and outlet.

Measurement cell No. 1: Flow cell with circulator

At first a flow cell with a copper pipe for temperature control was used. For the temperature stabilization of the cooling liquid in the copper pipe a circulator (Circulator f12-MV, Julabo) was used.

Figure 21 – Flow cell with temperature stabilized water circuit

In this cell a path length of 47µm was established. The exact optical path length was determined with a FTIR-spectrometer (Vertex 80V, Bruker Optics). A PID-control software was programmed in Labview for temperature stabilization. With this setup it was not possible to control the temperature of the flowing sample.

Measurement cell No. 2: Flow cell in T-design

Since the measurement cell No. 1 did not work satisfactorily, because relative temperature accuracy was too low, another two flow cells were designed. One of them is the T-design cell, which is shown in Figure 23.

With this cell, it was possible to stabilize the sample's temperature before it enters the flow cell. This happened in the inlet tube, which was placed in a meander around the windows (see Figure 22) (meander length = 1325mm). The cell was temperature-stabilized with 2 TEC-elements, each with 42 W nominal power. The advantage of this cell was that for cooling the TEC-elements a conventional heat sink, which was supplied with fresh air by a fan, could be used (see Figure 24). The disadvantage of the T-design was the great distance between sample liquid and the TEC-elements, which made it difficult to tightly control the temperature. For this reason, two temperature sensors were used, a control sensor for the main feedback loop, which was set nearby the TEC-elements and a flow cell sensor, which was located near the sample liquid. Furthermore, the whole cell was insulated with foam material to suppress external temperature influences as far as possible (see Figure 24). To bring the cell accurately in position during the measurements, it was mounted on an XYZ-stage. The construction plans of the flow cell can be found in Appendix B.

Figure 22 – Meander with the temperature-stabilized tubing

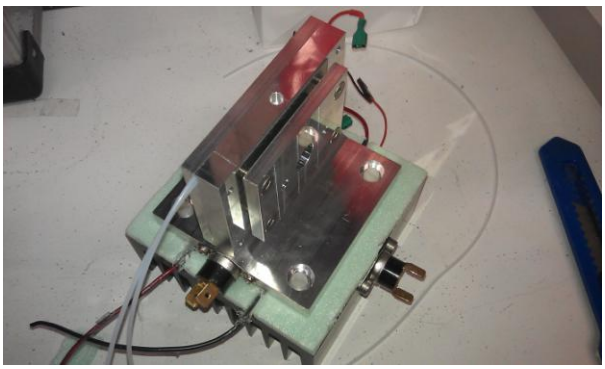

Figure 23 – Assembled T-design flow cell

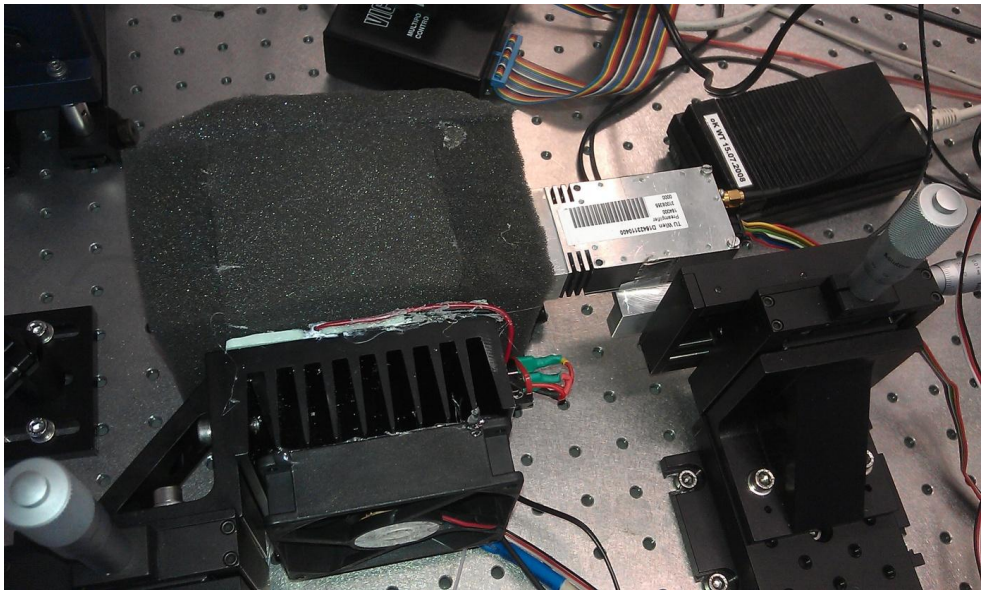

Figure 24 – Thermally isolated flow cell assembled and mounted in the measurement setup

Measurement cell No. 3: Flow cell in plate-design

This flow cell was designed according to Figure 27. In this flow cell also a meander (meander length = 1565mm) was provided for sample pre-cooling (see Figure 25). The difference and at the same time the biggest advantage of this flow cell was, that the TEC-elements were positioned directly behind the sample liquid so the temperature for the main feedback loop was measured nearby the sample liquid. For this reason, only one temperature sensor was needed. This flow cell eliminated the inertia of the temperature control from the T-design almost entirely, thus the desired temperature was now reached faster. The big disadvantage of this flow cell was the necessary liquid cooling for the TEC elements (see Figure 26). Because the laser beam was guided through the heat sink, using a fan was not possible and therefore also no conventional passive heat sink could be used. For this reason, cooling water was required for operation. Figure 26b shows the assembled flow cell, as employed in the measurements. Again, the flow cell was isolated from external influences (see Figure 15b, it shows the plate design in the measurement setup). The construction plans of the flow cell can be found in Appendix C.

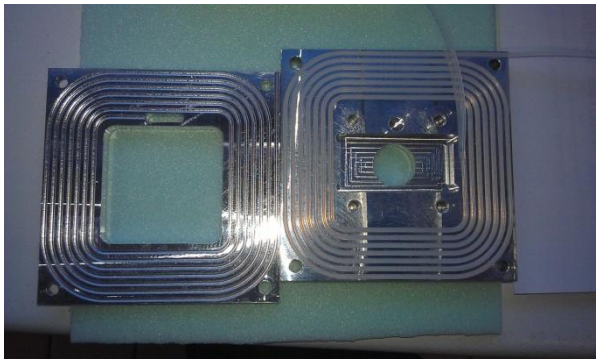

Figure 25 – Meander with the temperature stabilized tubing

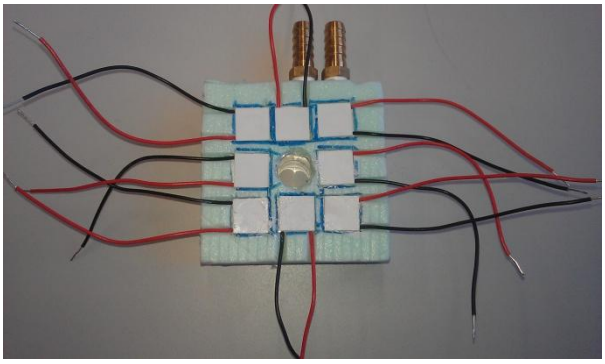

Figure 26 – Liquid cooling system with TEC-elements

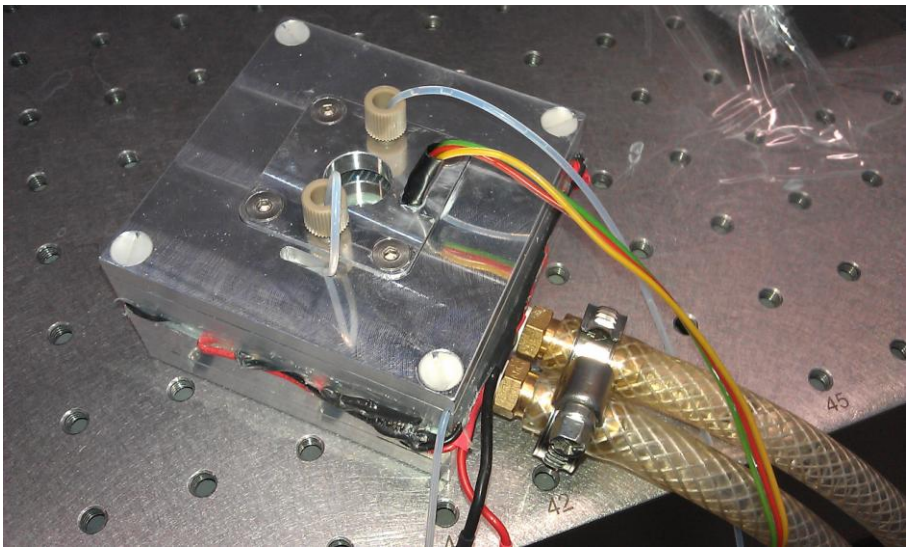

Figure 27 – Assembled plate design flow cell with liquid cooling system

2.1.6 Additional equipment

- Syringe Pump (XP 3000 Modular Digital Pump, Cavro Scientific Instruments Inc.)
- 6 port Selection Valve (6 port Selection Valve, VICI Valco Instruments Inc.)
- Ph-Meter (WTW 330i, WTW Wissenschaftlich-Technische Werkstätten GmbH)
- Mili-Q Direct Water System (Merck Millipore)
- FTIR spectrometer (Tensor 27, Bruker Optics)

2.2 Methods

2.2.1 Determination of the exact path length using a FTIR spectrometer

If light is transmitted through a measurement cell with thin plane-parallel layers interferences occur, which are noticeable in the spectrum by a superimposed sine. If the empty flow cell is positioned in the spectrometer and a measurement is made, the result is a spectrum with a superposed sine. From the position of the maxima, the thickness of the flow cell can be calculated by (6).

$$d = \frac{m}{2n} \frac{1}{\tilde{\nu}_1 - \tilde{\nu}_2} \quad (6)$$

$\tilde{\nu}_{1,2}$ ... wavenumbers

m ..... maxima between $\tilde{\nu}_{1,2}$

n ..... refraction index of air

d ..... path length

2.2.2 Acquisition of mid-IR-spectra using an EC-QCL

In order to take an absorption spectrum the laser was tuned over all wavenumbers at each single beam measurement (= one scan). For each background and sample measurement 16 scans were recorded, averaged and subsequently the corresponding absorption spectra were calculated using the Beer-Lambert law (equation 3). Each sample was measured five times and afterwards the resulting spectra were averaged. Subsequently, a Fourier filter for smoothing the noisy spectra was applied (described in [32]). The settings of the EC-QCL and the flow in the flow cell are given at the beginning of each chapter.

2.2.3 Preparation of the samples for the different measurement series

All samples, which were used for the measurements, were dissolved in deionized water from the Milli-Q Water System Direct.

a) Non Protein

The initial measurements were performed with N-methylacetmide as a model substance for the amide I band.
NMA has a melting point slightly above room temperature, thus the container with the chemical had to be slightly warmed. For the measurements the samples were weighed using a balance and filled into crimp top vials with 100ml of deionized water. The respective concentrations of the sample series are given in the corresponding subsection in chapter 3.

b) Proteins

The following proteins were measured in the course of this work:

- Albumin
- ß-lacto-globulin
- Casein
- Soya Protein

In this work Albumin and ß-lacto-globulin were additionally measured, since these proteins have in comparison to casein various secondary structures. Thus it can be shown that one can distinguish the different structure by measuring the amid I absorption band and thus the different proteins can be also distinguished using EC-QCL measurements. For each protein, a highly concentrated stock solution was prepared, which were appropriately diluted for the measurement series to the different concentrations. For sample preparation and also to measure the sample volume Eppendorf pipettes were used. The solution was prepared in 100ml crimp top vials again.

At this time the solution was prepared with a buffer solution as solvent because proteins change their properties with the pH-value (mentioned in chapter 1). For this purpose a phosphate buffer was prepared, having the following formulation:

- 1l deionized water (Milli-Q Direct water system)
- 1,2g Monosodium phosphate
- 0,885g Disodium hydrogen phosphate

Set-pH-value=7

Actual-pH-value=6.90 (measured using the pH-meter WTW 330i)

The respective concentrations of the sample series are given in the corresponding subsection in Chapter 3.

c) Casein

A stock solution of 8% casein in phosphate buffer was prepared from sodium caseinate powder, including the addition of 2-bromo-2 ni- tropropane-1,3-diol (20 mg/100 mL) and Natamicin (0.75 mg/100 mL) as a preservative. This solution was stored in a fridge and immediately before measurements were executed, the samples were established, preventing the sample from changes of proteins properties. The respective concentrations of the sample series are given in the corresponding subsection in chapter 3.

2.2.4 Milk samples

As a part of this thesis, the measurements with the following types of milk were performed:

- Unskimmed milk (3.5% fat)
- Long-life milk (1.5% fat)
- With casein spiked Long-life milk

The spiked milk solution should show the behaviour of casein in the natural environment of milk. The respective concentrations of the sample series are given in the corresponding subsection in chapter 3.

3. Results and Discussion

In this chapter the temperature dependence of the ν_2-band of water is shown and furthermore the measured spectra of the samples described in chapter 2.2 are discussed. The settings for each measurement are summarized at the beginning of each chapter.

3.1 Temperature dependence of the water absorption band at 1645 cm^{-1}

3.1.1 Temperature controlled flow cell (measurement cell No. 1)

To be sure that the temperature stabilization of the flow cell was sufficient, the intensity of the laser is measured with a MCT detector, while various cell temperatures were set. In this measurement the temperature stability of the flow cell is indirectly measured by the changes in the absorption spectrum of water. For that purpose, four wavenumbers were selected and at each wavenumber five different temperatures were set. The intensity at the 4 desired wavenumbers was measured (1710, 1640, 1645 and 1600 cm^{-1}, see figure 32) to obtain data on both sides of the O-H bending absorption band of and nearby its maximum at 1645 cm^{-1}. The course of the molar absorption coefficient is shown in Figure 32. The graph was plotted based on the data of John Bertie (see also chapter 1.3).

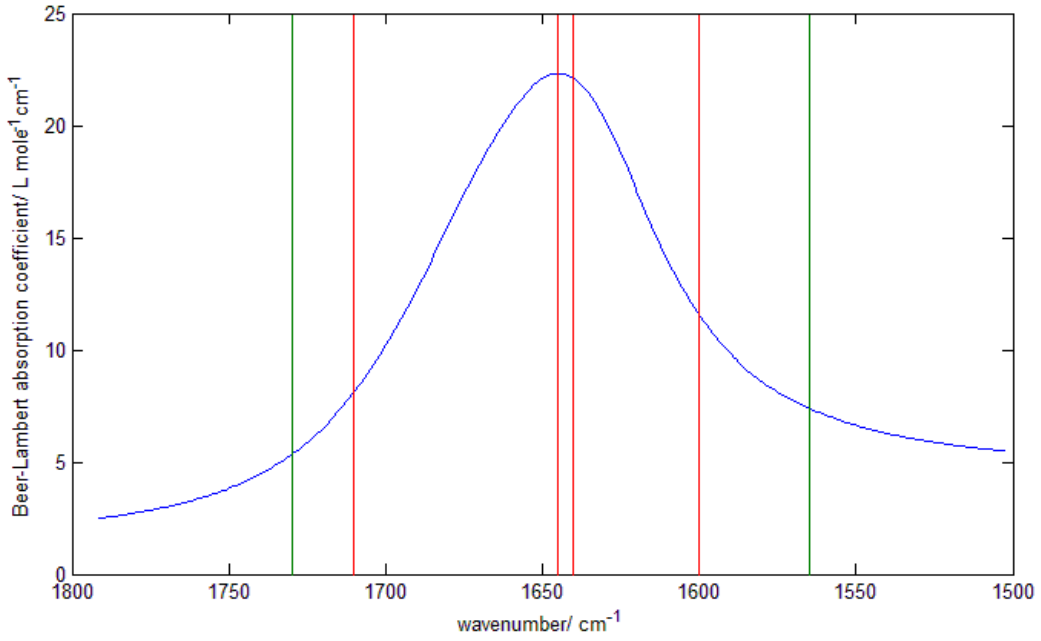

Figure 32 - Molar absorption coefficient based on the data of John Bertie - green lines: EC-QCL's spectral tuning range - red lines: wavenumbers that were measured for investigating the correlation of band intensity and temperature

The red vertical lines indicate the wavenumbers which were measured and the green lines indicate the spectral coverage of the employed EC-QCL.

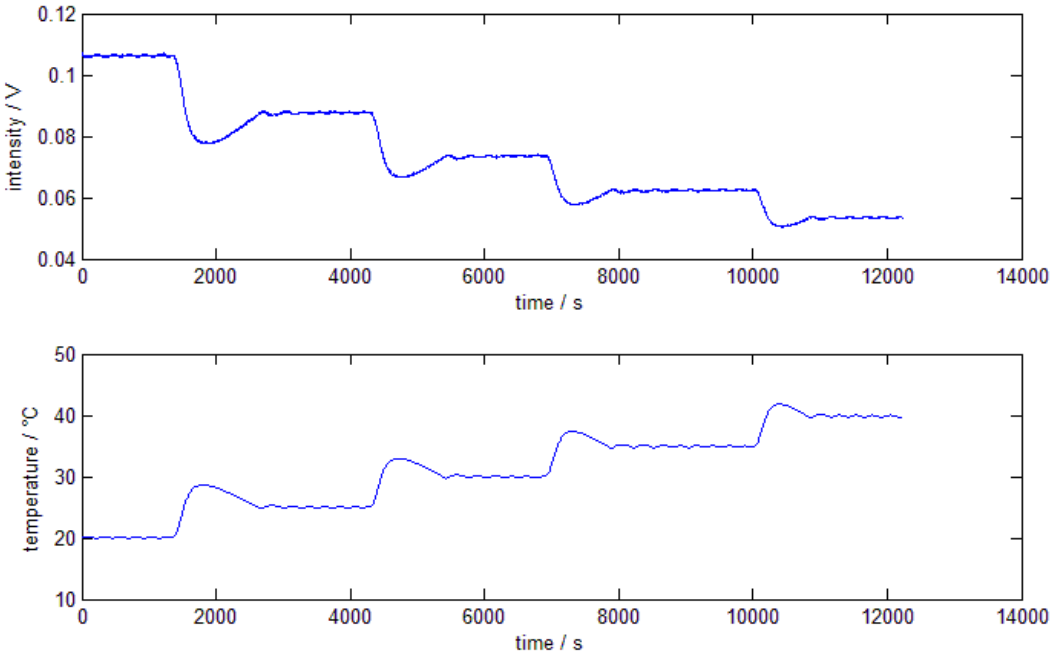

Figure 33 – Comparison of band intensity and temperature over time at 1640 cm^{-1}

Figure 33 clearly shows that the absorption of the water band correlates with the temperature (raising the temperature -> more intensity was absorbed). This effect can be explained on the one hand, by the fact that the spacer expands with increasing temperature, thereby causing the path length of the flow cell to increase. The major reason, however, is the dependence of the band position and intensity on the strength of hydrogen bonds which varying if the temperature changes.

Considering the results presented in Figure 32, Figure 34 and Figure 35, it can be seen clearly, that the v_2-band shifts towards lower frequencies with increasing temperature.

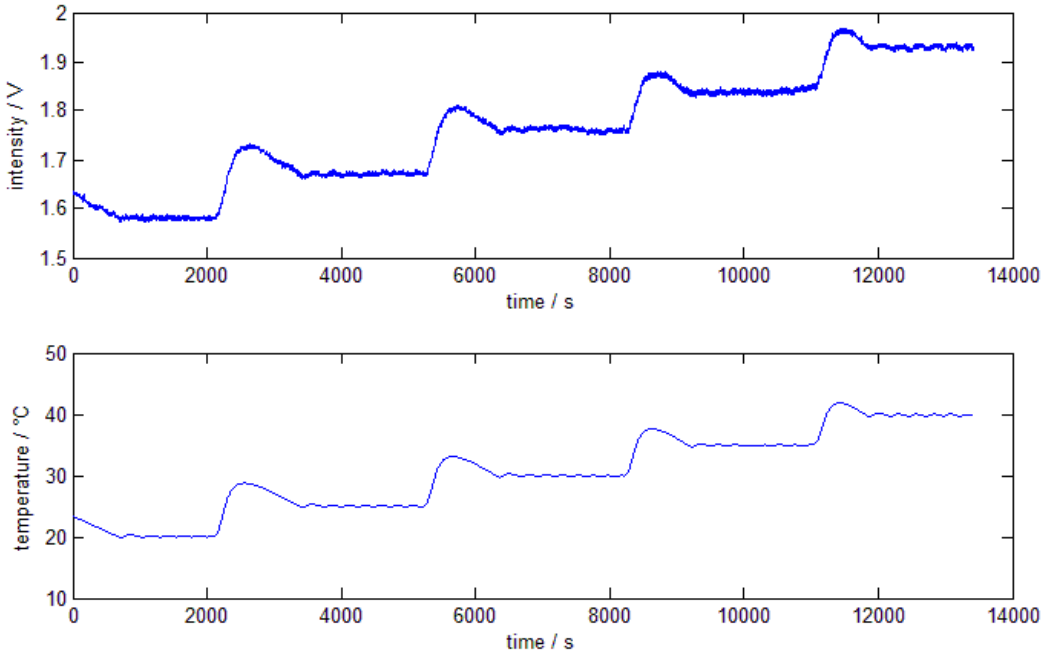

Figure 34 – Comparison of band intensity and temperature over time at 1710cm^{-1}

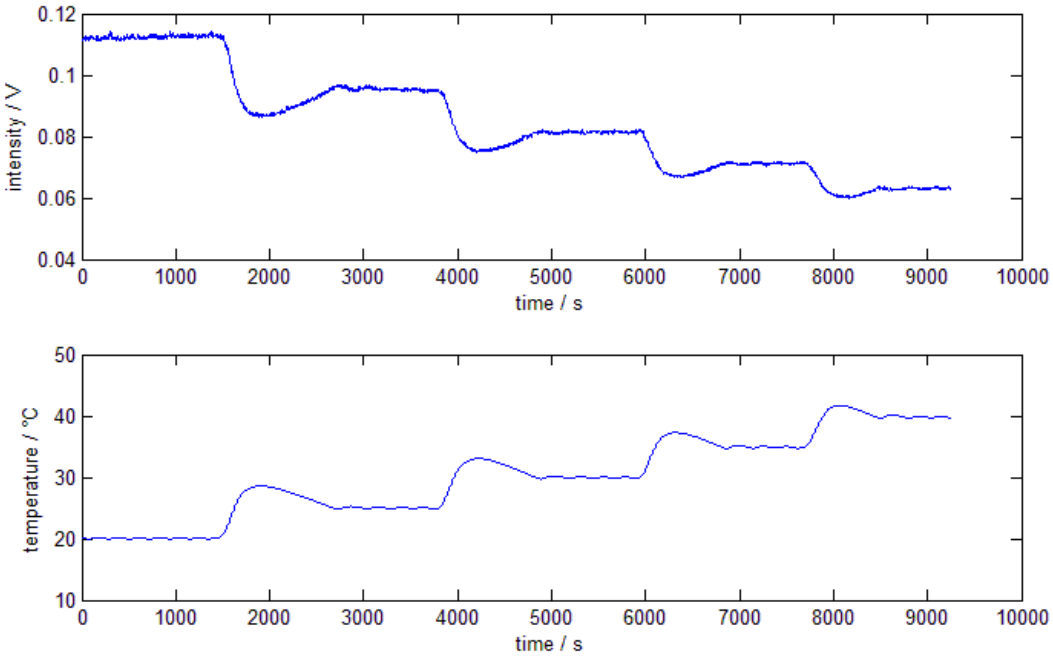

Figure 35 – Comparison of band intensity and temperature over time at 1645cm^{-1}

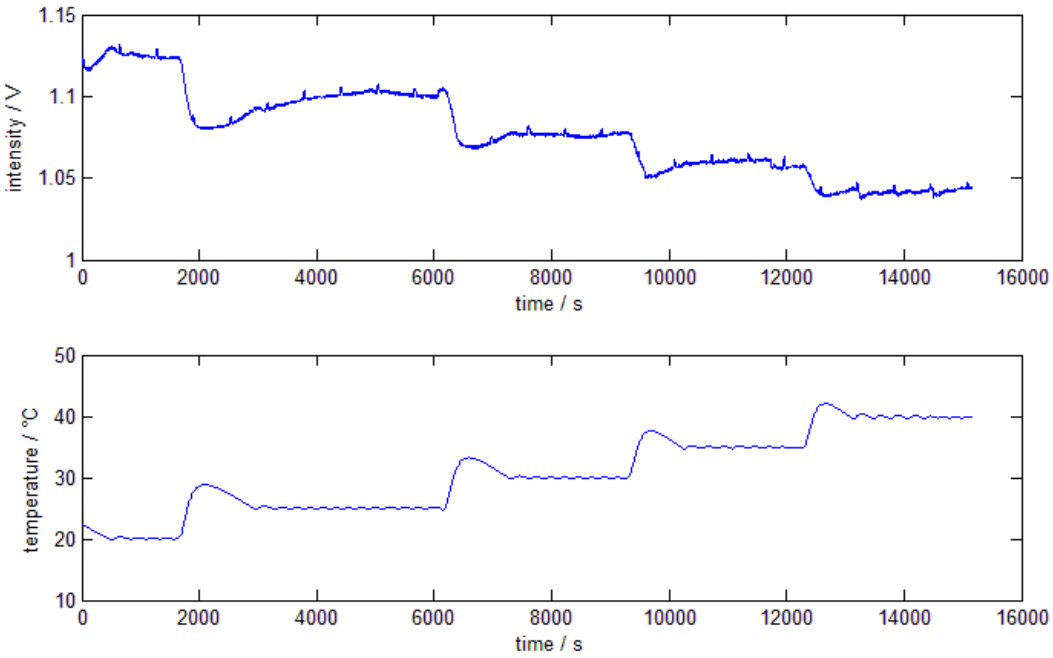

Figure 36 – Comparison of band intensity and temperature over time at 1600cm^{-1}

In Figures 34-36 it can be seen that short steps along the graph were produced while switching off the pump while a new sample was aspirated and thereby the pressure changes

in the flow cell. This steps show that also the pressure has a great influence on the absorption band and the path length of the flow cell.

Figure 34 shows that the low temperature fluctuations, which can be seen without zooming in, cause absorption band intensity fluctuations. Hence these measurements show that the temperature stabilization of the flow cell did not work sufficiently accurate (relative accuracy is important here), which is why improved flow cell designs were developed (see chapter 2). These cells were used for all further measurements.

100%-lines:

In the next measurement the laser was continuously scanned while changing the temperature stepwise. This experiment was performed without flow in the cell to exclude pressure fluctuations. The following three temperatures were adjusted on the temperature controller of the flow cell: 20, 30, 40°C. The resulting 100%-lines are shown in Figure 37 and the corresponding temperature log is shown in figure 38. Between the temperature jumps the process of achieving an equilibrium can be observed. 10 spectra were used to calculate the average at 20°C which was used as background, whereas the following spectra were used as sample single beam spectra. These spectra were calculated using Beer-Lambert Law and were plotted in Figure 37 (the spectra are plotted from blue to red -> from cold to warm).

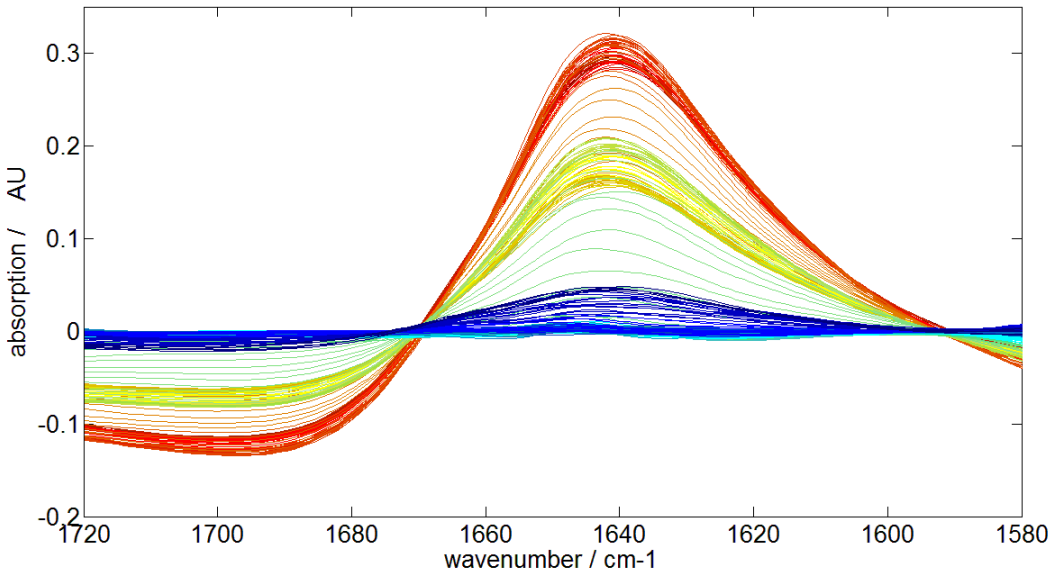

Figure 37 – 100%-lines of water while varying the temperature of the flow cell corresponding to the temperature log in Figure 38 (the spectra are plotted from blue to red)

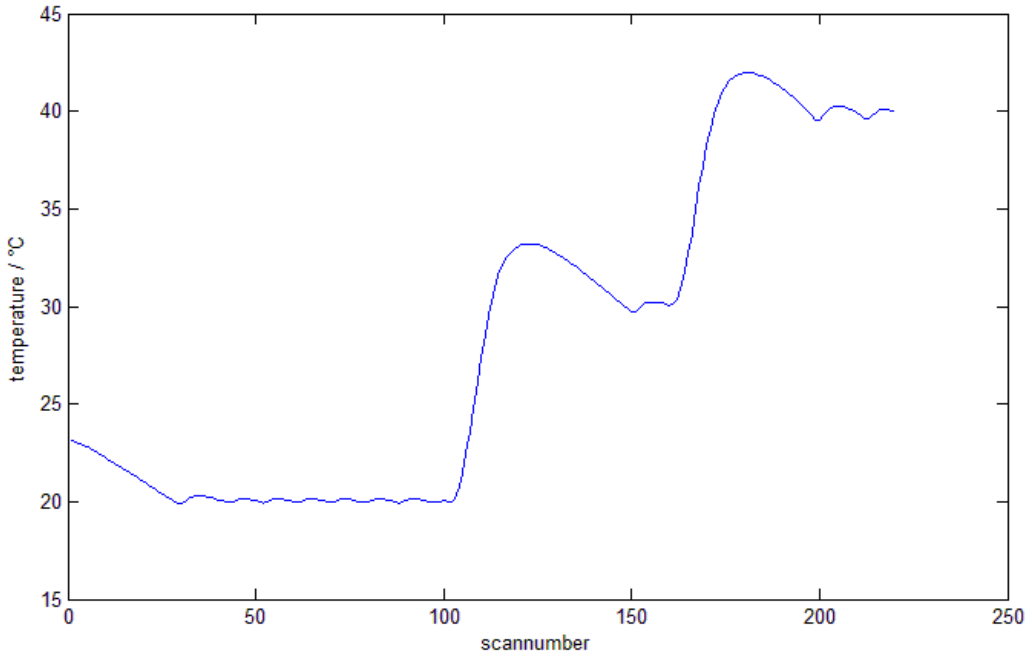

Figure 38 - Temperature log during the measurements, the temperature was sampled at the beginning of each scan

The temperature was sampled at the beginning of each scan. In Figure 37 it can be seen that a temperature change of 10°C caused an error of about 200mAU at 1645cm^{-1}. So a

temperature change of 0.1°C of the matrix would result in an error of about 2mAU, hence the temperature control of the flow cell should work better than 0.1°C.

3.1.2 TEC-controlled flow cell

Since the temperature control did not work well enough when using the conventional temperature controlled flow cell (measurement No. 1), two TEC-elements controlled flow cells were constructed and characterized (described in chapter 2.1.4).

a) T-design cell (measurement cell No. 2):

At first, the thermal stability of the T-design flow cell was measured. The measurement setup, which was used, is shown in Figure 39.

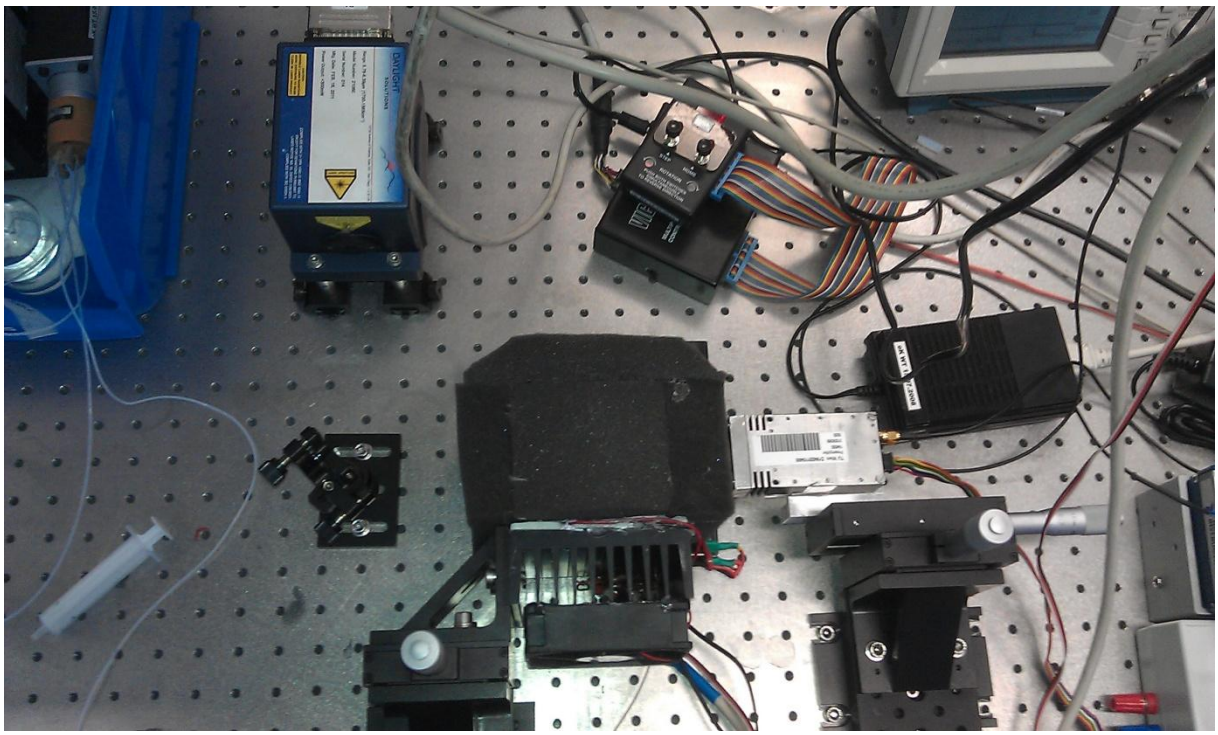

Figure 39 - Measurement setup with the T-design flow cell

The measurements were performed at 20, 25, 30, 35 and 40°C and each temperature was kept constant over a period of about 1200s per temperature; this resulted in a total recording time of 6000s. The results are summarized in Figure 40

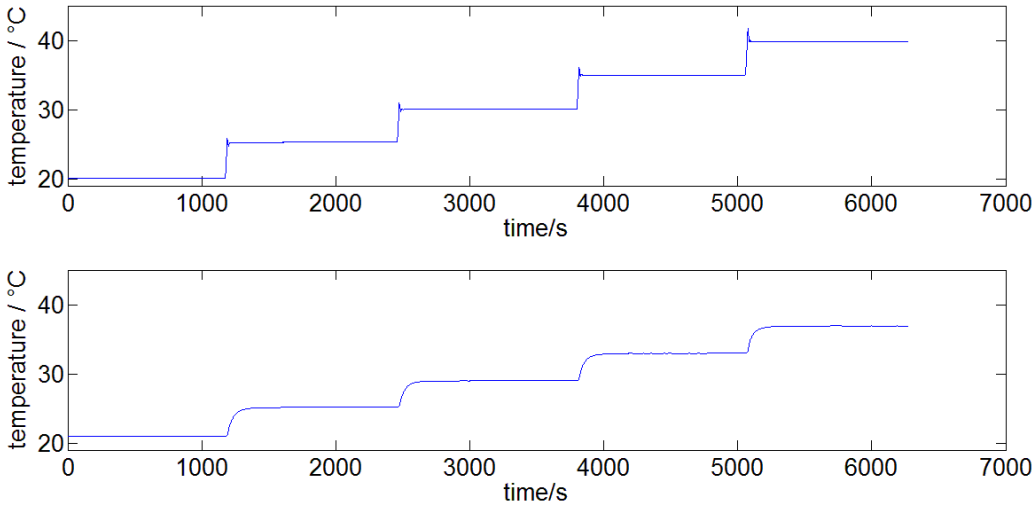

Figure 20 - Temperature logs of the control sensor (top) and the flow cell sensor (bottom) (see section 2.1.4)

Figure 41 shows that the temperature measured at the flow cell sensor ranges within an interval of about 30mK for about 6 min. At the control sensor, the stability was determined to be +/- 2mK. In order to achieve even more accurate temperature control, the sensor (or TEC-elements) had to be mounted closer to the sample volume to avoid a temperature gradient between loopback sensor and the sample liquid. Also the inertia of the temperature controller decreased with this method -> "Plate-Design" (measurement cell No.3). In order to characterize the inertia of the system in more detail, the temperature was lowered from 40°C to 20°C, while monitoring the temperature over time (see figure 42). Figure 43 shows, that after the flow cell reaches the thermal equilibrium, the temperature could be kept stable to about 0.004K. This improvement of the temperature stability was also assisted by the improved insulation.

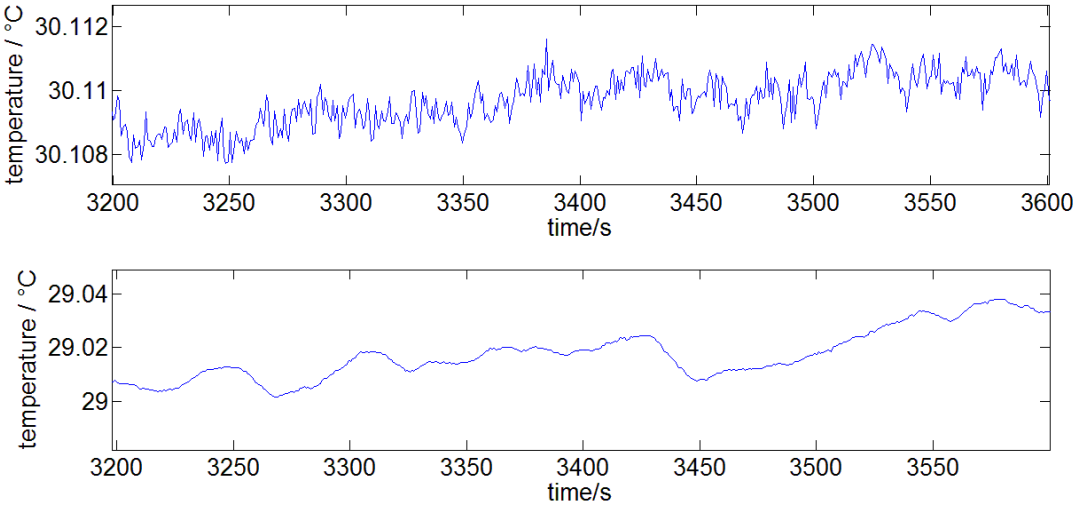

Figure 41 - Section of the temperature logs from figure 40 (control sensor at the top and the flow cell senor at the bottom)

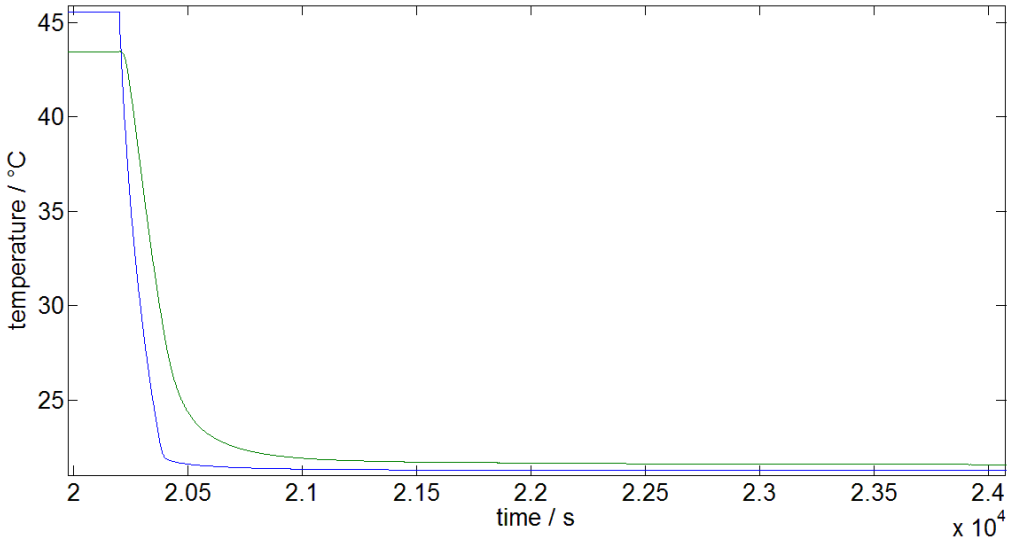

Figure 42 – Course of flow cell temperature when lowering the set value from 43°C to 22°C (blue=control senor, green=flow cell senor)

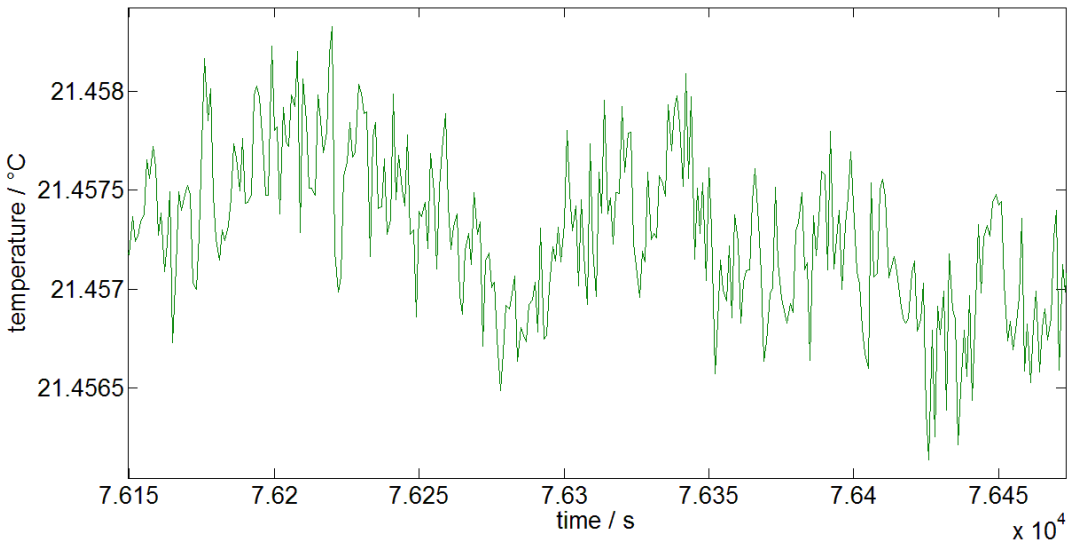

Figure 43 – Temperature at the flow cell sensor at the thermal equilibrium

100 %-lines:

Furthermore 100% lines were measured with water as sample and background to check the accuracy of the measuring cell in real conditions. The calculated spectra are summarized in Figure 44.

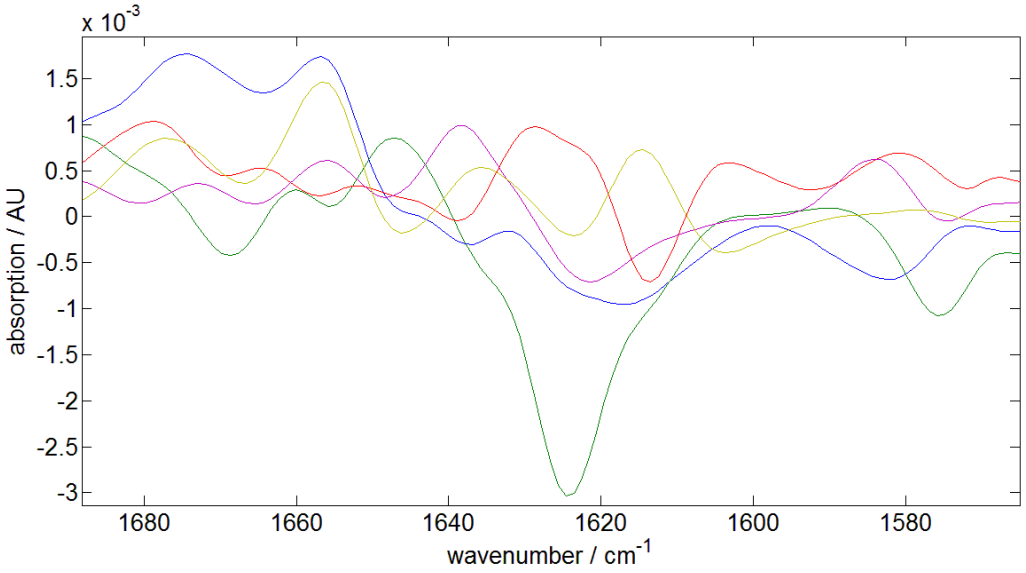

Figure 44 - 100%-Lines of deionized water using the "T-Design" flow cell

b) Plate-Design (measurement cell No. 3):

The temperature control of the measurement cell No. 2 approaches the adjusted value too not fast enough in case of a the temperature jump, so the setup was changed to the measurement cell No. 3 according to Figure 45. With this flow cell, it was assumed to be possible to obtain faster temperature changes.

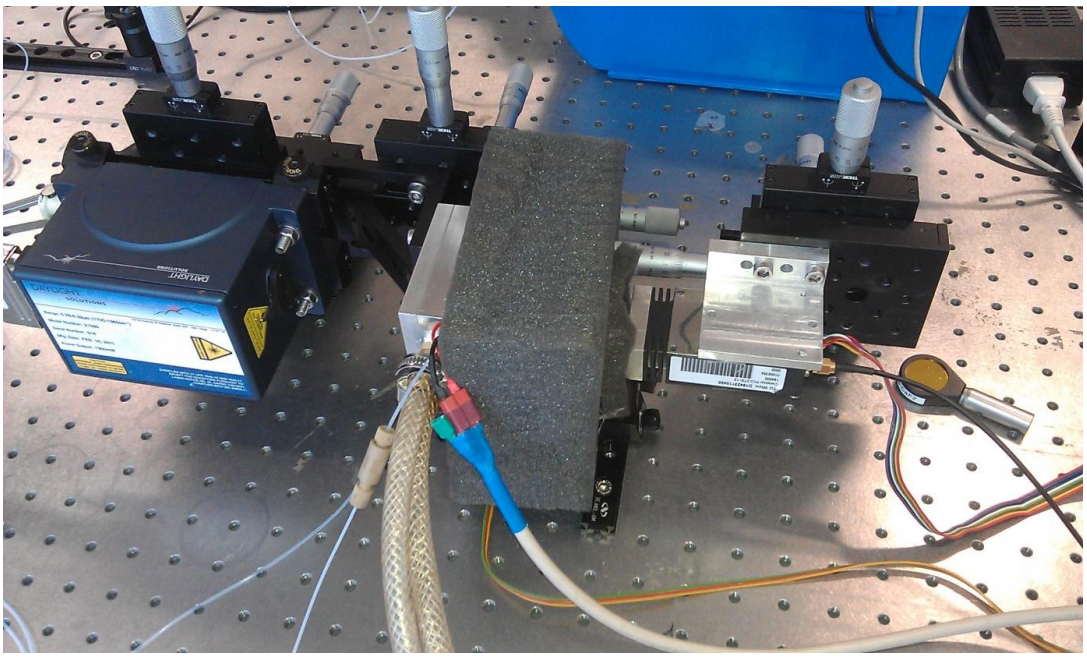

Figure 45 - New setup with plate design and liquid cooling

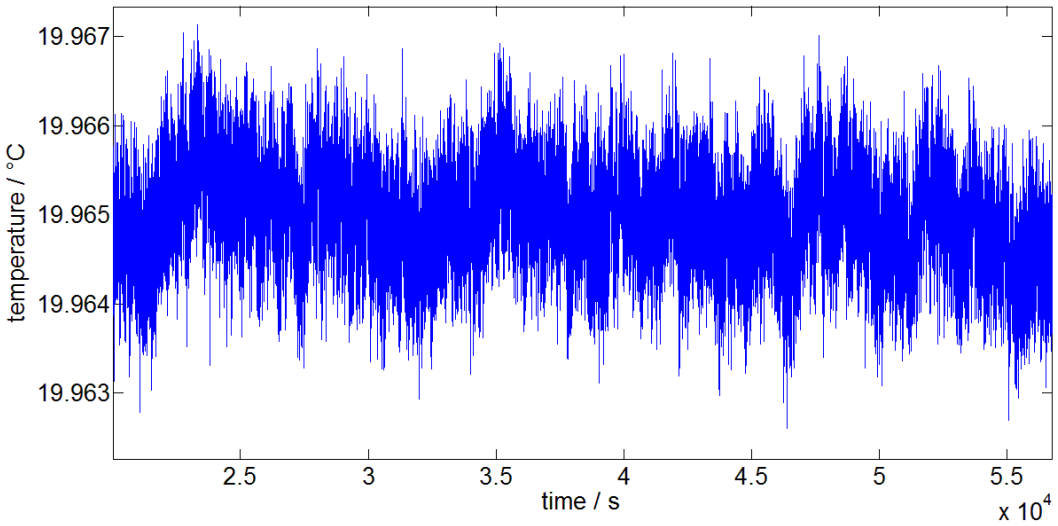

Figure 47 – Temperature log of the plate design flow cell at 20°C

Figure 47 show that the temperature stability and the response are sufficient for the further measurements. The 100%-lines, which are shown in figure 48 could confirm sufficient stability.

100 % - Lines:

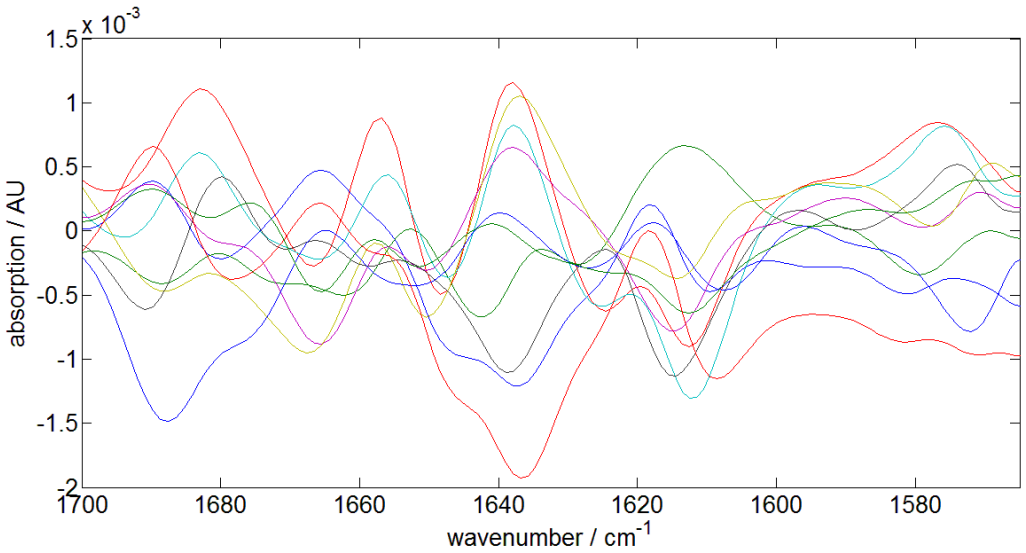

Figure 48 - 100%-lines with the new setup – sample: water

3.1.3 Determination of the temperature dependence on the water band

Settings for the following measurements:

- Path length: 44 µm
- Settings - EC-QCL:
  - Repetition rate: 100 kHz
  - Pulse width: 0,5 µs
  - Laser current: 1000 mA
  - Tuning range: 1565-1690 cm^{-1}
  - Scan rate: 6 µsteps/int
- Flow rate: stopped flow

- Data acquisition: 24 kS, 16 kS/s
- Flow cell: measurement cell No. 2

The next measurements deal with the change of the water band at 1645 cm^{-1} under the influence of temperature variations. For this purpose, the flow cell was rinsed with ethanol (absolute, denaturated with 0.5-1.5 vol% 2-butanone and aprox. 0.001% Bitrex (GC),> = 98% (GC)) until no water in the spectra could be seen. Then 5 100%-lines were recorded at 25°C. For the determination of the 100%-lines, 16 successive scans were averaged. The results are summarized in Figure 52.

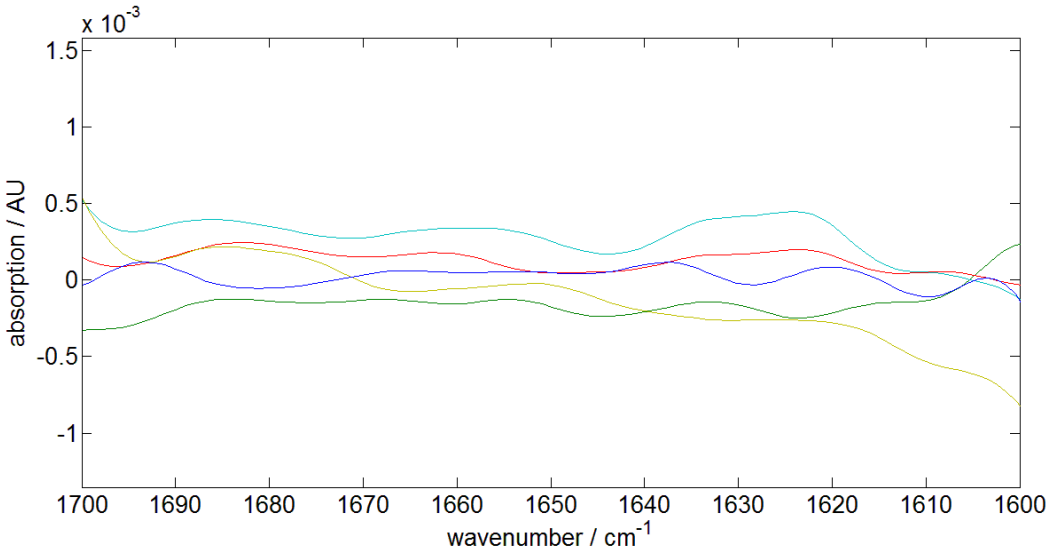

Figure 52 - 100%-lines of ethanol

Figure 52 shows that the measured 100%-lines reside within an interval of -0.001 and 0.001 AU, which is already quite good for using this setup.

Next, a background consisting in 200 g/l of water in ethanol and a sample consisting in 250 g/l of water in ethanol were measured at different temperatures, thereby for each measurement 16 scans were averaged. Each measurement carried out 5 times. The obtained absorption spectra are averaged and plotted in Figure 53.

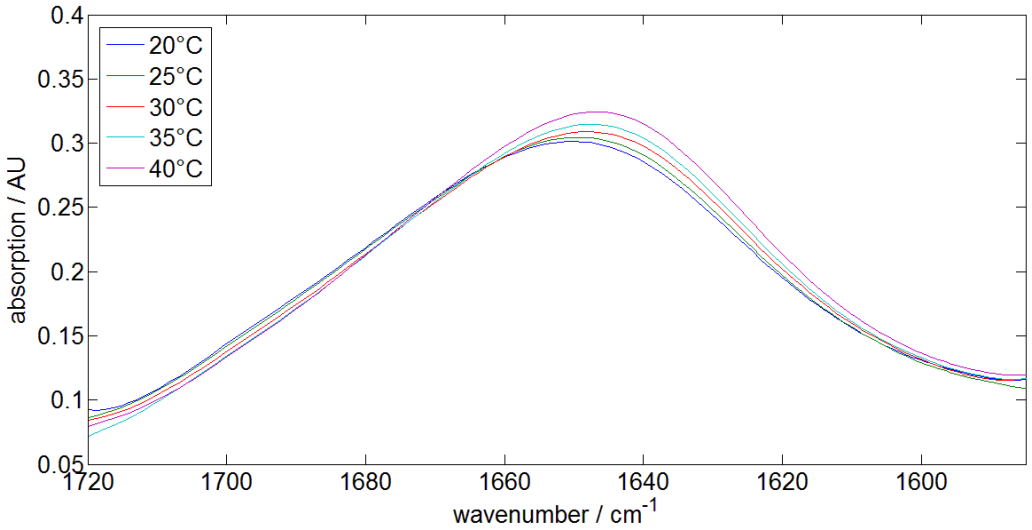

Figure 33 - Change of the absorption band of water (H_2O bending) due to temperature variation

As shown in Figure 53, the absorption band of the v_2-vibration of water shifts to lower frequencies (energies) due to the weakening of the hydrogen bonds. At the same time the intensity of the band increases, but the absorption away from the band decrease slightly (which was also expected). These results were expected like it was mentioned in chapter 2.

3.2 Validation of the detektor-Boxcar-drift

The drift of the data acquisition electronics (detector, boxcar, NI module 24bit, mentioned in chapter 2) was measured at laboratory conditions and plotted in Figure 49. Within a time period of 20 hours, data were recorded to receive the long-term drift and the noise of the electronics. In this measurement, the laser was switched off, and thereby the noise of the pure electronic was measured.

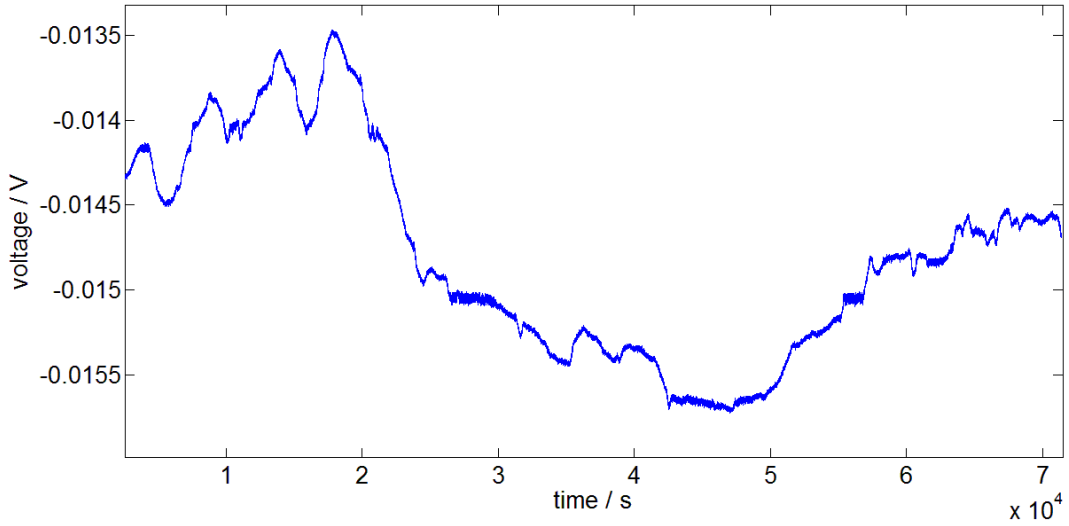

Figure 49 – Drift and noise of the data acquisition electronics over 20 hours

If one converts the peak to peak variation of figure 49 to AU using Beer-Lambert law, a value of about 17 mAU is calculated as drift that is introduced by the data acquisition electronics that is shown in Figure 50 over 20 hours. Therefore, it is very important to record always the offset of the electronics and also measure a background for each sample, to suppress the influence of the drift to the system. Corresponding to figure 51 the noise of the system over 10 minutes amounts to 1.9 mAU. The noise of all the measurements, which were taken, is lower because in these figures there were no averaged spectra. Due to the strong absorption of water in the range of 1645cm^{-1}, the signal at 1610-1690 cm^{-1} on the detector is small enough to get a poor signal in the absorption spectrum (important here is the signal-to-noise ratio of the raw signal). Therefore in Figure 51 can be clearly seen that the noise in the absorption spectrum around 1645 cm^{-1} increases by a multiple.

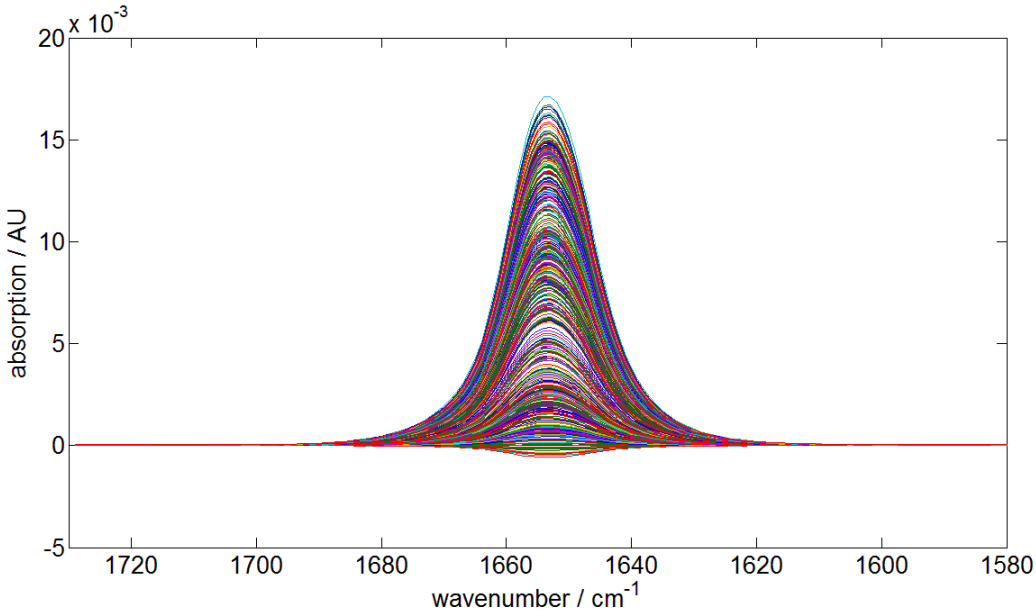

Figure 50 – Drift of the data acquisition electronics over 20 hours calculated with the Beer-Lambert law according to the data in Figure 49 (the Fourier filter was used to calculate these spectra, but there were averaged measurement)

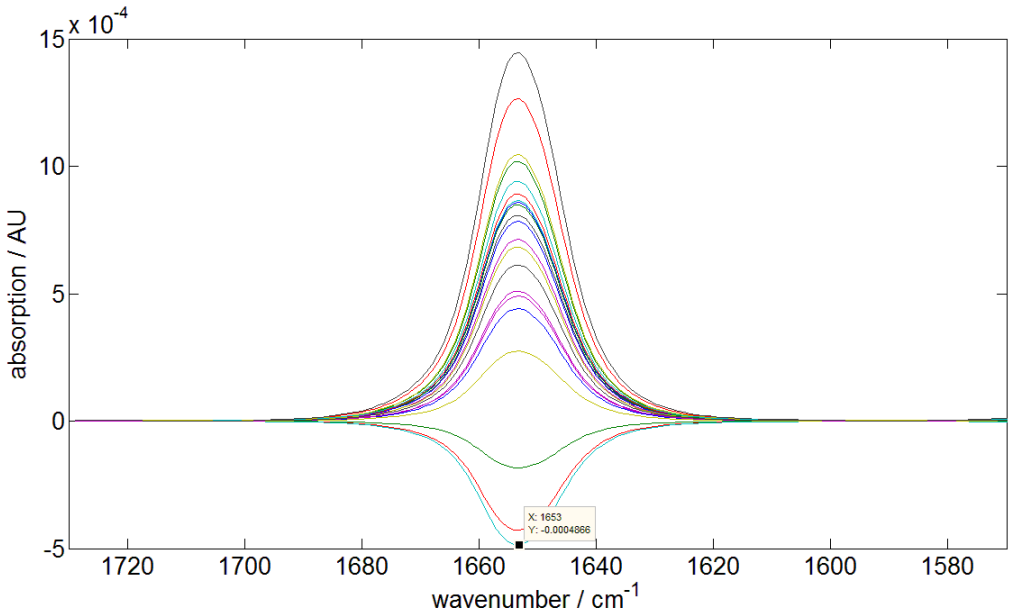

Figure 51 – Noise of the data acquisition electronics over 10 minutes calculated with the Beer-Lambert law according to the data in Figure 49 (the Fourier filter was used to calculate these spectra, but there were averaged measurement -> the noise decreases with the number averaged spectra)

3.2 Analysis of the amide I band of dissolved samples

Settings for the following measurements:

- Path length: 44 µm
- Settings - EC-QCL:
  - Repetition rate: 100 kHz
  - Pulse width: 0,5 µs
  - Laser current: 1000 mA
  - Tuning range: 1565-1690 cm^{-1}
  - Scan rate: 6 µsteps/int
- Flow rate: stopped flow
- Data acquisition: 24 kS, 16 kS/s
- Flow cell: measurement cell No. 3

3.2.1 N-Methyl Acetamide (NMA)

Initially measurements were performed using the model substance N-methylacetamide.

The first step was to take flow profiles of NMA to achieve information on the flow cell performance and the temperature dependence of the NMA absorption band. For that purpose, the flow cell was rinsed thoroughly with water. Subsequently, 2.5 ml of a solution consisting of 3.55g/l NMA in water were aspirated in the coil and afterwards water at a flow rate of 4µl/s was pumped through the coil while 140 scans were measured with the parameters given above. As background 20 averaged spectra of water were used. This results in continuous concentration distributions, which are plotted in Figure 54.

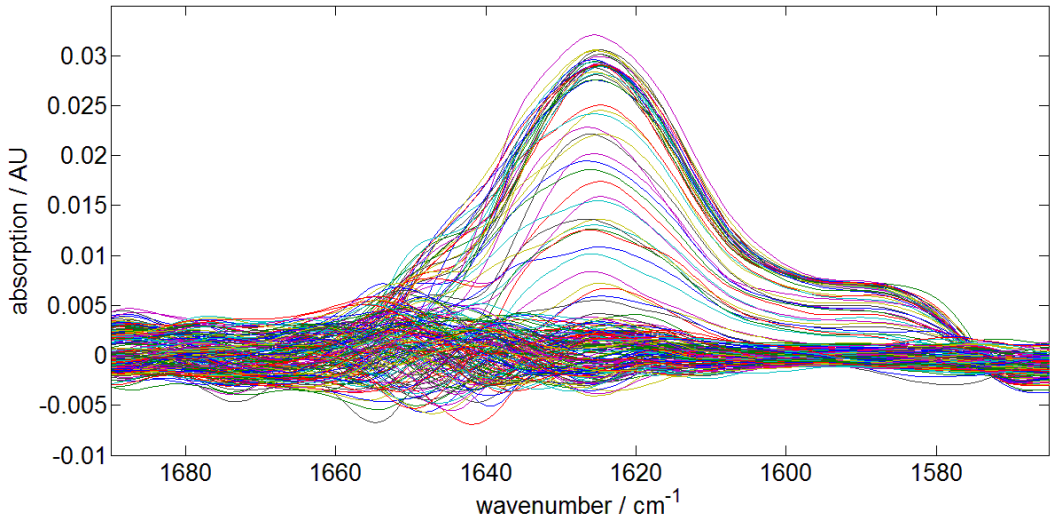

Figure 54 – Absorption spectra of NMA during the flow profile measurement

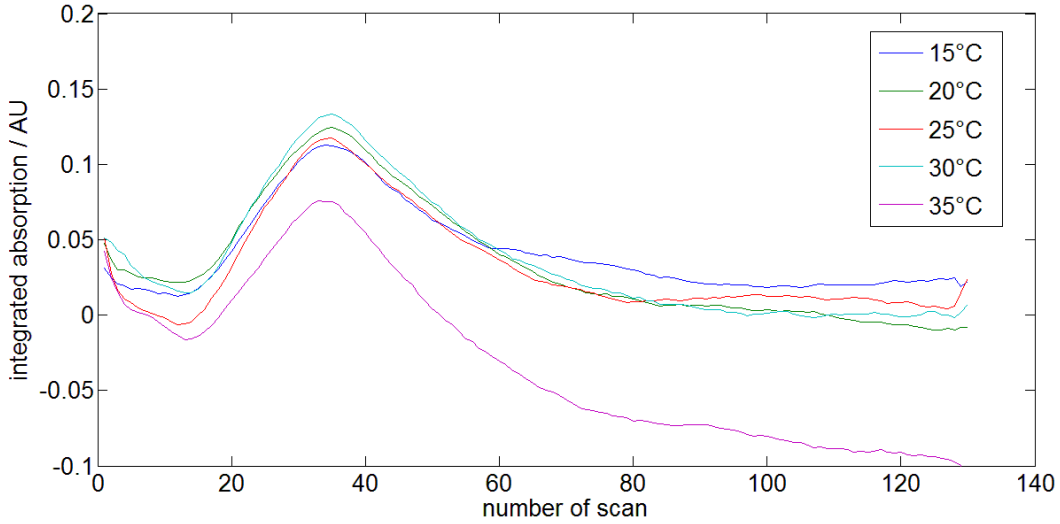

Figure 55 - Flow profiles of NMA at different temperatures (curves are smoothed); the unit of the abscissa is normalized to the scan number, thereby each scan takes about 10 seconds

Figure 55 shows the measured flow profiles. Due to slightly irregular mixing in the coil a slightly increased noise is recorded (see Figure 54 and 55).

In a next step, NMA in various concentrations was measured to establish a calibration curve. The results and the corresponding concentrations are summarized in Figure 56, whereby 16 scans for sample and background were averaged for the calculation of each spectrum. In figure 56 it can be seen that the graphs show a characteristic profile of the absorption spectra of NMA.

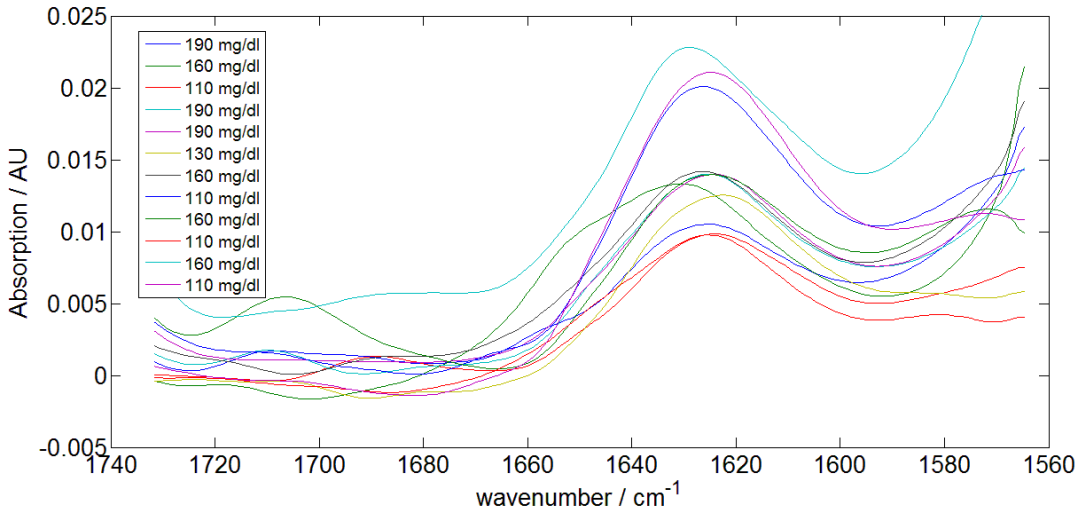

Figure 56 - Absorption spectra of NMA in various concentrations

Following the test measurements, a calibration measurement was carried out; again 16 averaged scans were used for background and sample to calculate the spectra. Figure 57 shows the measured spectra, which were used to calculate the calibration curve. To calculate the calibration curve the absorption bands were integrated from 1600 to 1650 cm^{-1} and the results are plotted in Figure 58. Furthermore, the data points were provided with a linear fit.

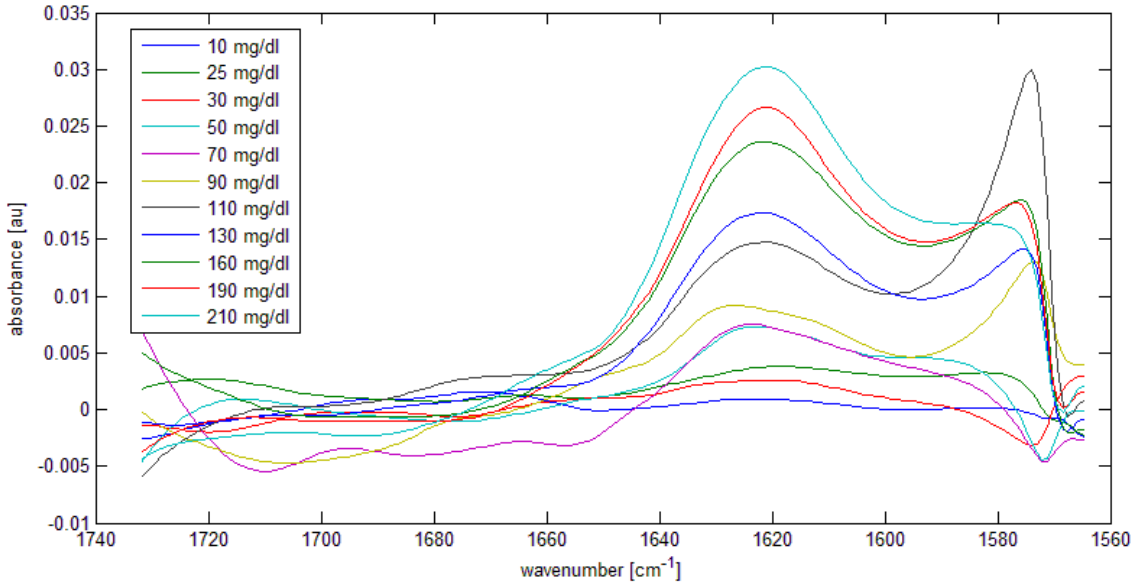

Figure 57 – Absorptions spectra of NMA for the calibration (see Figure 58)

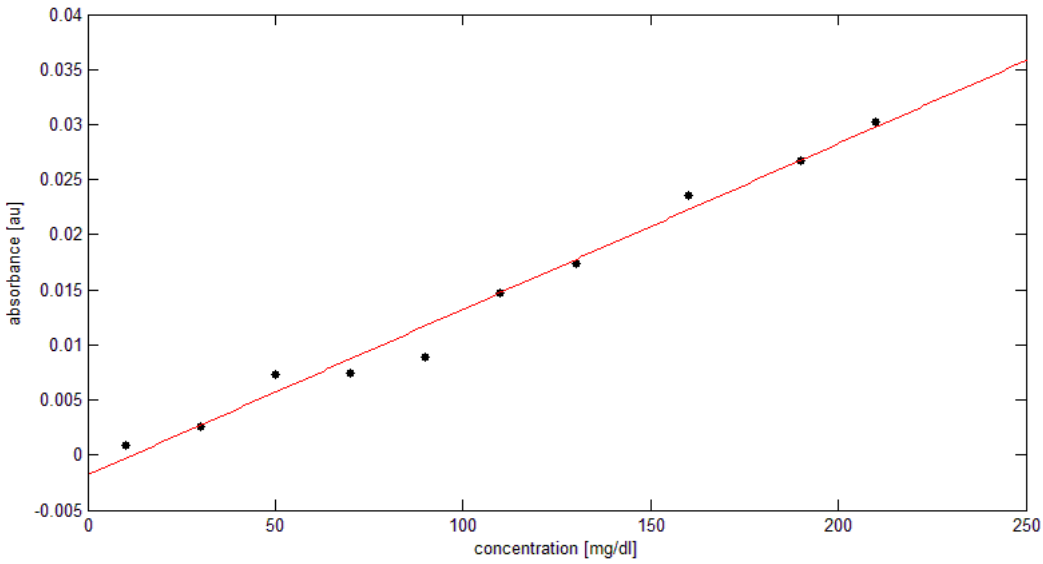

Figure 58 – calibration curve of NMA - R^2= 0.9841

The first test measurements of NMA suggest that more serious sources of interference in the measurement setup are present, since the noise is still too high. One of the greatest sources of error is certainly the laser system as the wave number setting does not work precisely enough. This fact is illustrated in Figure 59, where intentionally a spectrum with fringes was measured, that the shift of the successive scans can be seen clearly (no scans were

averaged). At the features in the absorption spectra (like water vapour bands) the noise due to the scan shift increases extremely (see Figure 59, the zoomed spectrum).

Another noise source is located in the data acquisition system, as it was already mentioned in chapter 2.

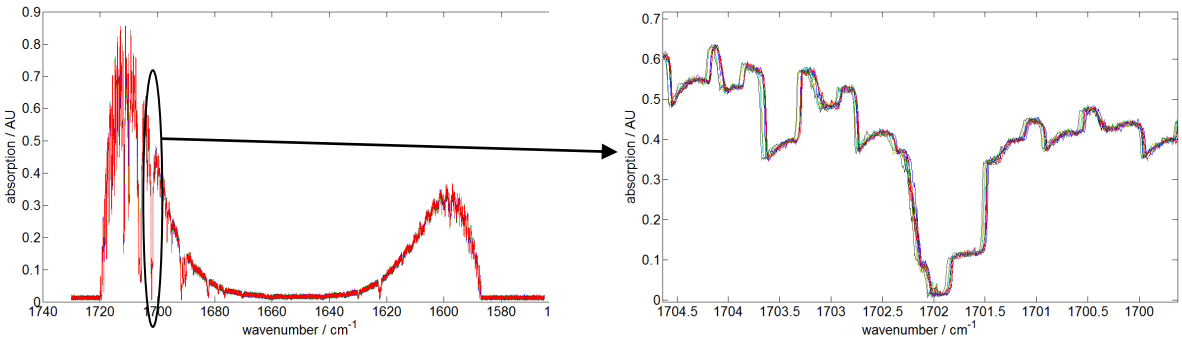

Figure 59 – Single beam spectrum with fringes and water vapour absorptions bands to illustrate the shift of successive scans. [32]

3.2.2 Albumin

Settings for the following measurements:

- Path length: 44 µm
- Settings - EC-QCL:
  - Repetition rate: 100 kHz
  - Pulse width: 0,5 µs
  - Laser current: 1000 mA
  - Tuning range: 1565-1690 cm^{-1}
  - Scan rate: 6 µsteps/int
- Flow rate: stopped flow
- Data acquisition: 24 kS, 16 kS/s
- Flow cell: measurement cell No. 3

After preparing the sample series as mentioned in section 2.2.3, a calibration measurement was carried out.

Sample Nummber	Konzentration (g/l)
Al1	4,6250
Al2	6,4833
Al3	9,7250
Al4	15,5667
Al5	19,4500

Table 4 – Concentrations of the albumin calibration for the measurements

The first spectra were recorded at 25°C, whereas five measurements were conducted and averaged at each concentration (the concentrations are shown in table 2). Furthermore, 16 consecutive scans were averaged for each sample and background measurement. The obtained results are shown in figure 60, where the amide I absorptions band can be clearly indentified.

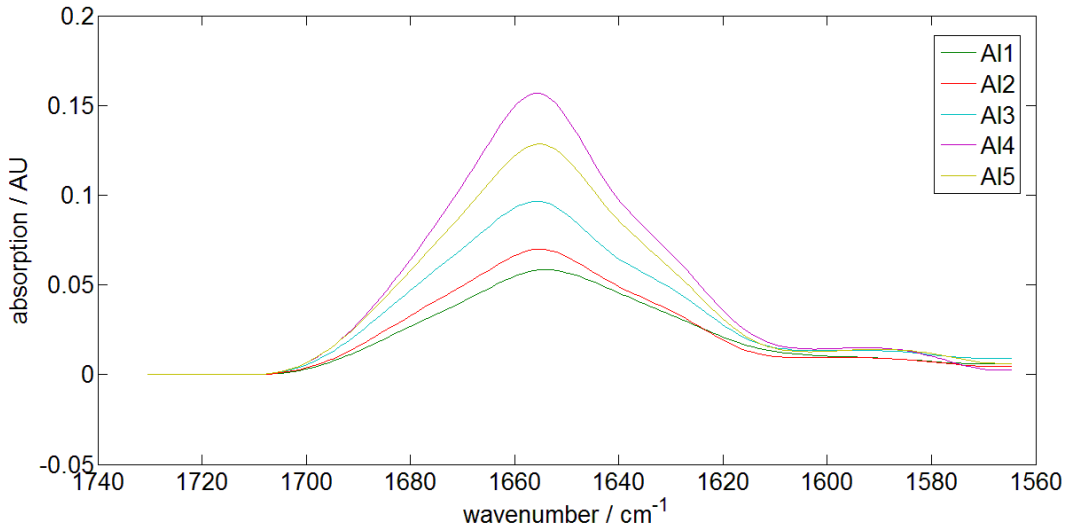

Figure 60 – Absorption spectra of albumin for various concentrations of albumin (see Table 4) at 25 ° C

To calculate the calibration curve the absorption bands were integrated over 1620-1690 cm^{-1} and the results are plotted in Figure 61.

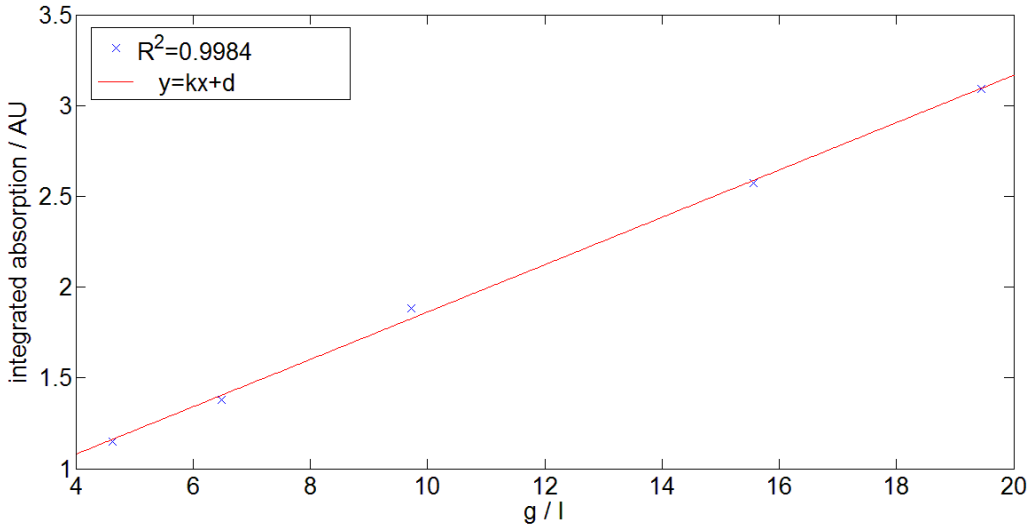

Figure 61 - Calibration curve of albumin in water at 25 ° C

Albumin at different temperatures:

Sample Number	Konzentration (g/l)
Al1	3,8900
Al2	4,6250
Al3	6,4833
Al4	9,7250
Al5	15,5667

Table 5 – Concentrations of albumin used for the measurements

The same measurements, as discussed above, were performed at four different temperatures (15°C, 20°C, 30°C, 35°C). The various concentrations (see table 5) were combined in different graphs (Figures 15-20) at different temperatures.

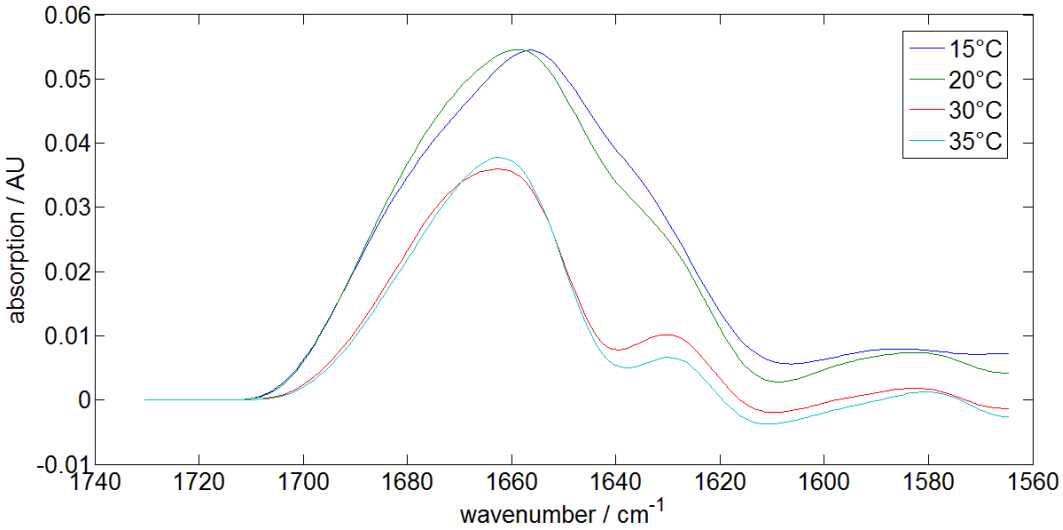

Figure 62 - Absorption spectra of albumin for the concentration Al1 according to table 5 at different temperatures

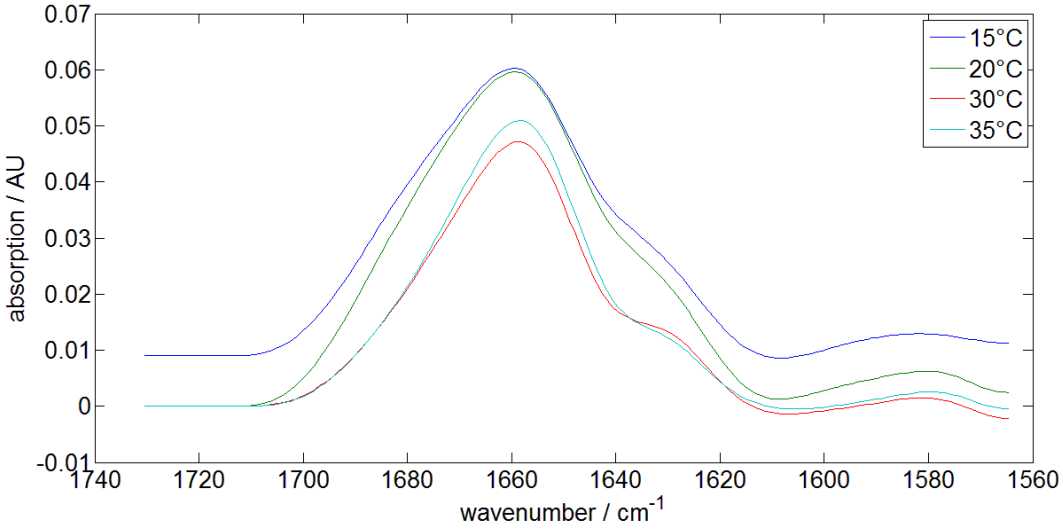

Figure 63 - Absorption spectra of albumin for the concentration Al2 according to table 5 at different temperatures

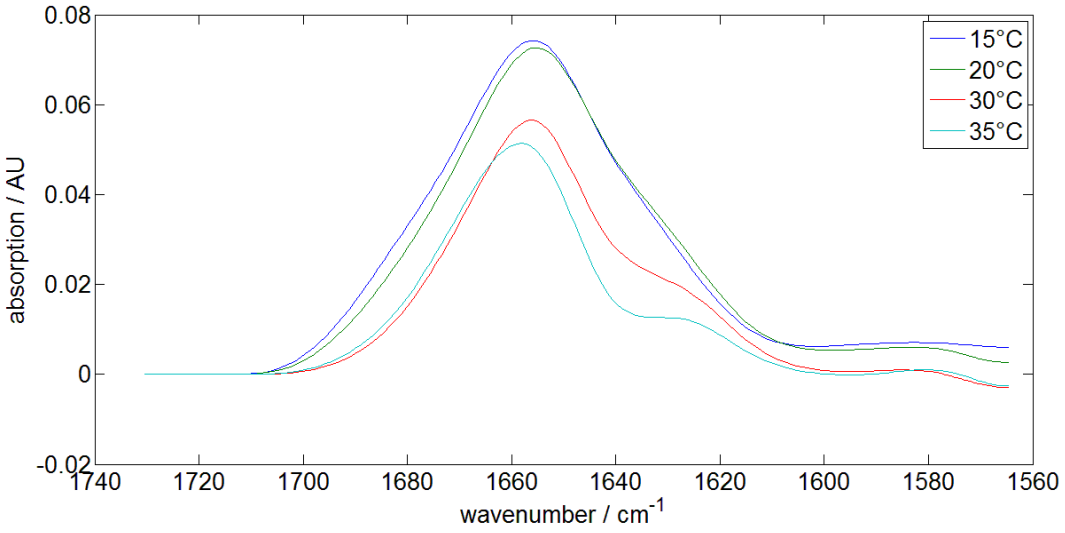

Figure 64 - Absorption spectra of albumin for the concentration Al3 according to table 5 at different temperatures

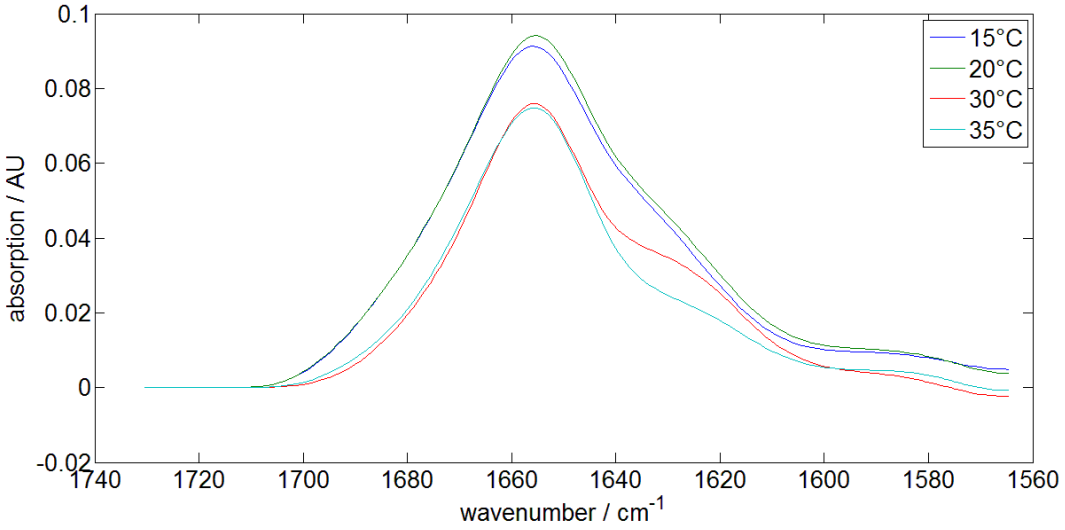

Figure 64 - Absorption spectra of albumin for the concentration Al4 according to table 5 at different temperatures

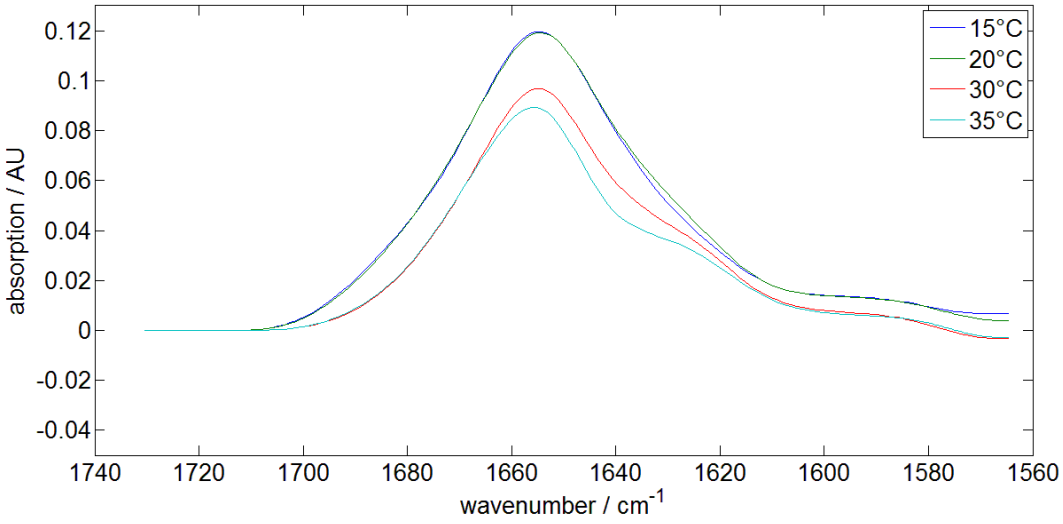

Figure 65 – Absorption spectra of albumin for the concentration Al5 according to table 5 at different temperatures

The data shown in Figures 60 - 65 suggest that the absorption band of albumin will change in strength and shape with the temperature according to changes in the secondary structure (see section 1.5.1). This fact can be seen clearly in Figure 62 and 63 where the main band decreases and an overlapping absorption band at 1625 cm^{-1} increases at higher temperature. This band is caused by the ß-sheet conformation band of the amid I band [4] [6]. Furthermore, it can be noticed that at higher temperatures, the reproducibility of measurement is poor and much more difficult to ensure than at lower temperatures. At higher temperatures, most of the measurements are incorrect due to the strong water absorption band which lowers the signal on the detector extremely (this is stronger with temperature). For this reason the following measurements are carried out at a flow cell temperature of 20°C.

3.2.3 Casein

Settings for the following measurements:

- Path length: 44 µm
- Settings - EC-QCL:
  - Repetition rate: 100 kHz
  - Pulse width: 0.5 µs
  - Laser current: 1000 mA
  - Tuning range: 1565-1690 cm^{-1}
  - Scan rate: 6 µsteps/int
- Flow rate: stopped flow
- Data acquisition: 24 kS, 16 kS/s
- Flow cell: measurement cell No. 3

After preparing the sodium caseinate sample series as mentioned in chapter 2.2.3, a test measurement at 25 °C was carried out with a concentration of 8.0236 g/l. The results are summarized in Figure 66 and show also clearly the amide I band.

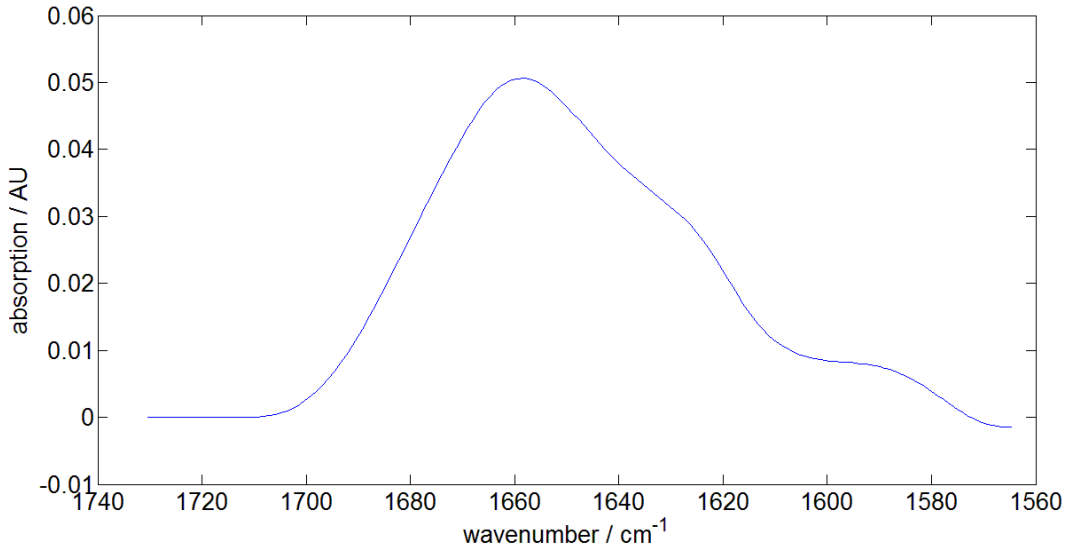

Figure 66 - Absorption spectrum of casein (8.0236 g / l)

Five different concentrations were prepared by diluting a stock solution with an Eppendorf pipette. The concentrations obtained are summarized in table 6.

Samplenummer	Konzentration g/l
Sample 1	1,9569
Sample 2	3,8208
Sample 3	5,0979
Sample 4	6,0236
Sample 5	9,3151

Table 6 – Concentrations of sodium caseinate

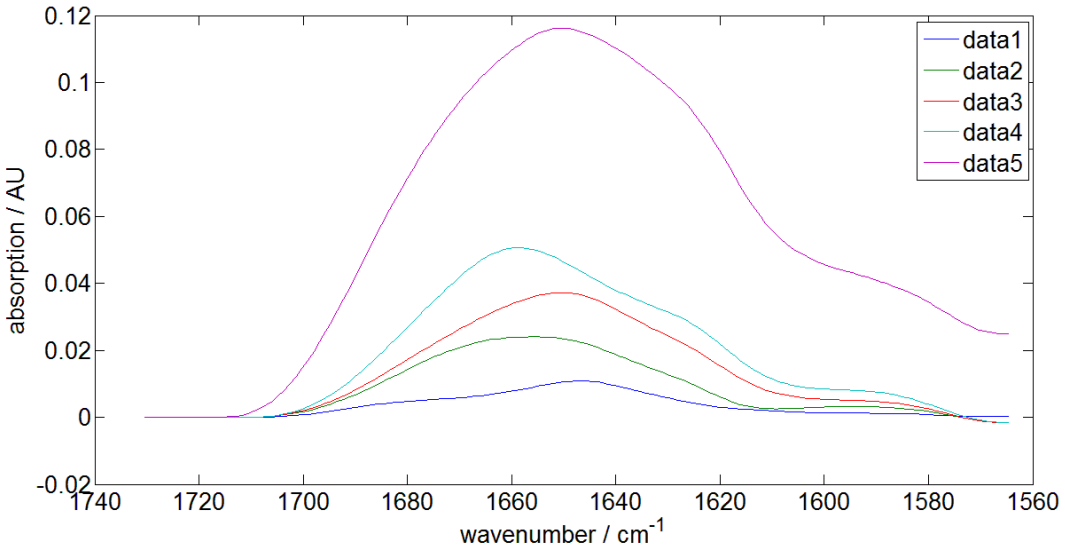

Figure 67 - Absorption spectra of various concentrations of sodium caseinate in water at 20°C according to table 6

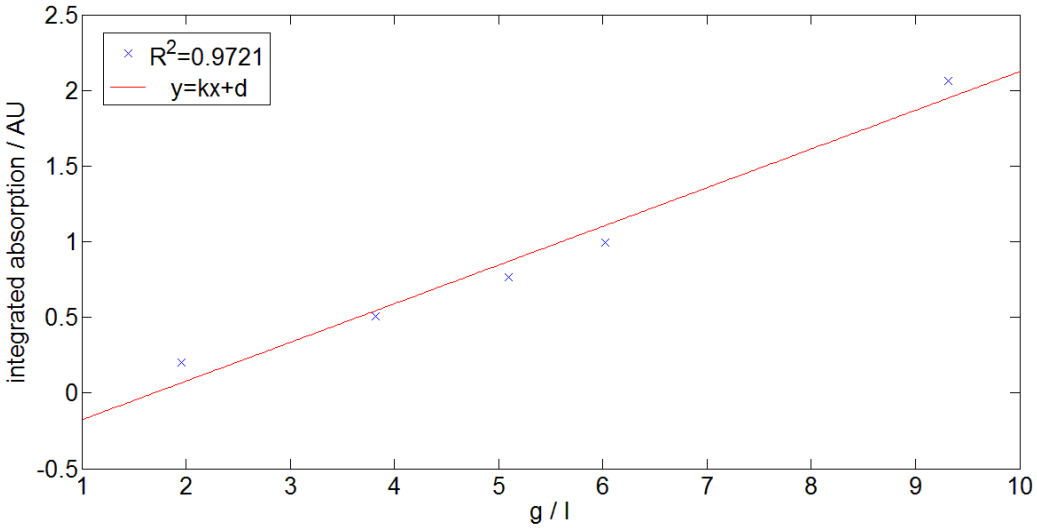

Figure 68 - Calibration curve of sodium caseinate in water at 20 ° C

To calculate the calibration curve the absorption bands were integrated from 1620 to 1680 cm^{-1} and the results are plotted in Figure 68. The linearity of the calibration curve is poor which can be an artefact of changes in the casein's properties between the various concentrations.

3.2.4 ß-lacto-globulin

Settings for the following measurements:

- Path length: 44 µm
- Settings - EC-QCL:
    - Repetition rate: 100 kHz
    - Pulse width: 0,5 µs
    - Laser current: 1000 mA
    - Tuning range: 1565-1690 cm^{-1}
    - Scan rate: 6 µsteps/int
- Flow rate: stopped flow
- Data acquisition: 24 kS, 16 kS/s
- Flow cell: measurement cell No. 3

After preparing the ß-lactoglobulin sample series of 6 samples as mentioned in chapter 2.2.3, a calibration measurement at 20°C with the concentration which are mentioned in table 7 was carried out.

Sample	Konzentration in g/l
ß1	1.0233
ß2	2,5783
ß3	3,5700
ß4	4,4200
ß5	5,1567
ß6	8,0523

Table 7 – Concentrations of ß-lacto-globulin for the calibration

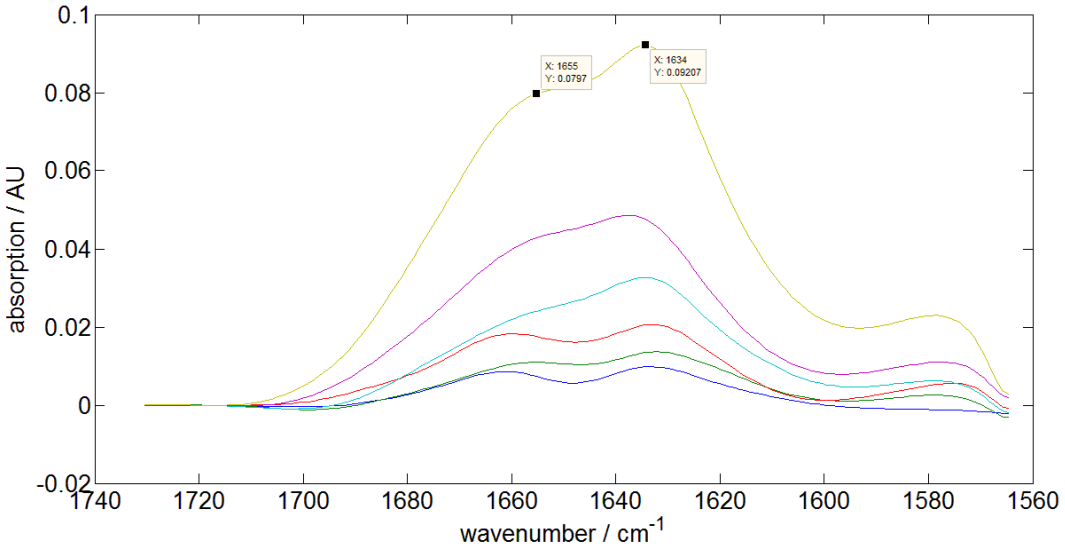

Figure 69 – Absorptions spectra of ß-lactoglobulin at different concentrations according to table 7

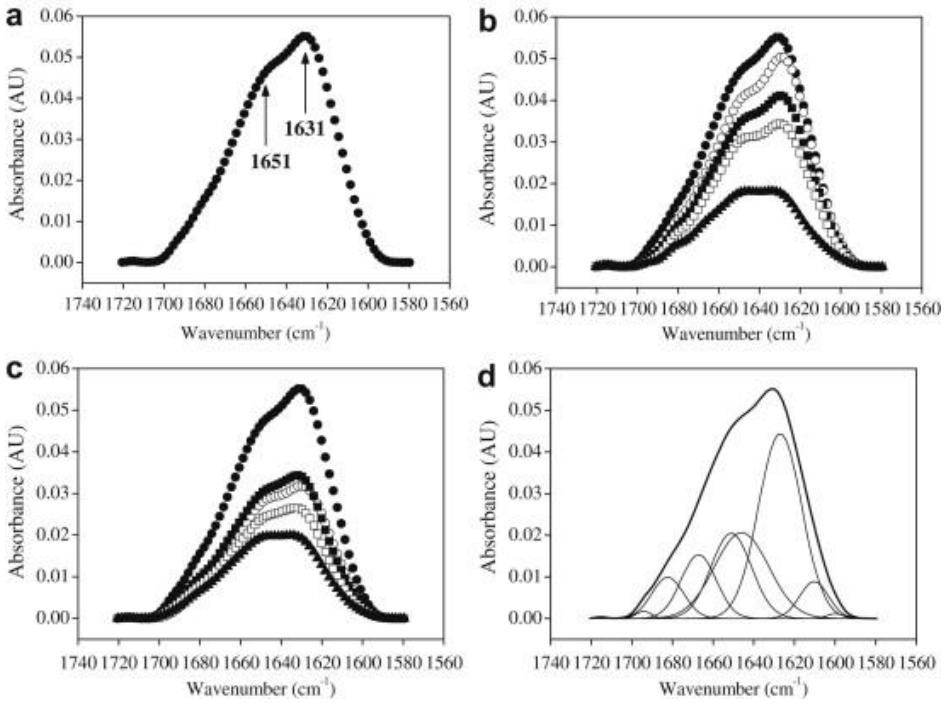

Figure 70 – Absorptions spectrum ß-lactoglobulin from literature as a reference spectrum [12]

Comparing Figure 69 and Figure 70, it can be seen clearly that the measured spectra agree well with the spectra from the literature. Furthermore, it can be seen that the peaks in figure 69, are shifted about 3 wavenumbers with respect to Figure 70, which can be attributed to the wavenumber fit which was used for plotting of all spectra.

To calculate the calibration curve the absorption bands were integrated around from 1610-1620 cm^{-1} and the results are plotted in Figure 71.

3.2.5 Soya protein

Settings for the following measurements:

- Path length: 44 µm
- Settings - EC-QCL:
    - Repetition rate: 100 kHz
    - Pulse width: 0,5 µs
    - Laser current: 1000 mA
    - Tuning range: 1565-1690 cm^{-1}
    - Scan rate: 6 µsteps/int
- Flow rate: stopped flow
- Data acquisition: 24 kS, 16 kS/s
- Flow cell: measurement cell No. 3

In the course of this thesis a soya protein sample which had a concentration of approximately 10 g/l. Although the exact concentration was unknown, this sample was measured for comparison purposes. The absorption spectrum is plotted in Figure 72. Although the absorption band shows a different shape due to different conformation, it still shows a characteristic profile of the amide I band.

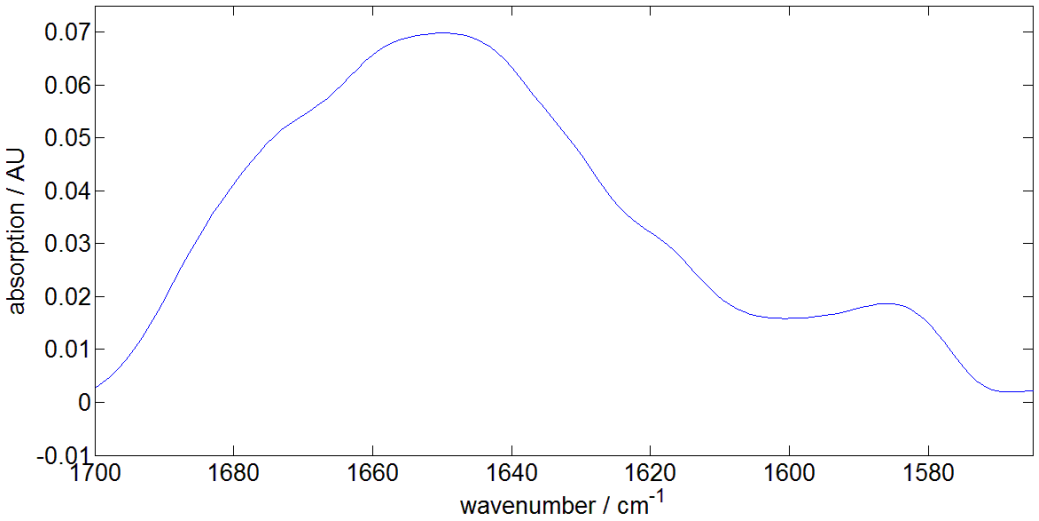

Figure 72 – Absorption spectrum of soya protein (approximately 10g/l)

3.3. Measurements with cow milk

Settings for the following measurements:

- Path length: 44 µm
- Settings - EC-QCL:
  - Repetition rate: 100 kHz
  - Pulse width: 0,5 µs
  - Laser current: 1000 mA
  - Tuning range: 1565-1690 cm^{-1}
  - Scan rate: 6 µsteps/int
- Flow rate: stopped flow
- Data acquisition: 24 kS, 16 kS/s
- Flow cell: measurement cell No. 3

The following measurements were carried out at a temperature of 20 °C.

Cow milk contains approximately 2.6 % casein (i.e., about 26 g/l), i.e. when milk measured using a pure water spectrum as background single beam spectrum, the resulting absorption spectrum should yield a clear maximum 1650-1660 cm^{-1}. Two different types of milk (long-life milk 1.5 %, unskimmed milk 3.5 %) were measured (background = deionized water). The resulting spectra are plotted in Figure 73 and Figure 74.

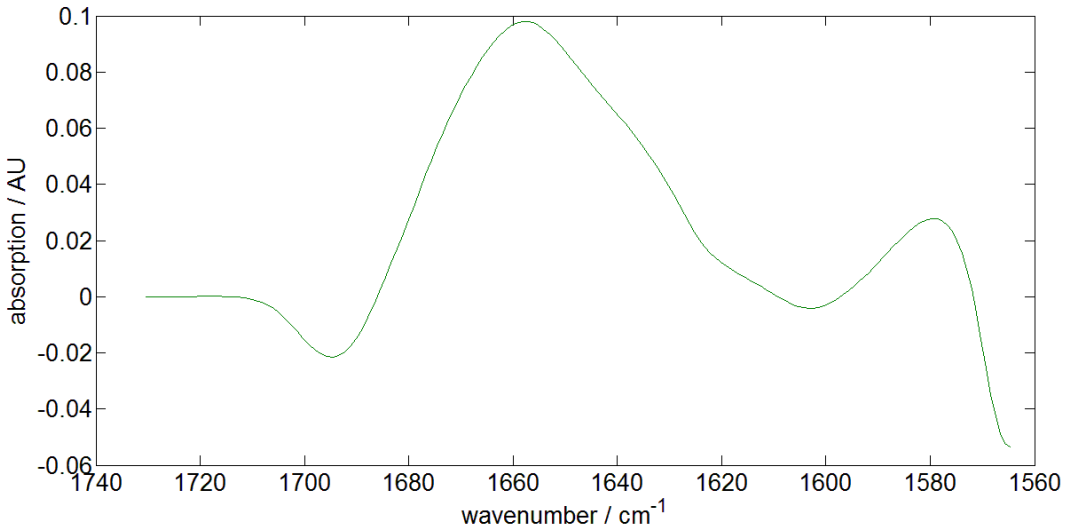

Figure 73 – Absorption spectrum of long-life milk with a fat content of 1.5 %

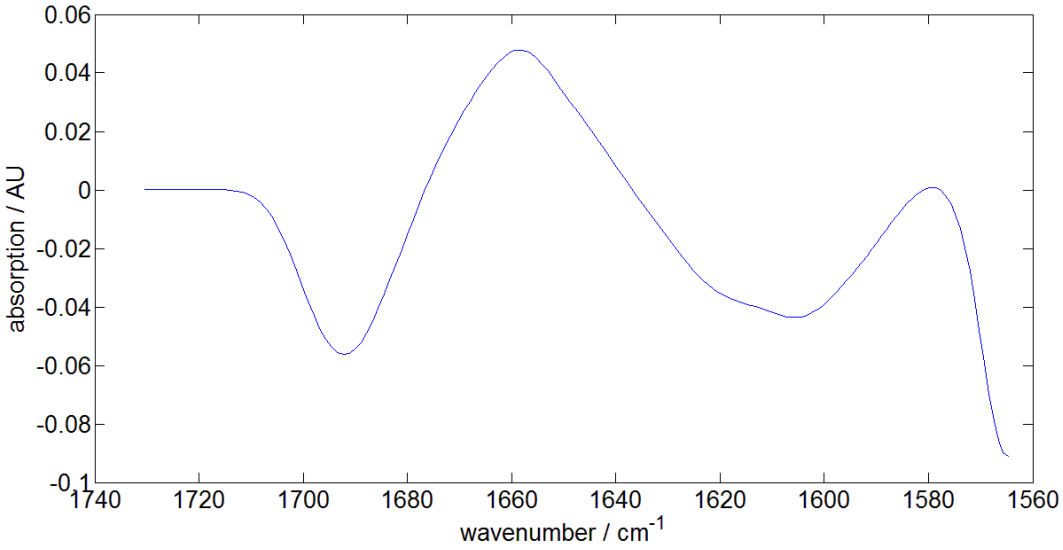

Figure 74 – Absorptions spectrum of unskimmed milk with a fat contant of 3.5 %

In Figure 75 a spectrum of sodium caseinate in water is plotted, which was measured using the same setup (with a concentration of 8.0236 g/l).

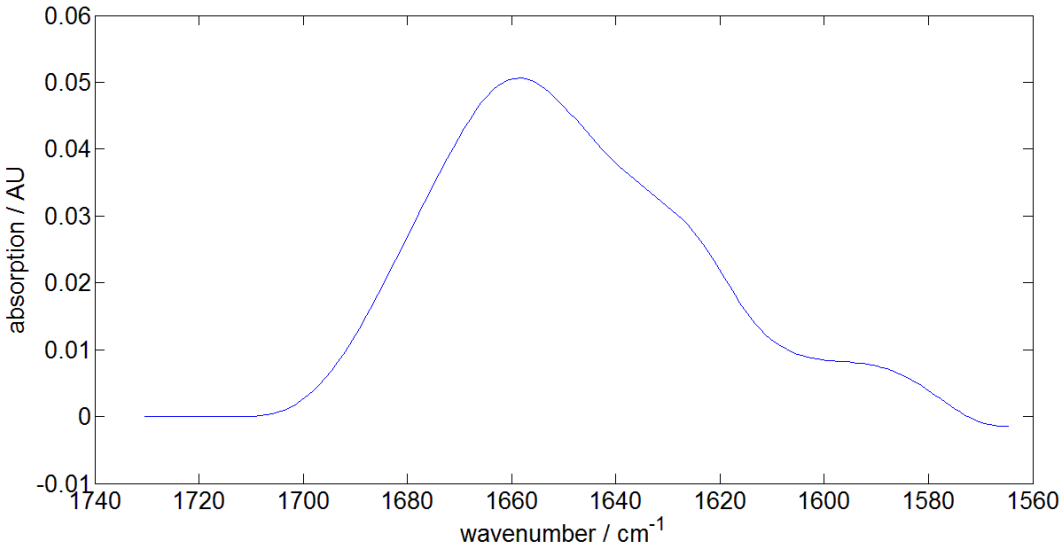

Figure 75 - absorption spectrum of casein in water (8.0236 g / l)

casein in water (8,0236 g/l)	long-life milk	unskimmed milk
1.6539 int. AU	4.1980 int. AU	3.5210 int. AU

Table 8 – Integrated absorption bands which are plotted in figure 73-75

Comparing Figures 73, 74, 75 and Table 8 it can be seen that the linear relationship between the concentrations and the absorbance units is not given satisfactory (if a concentration of 26 g/l of casein in milk will be adopted, based on: milk contains approximately 2.6 % casein). This fact is certainly also due to the different background, in which the casein is dissolved. However, a positive result is that the maximum of the spectra is approximately located at the same place. Furthermore, in Figures 73, 74 it can be seen, that the baseline varies greatly. The large variation of the baseline at the different samples can be explained by the fact that the samples contain varying amounts of other ingredients. These different contents of milk decrease the water content of the milk. An example of such a substance is fat (0-3.5%) in which the samples differ greatly regarding their fat content. Since deionized water was used as background, a negative water absorption band, which is dependent on the quantity of in milk dissolved ingredients, is overlapped by a positive amide I absorption band due to the protein content of the measured milk. Thus a negative water absorption band, which is superposed by an amide I band, is shown in Figures 73, 74. Another difficulty in the measurement of proteins in milk is the fact that milk is an inhomogeneous suspension which forms micelles, whereby the reproducibility of successive measurements is hard to ensure.

In a next step, a solution of 8.0023 g/l Sodium caseinate powder in milk was produced (see section 2.2.4) and was measured with the same setup, which was mentioned above using milk instead of water as background. Further experiments to dissolve caseinate powder in milk unfortunately fail, thus the one successful solution was measured. The resulting spectrum is plotted in Figure 76.

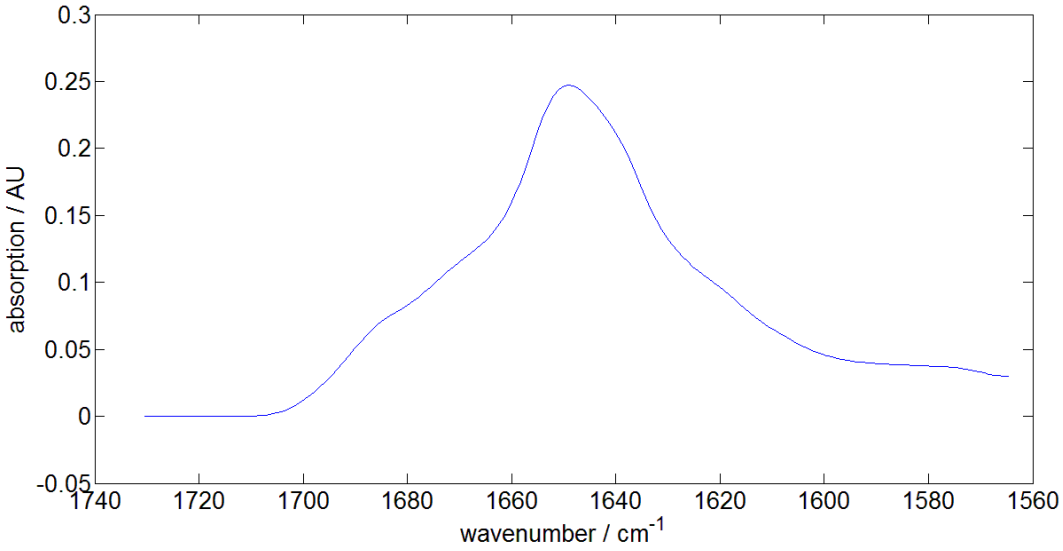

Figure 76 – Absorption spectrum of sodium caseinate powder in milk (8.0023 g/l)

The shape of the amide I band changes due to the altered matrix (=milk) and further this time no buffer solution was used to prepare the sodium caseinate sample. Comparing Figures 75 and 76, the position of the two absorption bands are located at the same point.

4. Conclusions and Outlook

The first part of this thesis dealt with the question of whether measurements of aqueous solutions in the region of the water bending vibration at about 1645cm^{-1} using an EC-QCL at large thick layer are possible. Furthermore, it was to show what is necessary for the quantitative measurement of such samples. In the second part should be shown that the amide I band of proteins, which is overlapped by the ν_2-water band, with layer thicknesses up to 40-50µm can be measured. For chemical analytical purposes, the amide I band has essential meaning, because it casts light on the secondary structure of proteins. The third part dealt with the actual motivation for this thesis; to show that it is possible to measure the amide I band of proteins in milk with sufficient accuracy for industry.

The investigations showed that it will be difficult to assert against a spectrometer measurement with low path lengths or an ATR measurement with the existing equipment. It was possible to show that an accurate temperature stabilization of the flow cell during the measurements is necessary due to the strong water absorption which is strongly influenced by the temperature. Furthermore, also a sample temperature stabilization during the measurement is essential, because a not temperature stabilized sample causes a deterioration of the flow cell's temperature control. Due to the small response at the using flow cells, the path length should not be further lowered. Instead the laser emission should be increased, and the data acquisition system should get free from noise and drift as far as possible. Increasing the laser power will not lead to success if a MCT detector with such low dynamic range would be used further. Increasing the laser emission power the existing setup would cause the saturation of the detector at the edges of the water band, which results in the loss of information at the amide I band. One possible approach to solve this problem would be the use of a pyro-electric detector, which supplies a signal that is also dependent on the pulse length of the used laser. This would make it possible to use short pulses at the edges of the water band and long at the maximum. This could be achieved by applying an external signal source for modulation over a laser scan.

A further major problem in measuring by means of using an EC-QCL from Daylight Solutions is the displacement between each successive laser scan, which causes much noise at features in the absorption spectrum (such as water vapour lines).

In milk measurements samples with different fat concentrations generate a large offset in the form of the bending vibration band due to the strong water absorption. This offset strongly depends on the quantity of fat or other ingredients. Attempts should be made to find a calibration, which suppresses the errors of other ingredients as much as possible. Also a great challenge measuring milk is that milk is an inhomogeneous suspension because milk builds micelles. This results in a bad reducibility of transmissions measurements.

5. Acknowledgements

Abschließend möchte ich die Möglichkeit nutzen, mich bei jenen Personen, welche mich bei der Erstellung dieser Arbeit tatkräftig unterstützt haben, ganz herzlich zu bedanken. Damit diese Botschaft auch für jene zu verstehen ist, die kein Englisch sprechen, möchte ich diesen Teil meiner Arbeit gerne in Deutsch verfassen.

Ich bedanke mich recht herzlich bei:

Ao.Univ.Prof. Dipl.-Ing. Dr.techn. Bernhard Lendl, der meine Masterarbeit im Rahmen der Arbeitsgruppe betreute und immer für Fragen während meiner Zeit bei ihm bereitstand. Weiters möchte ich mich bei ihm für die Hilfe, bei meinem weiteren Berufsweg Fuß zu fassen, bedanken.

Dipl.-Ing. Markus Brandstetter, welcher mich bei meiner Arbeit tatkräftig unterstützt hat, sich immer Zeit genommen hat, meine Ergebnisse zu diskutieren. Ich bedanke mich ebenfalls für die großartige Betreuung auf fachlicher Ebene.

Ao.Univ.Prof. Dipl.-Ing. Dr.techn. Martin Gröschl, welcher meine Masterarbeit seitens der TU Wien betreute.

Wolfgang Tomischko, der mich seitens der Elektronik mit großem Eifer unterstützt hat und mich an seiner umfangreichen Erfahrung teilhaben ließ.

Johannes Frank, welcher die von mir konstruierten Flusszellen mit großer Kompetenz und hoher Qualität herstellte.

Dipl.-Ing. Georg Ramer, der immer für eine Diskussion bereitstand und mir bei so einigen programmiertechnischen Problemstellungen helfen konnte.

Ich bedanke mich weiters bei der ganzen Arbeitsgruppe, welche mir immer hilfsbereit zur Seite stand.

Ein besonderer Dank gilt meiner Mutter, die mich zu Zeiten meiner schulischen Laufbahn ermutigt hat, doch das Gymnasium mit Matura abzuschließen, wodurch dieses Studium erst möglich wurde.

Der größte Dank gebührt meiner Ehefrau Tanja, die mich seit Anfang meines Studiums unterstützte, immer für mich da war und stets meine Interessen tatkräftig förderte und nie einschränkte. Ohne sie wäre dieses Studium nicht möglich gewesen.

6. References

[1] “Handbook of Instrumental Techniques for Analytical Chemistry”, Hsu, C Sherman Ph, D

[2] “FTIR Analysis of Protein Structure”, Warren Gallagher

[3] “Fourier Transform Infrared Spectroscopy Analysis of Protein Secondary Structures”, Jilie Kong, Shaoning Yu

[4] “Infrared spectroscopy of proteins”, Andreas Barth

[5] “Handbook of vibrational Spectroscopy”, John M. Chalmers , Peter R. Griffiths

[6] http://jenalib.fli-leibniz.de/ImgLibDoc/ftir/IMAGE_FTIR.html

[7] http://www.bph.rub.de/faltung-body.htm

[8] “Dairy Processing Handbook/chapter 2”, Gösta Bylund

[9] “New applications of Mid-infra-red Spectrometry for the Analysis of Milk and Milk Products”, Bulletin of the International Dairy Federation 406/2006, Christian Robert

[10] “Spektroskopie”, Jürgen Böcker

[11] “Determination of protein concentration in raw milk by mid-infrared fourier transform infrared/attenuated total reflectance spectroscopy”, Etzion, Y; Linker, R; Cogan, U; Shmulevich, I

[12] „Food Hydrocolloids –Elsevier“

[13] http://www1.lsbu.ac.uk/water/sitemap.html, Emeritus Professor of Applied Science London South Bank University, Martin Chaplin BSc PhD CChem FRSC

[14] http://www.ualberta.ca/~jbertie/JBDownload.HTM#Spectra, John Bertie

[15] “Possible amplification of electromagnetic waves in a semiconductor with superlattice.”, Fizika I Tekhnika Poluprovodnikov 5, 797-800, Kazarinov, R.F., Suris, R.A. 1971.

[16] “Quantum Cascade Laser.”, Science 264, 553-556, Faist, J. et al. 1994.

[17] “Klassisches Konzept von Quanten-Kaskaden Lasern“, 2013 Walter Schottky Institut.

http://www.wsi.tum.de/Research/AmanngroupE26/AreasofResearch/QuantumCascadeLasers/tabid/111/Default.aspx

[18] “Quantum Cascade Lasers for Infrared Spectroscopy: Theory, State of the Art, and Applications”, Laura Bush 2013

[19] “Experimentalphysik 1“, Demtröder Wolfgang, S 280

[20] http://www.chemguide.co.uk/organicprops/aminoacids/proteinstruct.html

[21] “IR-Spektroskopie”, Günzler, Helmut, Gremlich, Hans-Ulrich

[22] “Molekülphysik”, Demtröder Wolfgang

[23] http://commons.wikimedia.org/wiki/File:Protein-Sekund%C3%A4rstruktur.png

[24] “Changes in the Secondary Structure of Bovine Casein by Fourier Transform Infrared Spectroscopy Effects of Calcium and Temperature”, Curly, Kumosinski, Unruh, Farrell

[25] “WT Boxcar mit Anzeige REV_C Manual”, Tomischko Wolfgang

[26] http://www.vigo.com.pl/products/measurement-equipment/MIPxC

[27] http://de.wikipedia.org/wiki/Infrarotspektroskopie

[28] “Tunable external cavity quantum cascade laser for the simultaneous determination of glucose and lactate in aqueous phase.”, The Analyst. 135 (2010) 3260–3265, M. Brandstetter, A. Genner, K. Anic, B. Lendl

[30] “Application of microfluidic devices for time resolved FTIR spectroscopy”, Christoph wagner

[31] http://www.vigo.com.pl/products/measurement-equipment/MIPXC

[32] “Tunable mid-infrared lasers in physical chemosensors towards the detection of physiologically relevant parameters in biofluids”, Markus Brandstetter, Bernhard Lendl

[33] http://www.foss.dk/industry-solution/dairy/papers - “Intrument standardisation“ (US Pat. No. 5,933,792)

[34] “What vibrations tell us about proteins”, Andreas Barth, Christian Zscherp

[35] “External cavity quantum cascade laser”, Topical Review, Andreas Hugi, Richard Maulini and Jerome Faist

Appendix A

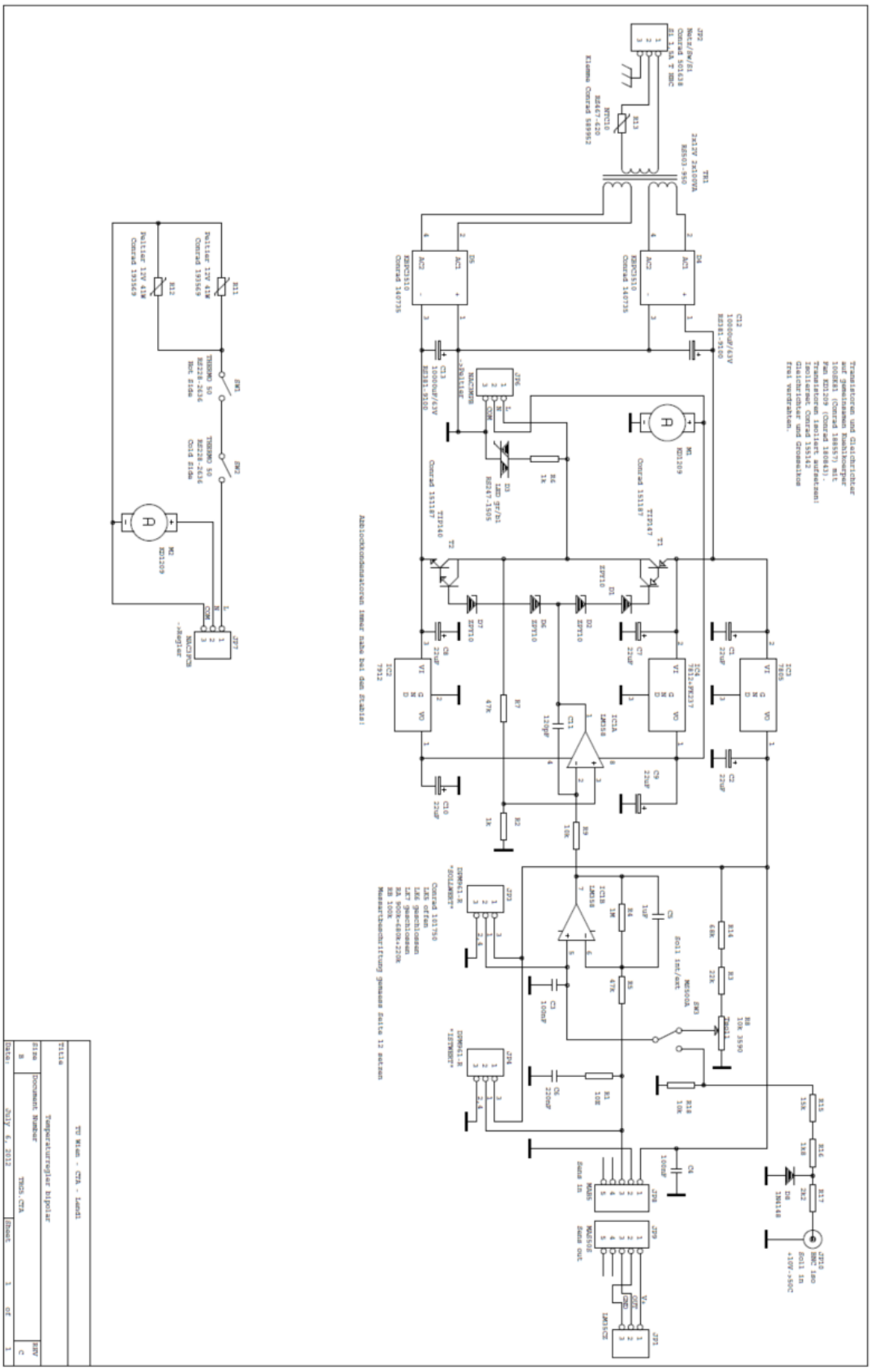

Appendix B

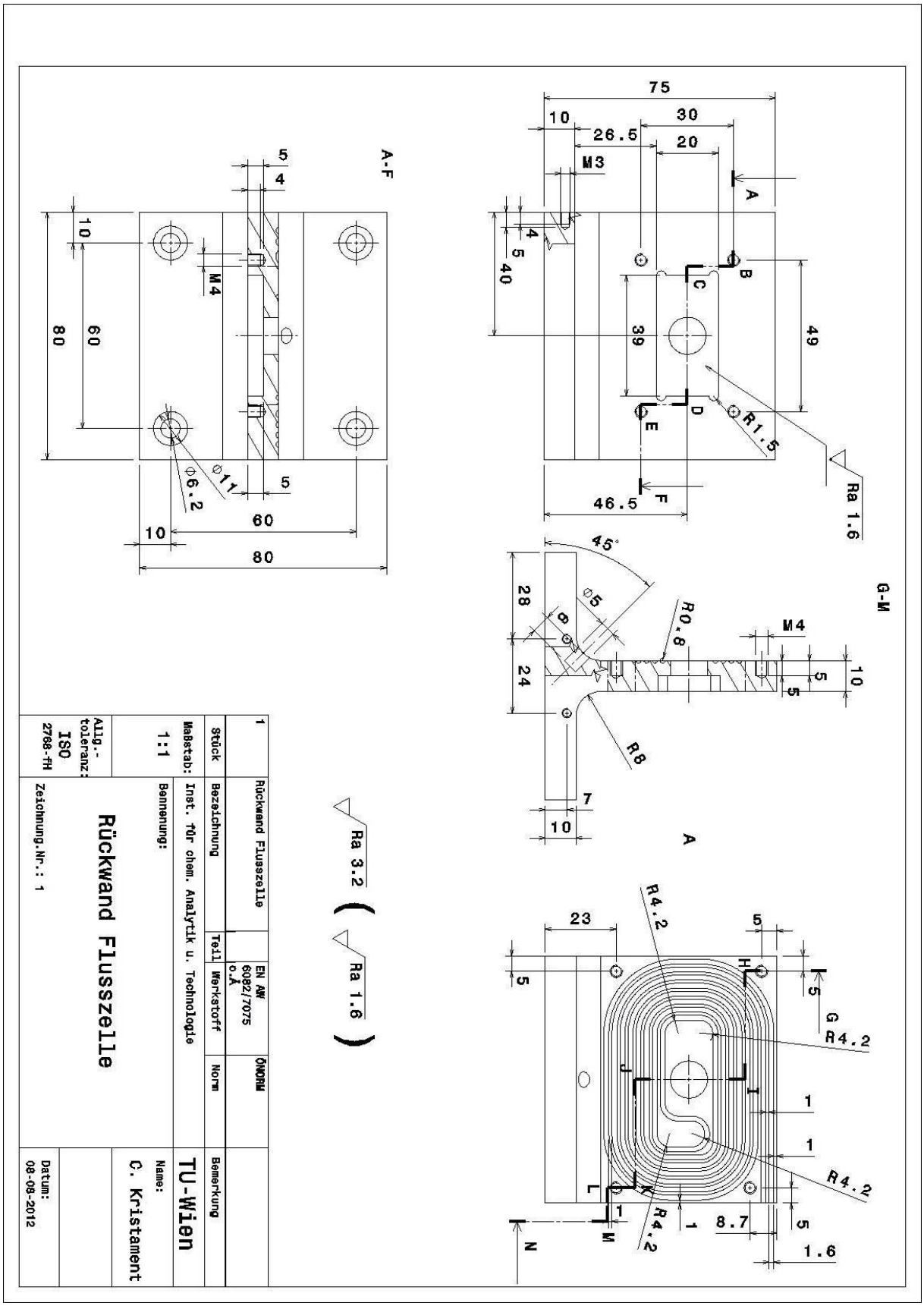
A-F
G-M
A
Ra 3.2
Ra 1.6
Rückwand Flusszelle
EN AW 6082/7075 o.Ä
ÖNORM
Inst. für chem. Analytik u. Technologie
TU-Wien
C. Kristament
Rückwand Flusszelle
1:1
ISO 2768-fH
08-08-2012
Zeichnung-Nr.: 1

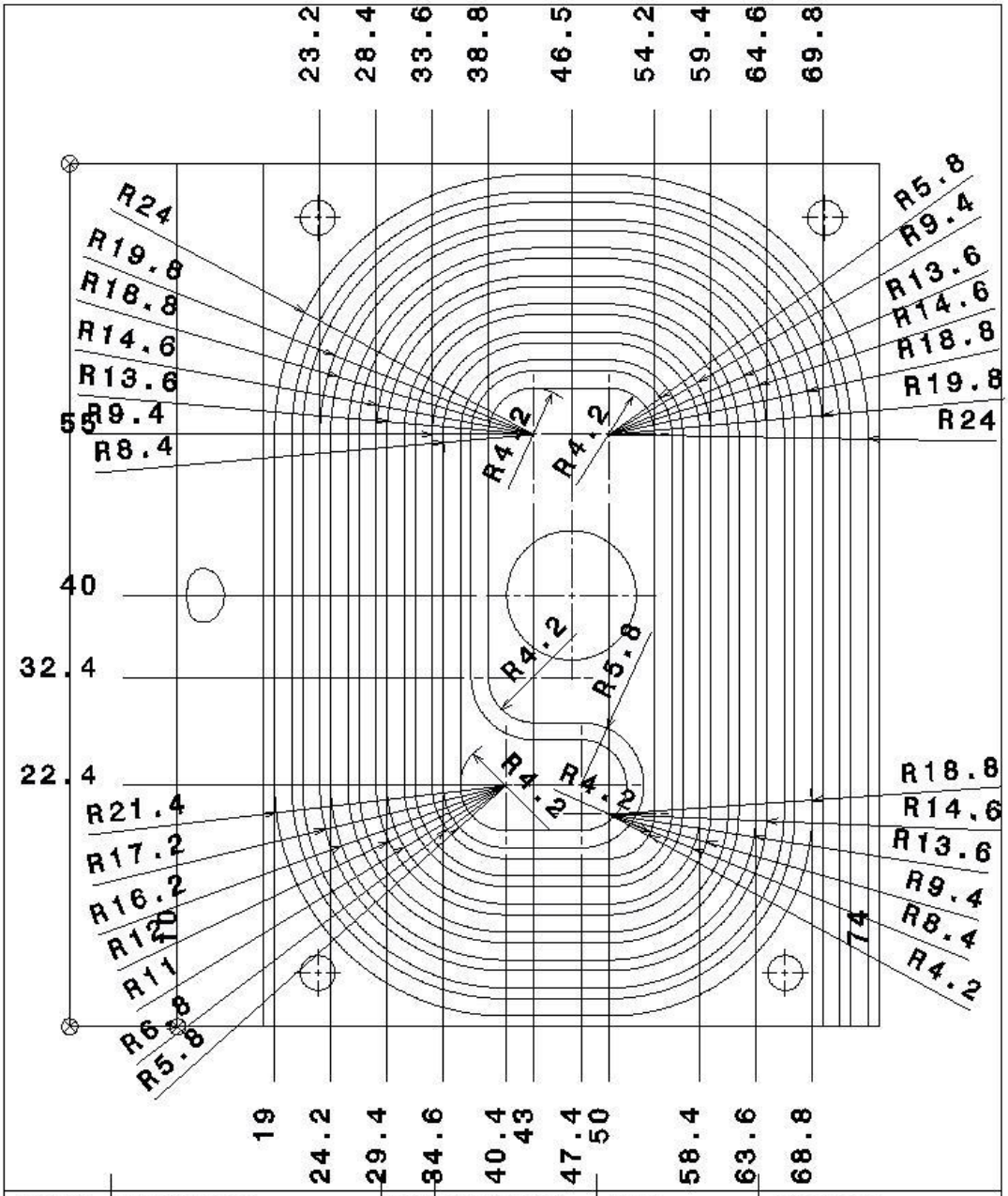

Stück	Bezeichnung	Teil	Werkstoff	Norm	Bemerkung
Maßstab: 2:1					TU-Wien
	Bennenung: Mäander Rückwand				Name: C. Kristament
Allg.-toleranz:					
	Zeichnung.Nr.: ad 1.1				Datum: 05-09-20xx

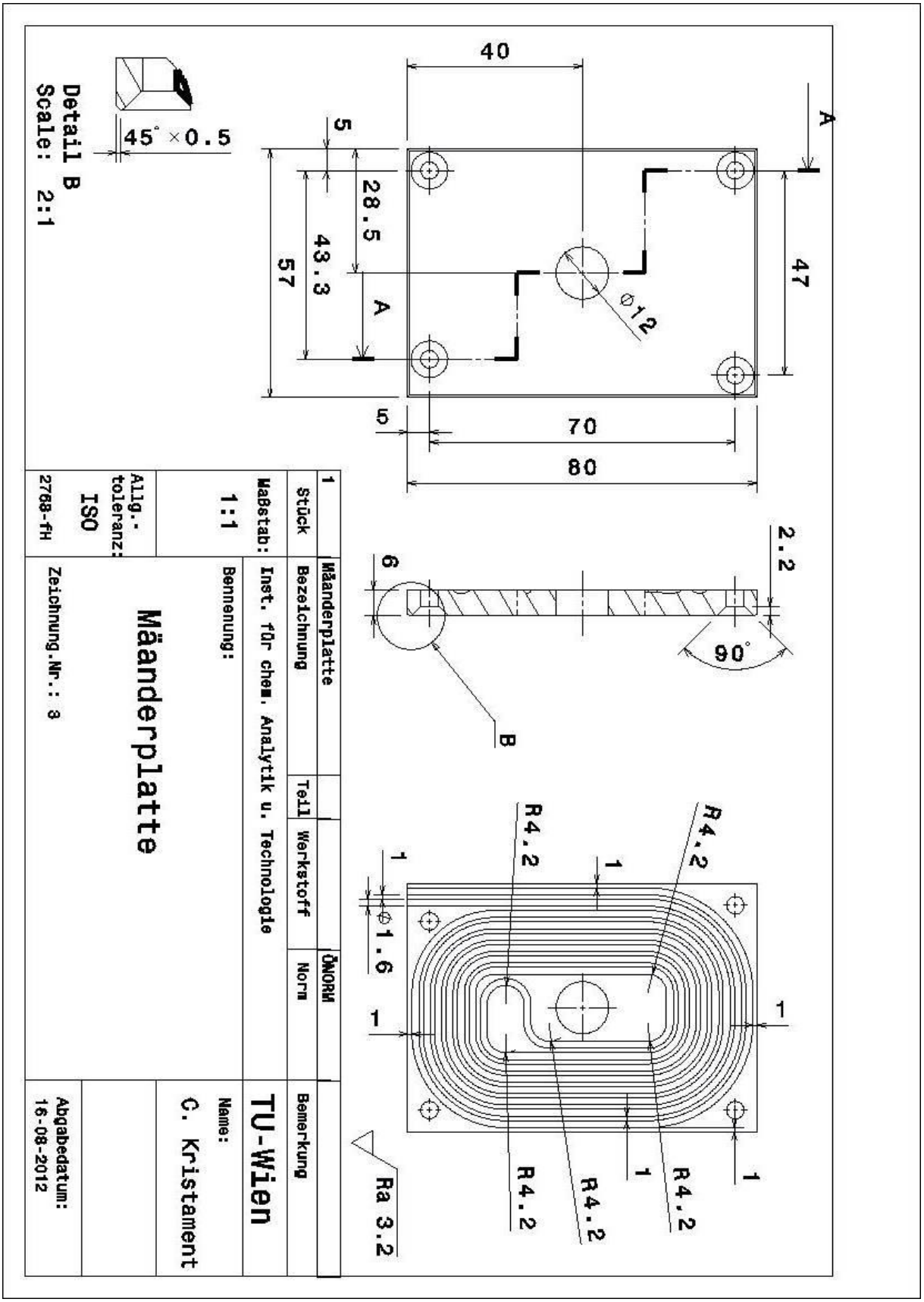
Detail B
Scale: 2:1
45° ×0.5
40
5
28.5
43.3
57
A
47
Ø12
5
70
80
2.2
6
90°
B
R4.2
1
Ø1.6
Ra 3.2
1
Mäanderplatte
Stück
Bezeichnung
Teil
Werkstoff
Norm
ÖNORM
Bemerkung
Maßstab:
1:1
Inst. für chem. Analytik u. Technologie
TU-Wien
Allg.-toleranz:
ISO
2768-fH
Benennung:
Mäanderplatte
Name:
C. Kristament
Zeichnung.Nr.: 8
Abgabedatum:
16-08-2012

Appendix C

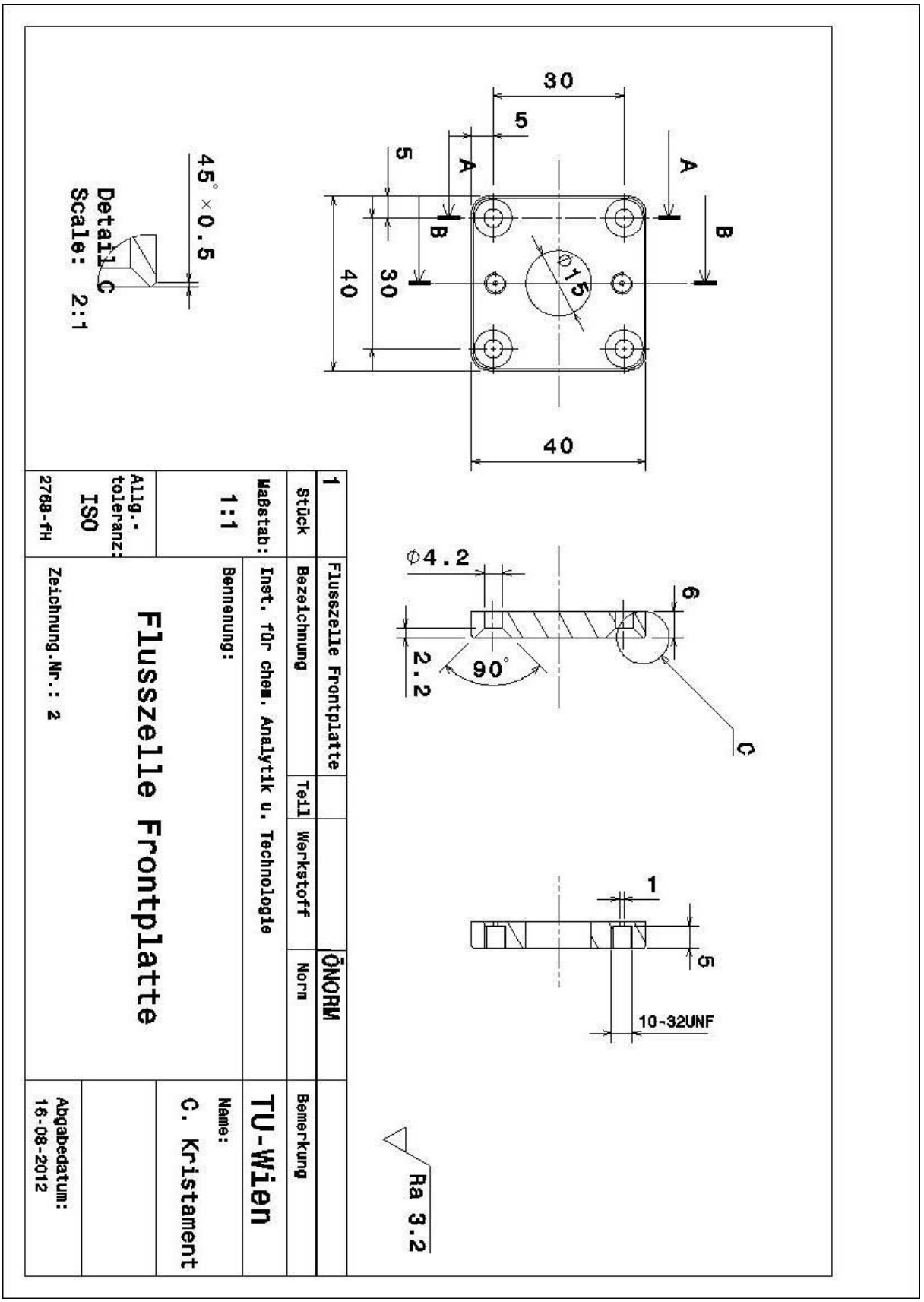
30
5
5
A
B
40
30
Ø15
40
45° ×0.5
Detail C
Scale: 2:1
Ø4.2
6
2.2
90°
C
1
5
10-32UNF
Ra 3.2
1
Flusszelle Frontplatte
Stück
Bezeichnung
Teil
Werkstoff
Norm
ÖNORM
Bemerkung
Maßstab:
1:1
Inst. für chem. Analytik u. Technologie
TU-Wien
Allg.-toleranz:
ISO
2768-fH
Benennung:
Flusszelle Frontplatte
Name:
C. Kristament
Zeichnung-Nr.: 2
Abgabedatum:
16-08-2012

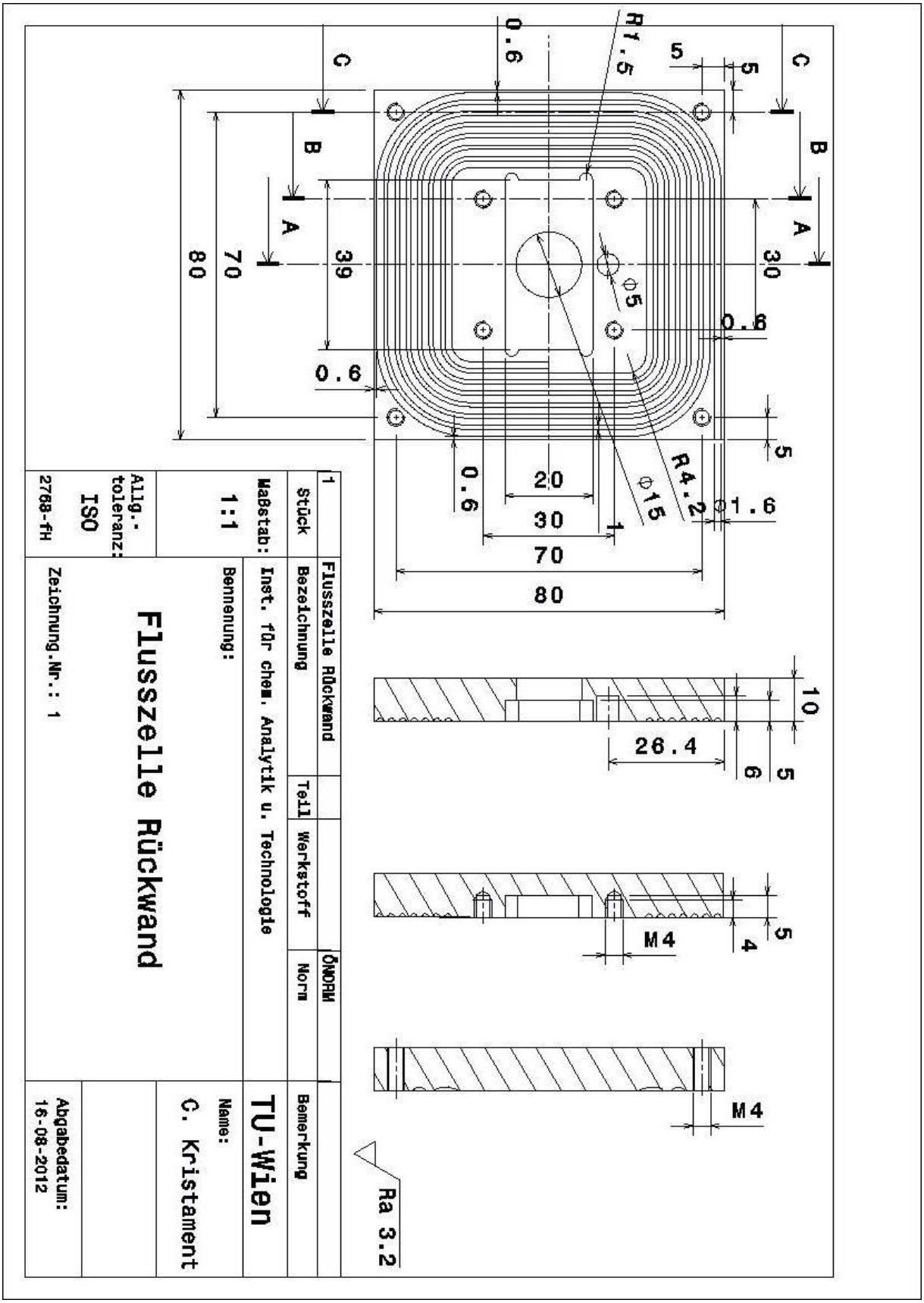
R1.5
0.6
5
5
C
B
A
39
30
80
70
Ø5
0.6
0.6
5
R4.2
Ø15
Ø1.6
0.6
20
30
70
80
1
10
26.4
6
5
M4
4
5
M4
Ra 3.2
1
Stück
Maßstab:
1:1
Allg.-toleranz:
ISO
2768-fH
Flusszelle Rückwand
Bezeichnung
Teil
Werkstoff
ÖNORM
Norm
Bemerkung
Inst. für chem. Analytik u. Technologie
Benennung:
Flusszelle Rückwand
Zeichnung.Nr.: 1
TU-Wien
Name:
C. Kristament
Abgabedatum:
16-08-2012

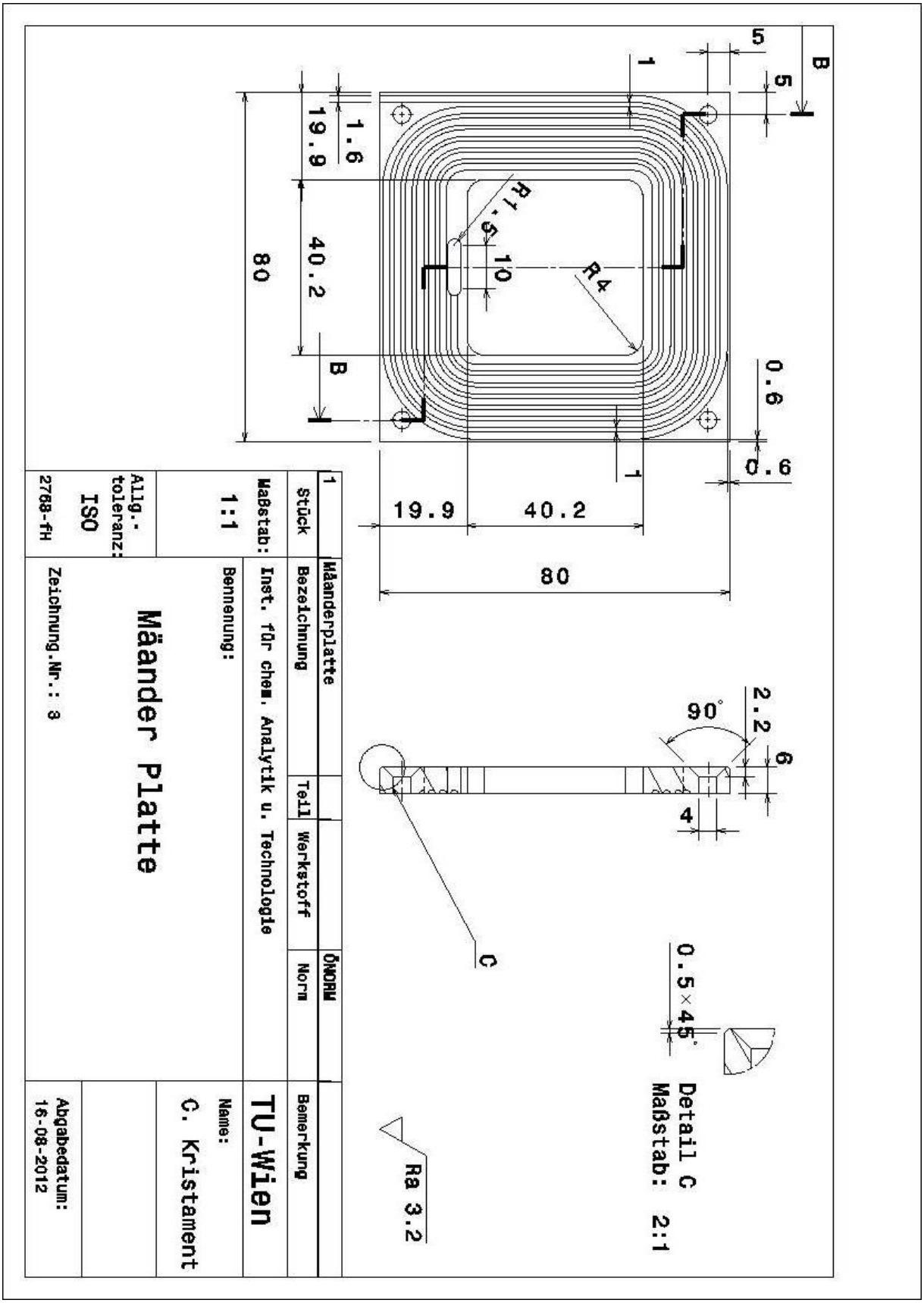
B
5
5
1
1.6
19.9
40.2
80
R1.5
10
R4
B
0.6
0.6
1
19.9
40.2
80
90°
2.2
6
4
C
0.5×45°
Detail C
Maßstab: 2:1
Ra 3.2
1
Mäanderplatte
Stück
Bezeichnung
Teil
Werkstoff
Norm
ÖNORM
Bemerkung
Maßstab:
1:1
Inst. für chem. Analytik u. Technologie
TU-Wien
Allg.-toleranz:
ISO
2768-fH
Benennung:
Mäander Platte
Name:
C. Kristament
Zeichnung.Nr.: 8
Abgabedatum:
16-08-2012

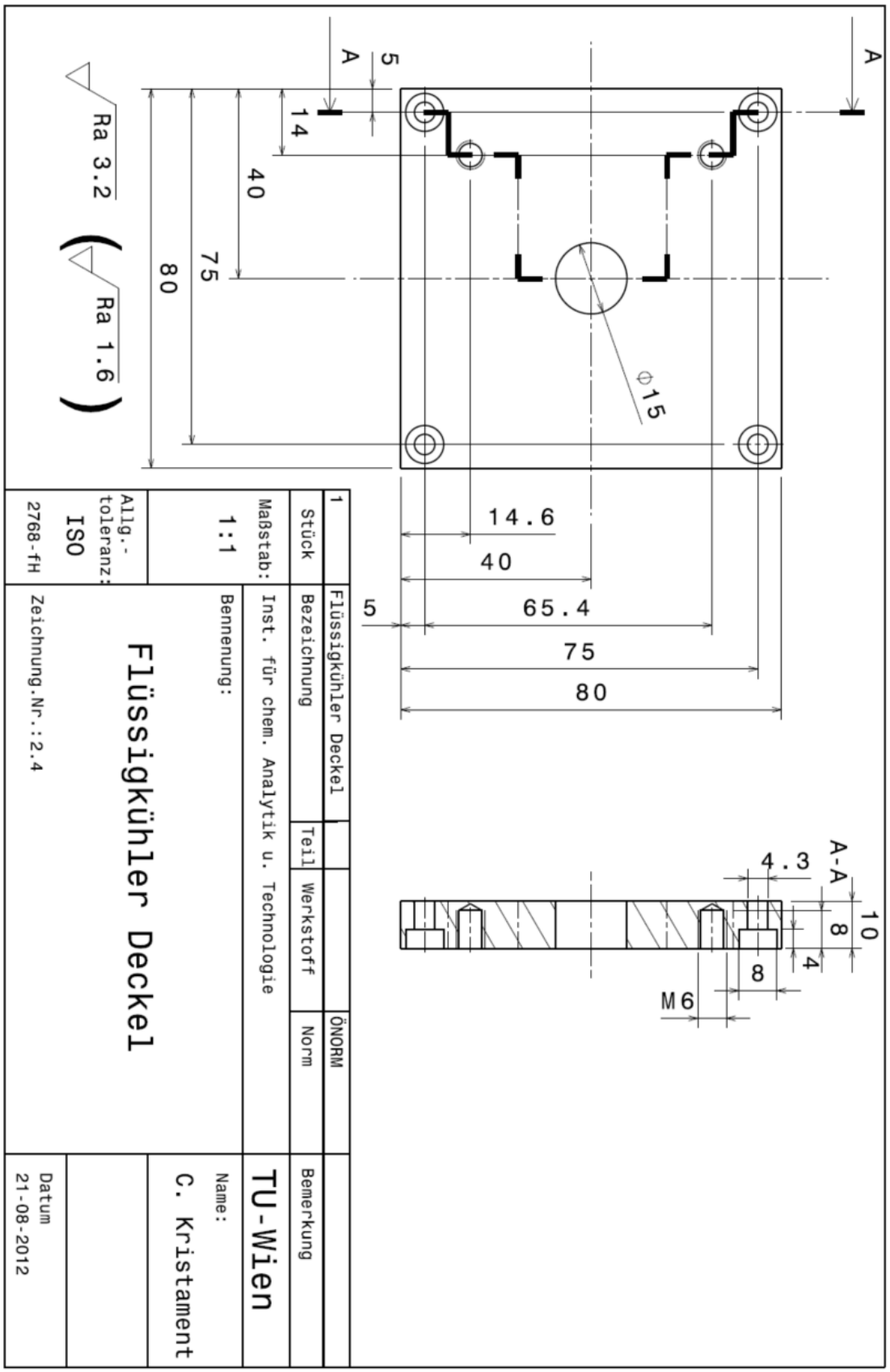

1	Flüssigkühler Deckel			ÖNORM	
Stück	Bezeichnung	Teil	Werkstoff	Norm	Bemerkung
Maßstab: 1:1	Inst. für chem. Analytik u. Technologie			TU-Wien	
Allg.-toleranz: ISO 2768-fH	Bennenung: Flüssigkühler Deckel			Name: C. Kristament	
	Zeichnung.Nr.: 2.4			Datum 21-08-2012	

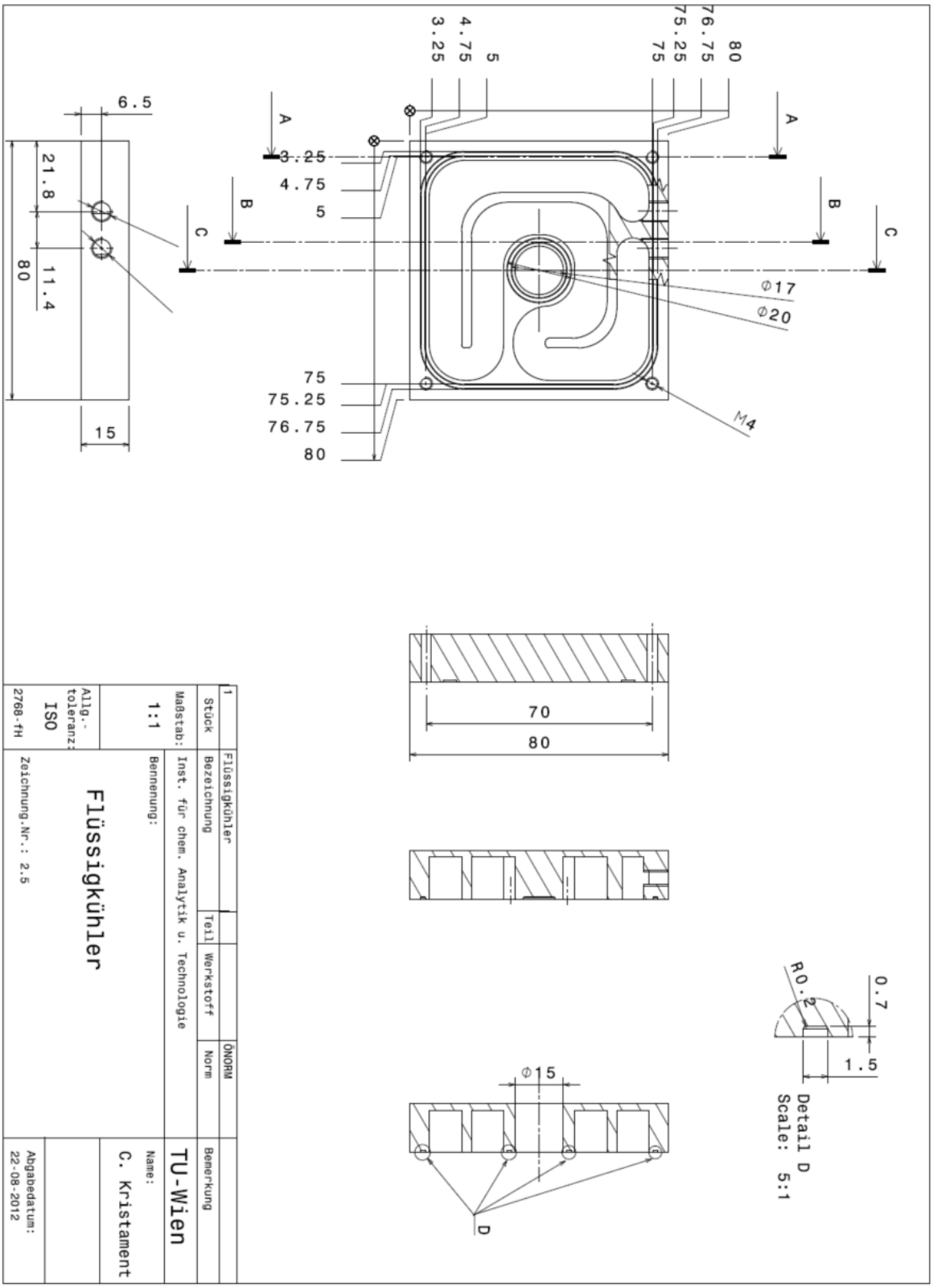
6.5
21.8
11.4
80
15
A
B
C
3.25
4.75
5
75
75.25
76.75
80
Φ17
Φ20
M4
70
80
Φ15
D
R0.2
0.7
1.5
Detail D
Scale: 5:1
1
Stück
Flüssigkühler
Bezeichnung
Teil
Werkstoff
Norm
ÖNORM
Bemerkung
Maßstab:
1:1
Allg.-toleranz:
ISO
2768-fH
Inst. für chem. Analytik u. Technologie
TU-Wien
Benennung:
Flüssigkühler
Zeichnung.Nr.: 2.5
Name:
C. Kristament
Abgabedatum:
22-08-2012